Theses and Dissertations

2017

The regenerating fin as a model to examine the skeletal defects of Roberts Syndrome

Rajeswari Banerji
Lehigh University

The regenerating fin as a model to examine the skeletal defects of Roberts

Syndrome

by

Rajeswari Banerji

A Dissertation

Presented to the Graduate and Research Committee

of Lehigh University

in Candidacy for the Degree of

Doctor of Philosophy

in

Cell and Molecular Biology

Lehigh University

May 2017

Approved and recommended for acceptance as a dissertation in partial fulfillment of the requirements for the degree of Doctor of Philosophy

Rajeswari Banerji
The regenerating fin as a model to examine the skeletal defects of Roberts Syndrome

04.20.2017
_____
Defense Date

_____
Dissertation Director
M. Kathryn Iovine, PhD

_____
Approved Date

Committee Members

_____
Robert V. Skibbens, PhD
(Co-advisor)

_____
Linda Lowe-Krentz, PhD
(Internal member)

_____
Robert A. Cornell, PhD
(External member)

so easy to do my experiments. My PhD journey has been memorable because I was a part of a fantastic and helpful department. I would like to thank all the members of the Biological Science department- faculty, graduate students and office staff for making my journey great.

Lastly, I would like to express my deepest gratitude to my family for all the support. My husband, Dr. Soutir Bandyopadhyay has always motivated and supported me to fulfill my dreams. Without his support I wouldn't have completed my PhD work. He has spent long hours taking care of our daughter, Anushka, which gave me more time to complete my studies and research work. I am equally grateful to my parents and in-laws for having faith in me and motivating me from long distance. Thank you.

TABLE OF CONTENTS

LIST OF FIGURES AND TABLES

LIST OF ABBREVIATIONS

AEC   Apical epithelial cells
ANOVA   Analysis of Variance
BCIP   5-Bromo-4-chloro-3-indolyl-phosphate
BME   Beta-mercaptoethanol
Bp   Base pairs
BrDU   Bromodeoxyuridine
BSA   Bovine serum albumin
3C   Chromosome conformation capture
$CaCl_2$ Calcium Chloride
CTCF   CCCTC-binding factor
cDNA   Complementary DNA
CdLS   Cornelia de Lange Syndrome
ChIP   Chromatin immunoprecipitation
CNS   Central nervous system
CoREST   Corepressor for element-1-silencing transcription factor
CX   Connexin
DAPI   4', 6-diamidino-2-phenylindole
DIG   Digoxygenin
dmb   Distal-most blastema
DMEM   Dulbecco's Modified Eagle's Medium
DNA   Deoxyribonucleic acid
Dpa   Days post amputation
Dpe   Days post electroporation
E   Enhancer
EDTA   Ethylene diamine tetra acetic acid
EGTA   Ethylene bis-tetra acetic acid
EL   Extracellular loop
ESCO   Establishment of Sister Chromatid Cohesion
Fp   Forward primer
Gja   Gap junction
GST   Glutathione S-transferase
GFP   Green Fluorescent Protein
Hapln   Hyaluronan and proteoglycan link protein
HCl   Hydrochloric acid
HDAC8   Histone deacetylase
HEPES   4-(2-hydroxyethyl)-1-piperazineethanesulfonic acid
Hos   Hda One Similar
Hpa   Hours post amputation
Hpe   Hours post electroporation
Hpf   Hours post fertilization
H3P   Histone 3 Phosphate
Hox   Homeobox protein
HR   Heterochromatin repulsion

HS	Heat shock
Hsp	Heat shock protein
HYB	Hybridization solution
IACUC	Institutional Animal Care and Use Committee
IL	Intracellular loop
ISH	In situ hybridization
IgG	Immunoglobulin G
IDT	Integrated DNA Technologies
Kb	Kilo base
KCl	Potassium chloride
KD	Knockdown
KDa	Kilodalton
KH_2PO_4	Potassium phosphate (monobasic)
K_2PO_4	Potassium phosphate (dibasic)
L	Liter
LSD	Lysine-specific demethylase
MCD	Mitotic Chromosome Determinant
Med	Mediator
μg	Microgram
μL	Microliter
μm	Micrometer
μs	Microsecond
μM	Micromoles
mM	Milimolar
Ms	Milisecond
Mg	Miligram
Ml	Mililiter
miRNA	MicroRNA
MO	Morpholino
MM	Mismatch
MABT	Maleic acid buffer Tween 20
Mps	Monopolar spindle
Mg_2SO_4	Magnesium sulfate
$MgCl_2$	Magnesium chloride
Min	Minutes
mRNA	Messenger RNA
Msx	Muscle Segment Homeobox
NBT	Nitro blue tetrazolium
NIPBL	Nipped-B like
Nkx	NK2 Homeobox
Notch	Neurogenic Locus Notch Homolog Protein
Nl	Nanoliter
NaCl	Sodium chloride
NaOH	Sodium hydroxide
Na_2HPO_4	Sodium hypophosphate
ODDD	Oculodentodigital dysplasia
P	Promoter
Pz	Proliferative zone
PCD	Programmed cell death
PCS	Premature centromere separation
PDS	Precocious Dissociation of Sisters

PFA	Paraformaldehyde
PBS	Phosphate base saline
PBST	Phosphate base saline with Tween 20
PCR	Polymerase Chain Reaction
qRT-PCR	Quantitative real-time PCR
RAD	Radiation-sensitive mutant
RBS	Roberts Syndrome
RNAPII	RNA Polymerase II
RT	Room temperature
RT-PCR	Reverse transcriptase PCR
RNA	Ribonucleic acid
rRNA	Ribosomal RNA
Rp	Reverse primer
runx	Runt-related transcription factor
S	Seconds
SCC	Sister Chromatid Cohesion
SA	Stromal antigen protein
Sema	Semaphoring
SEM	Standard error of mean
SETDB	SET domain bifurcated
SDS	Sodium dodecyl sulphate
Shh	Sonic hedgehog
SMC	Structural Maintenance Of Chromosomes
Sof	Short fin
Sox	SRY Box
Spry	Sprouty RTK signaling Antagonist
Std	Standard
Suv	Suppressor of variegation
Tbx	T Box transcription factor
TILLING	Targeted Induced Local Lesions in Genomics
TUNEL	Terminal deoxynucleotidyl transferase dUTP Nick-End Labeling
Tg+	Transgene positive
Tg-	Transgene negative
TdT	Terminal deoxynucleotidyl transferase
UTR	Untranslated region
UN	Uninjected
V	Volts
WT	Wild type

ABSTRACT

Roberts syndrome (RBS) is a human developmental disorder characterized by craniofacial abnormalities, limb malformation and often severe mental retardation. RBS arises from mutations in the cohesin auxiliary factor *ESCO2* that targets the SMC3 subunit of the cohesin complex. Mutations in cohesin subunits and a subset of cohesin auxiliary factors gives rise to a related developmental malady termed Cornelia de Lange Syndrome (CdLS). They are collectively termed cohesinopathies since both disorders comprise overlapping phenotypes and the causative genes for both syndromes perform common activities. The underlying cause of CdLS is largely modeled as occurring through transcriptional deregulation. Whereas, the mechanism that underlies RBS, remains unknown. A popular model states that RBS arises due to mitotic failure that leads to elevated levels of apoptosis. My thesis is based on developing a new vertebrate model system for examining RBS-like skeletal defects in order to better understand the mechanisms underlying the disease. Using the zebrafish regenerating fin model, I discovered a transcriptional role of *esco2* during fin regeneration. First, my results show that Esco2 contributes to skeletal growth and patterning independent of elevated levels of apoptosis – negating a model for mitotic failure. Second, I provide the first characterization of Esco2-dependent gene expression of a skeletal gene, *cx43*, which encodes the gap junction connexin subunit required for cell-cell communication and skeletal development in all vertebrates. Mutations in human *CX43* gives rise to a skeletal disorder, Oculodentodigital dysplasia (ODDD). My results conceptually link ODDD to cohesinopathies and provide evidence that ESCO2 may play a transcriptional role critical for human development. I next addressed the mechanism through which Esco2 regulates

cx43 expression, focusing on the Esco2 target Smc3. My results show that the Smc3

knockdown perturbs bone and tissue growth that recapitulates RBS-type phenotypes in

the regenerating fin model. Importantly, Smc3 regulates *cx43* expression, similar to that

of Esco2. Moreover, Chromatin Immunoprecipitation (ChIP) assays revealed that Smc3

binds to a discrete region of the *cx43* promoter, suggesting that Esco2 exerts

transcriptional regulation of *cx43* through modification of Smc3 bound to the *cx43*

promoter. These findings unify RBS and CdLS as transcription-based mechanisms.

CHAPTER 1

Introduction

1.1 The Cohesin ring complex and its auxiliary factors

The fundamental component of many cellular processes is the tethering together of two DNA segments, either in *cis* (intramolecular) or *trans* (intermolecular) conformations (Zakari et al., 2015; Skibbens, 2016). For instance, DNA segment *trans*-tethers between two separate DNA molecules, such as sister chromatids, identify the products of chromosome replication as sisters from S phase until anaphase onset. In addition to ensuring high fidelity chromosome segregation, *trans* tethers ensure proximity of template DNA required for error-free DNA repair events. On the other hand, *cis*-DNA tethering occur at the base of a single DNA molecule forming looped structures that brings into registration regulatory elements such as enhancers, promoters, insulators, terminators, etc. that deploy developmental transcription programs largely thought to occur during the G1 stage of the cell cycle. DNA segment *cis*-tethers also promote longitudinal compaction of DNA molecules that is required for regional changes in chromatin structure during G1 and genome-wide chromosome condensation during mitosis. Interestingly, a single complex that participates in various essential cellular activities via both *cis* and *trans*-DNA-tethering conformations is the multi-subunit cohesin complex and along with its auxiliary factors (Figure 1.1).

Cell division is a fundamental process by which cells replicate and generate identical daughter cells. The process of cells duplicating themselves starts with the S phase in which each parent cell replicates its chromosomes and ends with Mitosis in which sister chromatids segregate into newly formed daughter cells. For proper functioning of the cell cycle, it is essential for the sister chromatids to be tethered together until the chromosomes are ready to separate. This process is collectively termed

4

as cohesion and is maintained by the multi-protein cohesin complex along with numerous auxiliary factors (Skibbens, 2009).

Cohesin complexes are evolutionarily conserved from yeast to humans and are composed of five core subunits, SMC1A, SMC3, RAD21/MCD1/SCC1, SA1,2/STAG1,2/Irr1/Scc3 and PDS5 (Figure 1.1). SMC1A and SMC3 are elongated ATPase proteins that together form a ring, which is stabilized by RAD21/ MCD1/SCC1. RAD21 in turn recruits the remaining components (PDS5 and either SA1 or SA2) (Jeppssen 2014; Marston 2014; Skibbens 2016). The exact mechanism through which DNA becomes entrapped within this flattened cohesin ring remains enigmatic, but could involve one, or more than one, cohesin rings. Cohesins are incapable of binding DNA spontaneously. Instead, a series of auxiliary factors are required for cohesins to bind DNA prior to functioning in chromosome segregation, chromatin condensation, DNA repair, and transcriptional regulation. The NIPBL/SCC2 and MAU-2/SCC4 deposition heterocomplex is required to load cohesins onto DNA segments (Ciosk 2000; Seitan 2006; Rollins 1999; Rollins 2004). The rules governing cohesin deposition are poorly understood. Once chromatin-bound, however, cohesins must become activated (promoting cohesin oligomerization and/or stabilizing DNA entrapment). The N-acetyltransferase family of proteins, ESCO2/EFO2/ESCO1/EFO1/Ctf7/Eco1 supplies this role. The ESCO families of protein are highly conserved acetyltransferases that activates SMC3 through acetylation, which is required for all subsequent cohesin-dependent activities (Skibbens et al., 1999; Toth et al., 1999; Ivanov et al., 2002; Bellows et al., 2003; Hou and Zou, 2005; Rolef Ben-Shahar et al., 2008; Zhang et al., 2008). Cohesins must also be turned off, either to allow for sister chromatid separation at anaphase onset

or to respond to transcriptional responses to external cues through tether disassembly/reassembly. Cohesin inactivation at anaphase onset is irreversible and occurs through RAD21 degradation, although a non-proteolytic release mechanism can reduce cohesin binding during prophase (Funabiki 1996; Ciosk 1998; Uhlmann and Nasmyth 1999; Shintomi and Hirano, 2010). On the other hand, cohesin inactivation during G1 likely occurs through disassociation of cohesin dimers. In both cases, HDAC8/Hos1 deacetylase helps reset the acetylation state of SMC3 (Xiong et al., 2010; Borges et al., 2010; Beckouet et al., 2010; Deardorff et al., 2012a).

1.2 Cohesion-mediated *trans* and *cis*-DNA tethering functions

Historically, cohesins were identified for their role in the *trans*-DNA tethering mechanisms such as sister chromatid cohesion and segregation. But recently, numerous findings brought to light the *cis*-DNA tethering functions of cohesins (Figure 1.1). Cohesins function in stabilizing DNA loops by promoting or precluding registration of enhancers and promoters in close proximity. Other *cis*-DNA tethering roles of cohesins include condensation and ribosome biogenesis. Genome-wide studies report direct association of cohesin subunits and cohesin auxiliary factors with developmental genes. Thus one of the possible mechanisms that underlie the transcriptional regulation of cohesin is via long distance DNA looping. Additional studies from various groups show cohesin facilitates long distance DNA looping (Hadjur et al., 2009; Mishiro et al., 2009; Nativio et al., 2009; Hou et al., 2010). Interestingly, in mouse embryonic stem cells cohesin binding initiates enhancer-promoter interaction via DNA loops in transcriptionally active genes (Figure 1.2; Kagey et al., 2010). They provide *in vivo*

evidence of physical interaction and co-occupancy of the cohesin, mediator and NIBPL at the enhancer and core promoter regions of active genes. This group of researchers suggested that co-activator- bound mediator complex undergoes conformational changes and binds to the cohesin and NIBPL. This leads to the enhancer- promoter DNA loop formation and eventually overall gene activation. This study suggests the possibility that such long distance DNA looping may exist that affects the gene expression and thus results in various developmental disorders.

1.3 Cohesion pathway mutations leads to cohesinopathies

Skeletal defects, especially long bone growth and morphogenesis, are components of a number of multi-spectrum developmental abnormalities. These include Roberts syndrome (RBS), Cornelia de Lange Syndrome (CdLS) (Krantz et al., 2004; Tonkin et al., 2004; Schule et al., 2005; Vega et al., 2005; Musio et al., 2006; Deardorff et al., 2007; Gordillo et al., 2008; Deardorff et al., 2012a; Deardorff et al., 2012b). Genetic mapping studies revealed that mutations in the genes of the cohesion pathway give rise to these diseases and thus grouped them into a common disease category collectively termed cohesinopathies.

RBS is characterized by pre- and postnatal growth retardation affecting the limbs and craniofacial bone structures. Dr. John B. Roberts reported the earliest case back in 1919 and thus named in his honor. All four limbs are affected in RBS patients such that children are born with shortened arm and leg bones. Facial abnormalities are significant symptoms of RBS, which includes cleft lip, cleft palate, small chin and corneal clouding (Berg and Francke, 1993; Vega et al., 2005). Infants born with severe forms of RBS are

stillborn and the mortality rate is quite high (Schule et al., 2005). To date, roughly 150 cases of RBS have been reported.

CdLS is a similar disorder that exhibits significantly overlapping and severe phenotypes as RBS. Both RBS and CdLS patients, in addition to severe long-bone growth defects and missing digits, exhibit craniofacial abnormalities, cleft palate, syndactyly, organ defects and severe mental retardation (Van den Berg and Francke, 1993; Schule et al., 2005; Vega et al., 2005; Liu and Krantz, 2009; Mannini et al., 2010). Figure 1.3 depicts the phenotypes observed in RBS and CdLS patients.

1.4 Genetic basis of RBS and CdLS

RBS is an autosomal recessive disorder that arises from mutations in the acetyltransferase *ESCO2* (Vega et al., 2005; Schule et al., 2005; Gordillo et al., 2008). In 2005, the gene responsible for RBS was identified and characterized as *ESCO2* (Establishment of Cohesion 1 homolog 2). The 30.3kb coding sequence is divided into 11 exons, with the start and stop codon on exon 2 and exon 11 respectively (Figure 1.4). ESCO2 has a predicted size of 68.3 kDa and is evolutionarily conserved among vertebrate species (Vega et al., 2005). The C-terminal of *ESCO2* is similar to *Eco1/Ctf7* of yeast (Skibbens et al., 1999; Ivanov et al., 2002). ESCO2 C-terminal is evolutionary conserved and belongs to the Eco1p family of proteins. These proteins have N-acetytransferase activity and play an important role in the process of sister chromatid cohesion during the S phase of cell cycle. Table 1.1 lists the different names of the protein in various model organisms (Horsfield et al., 2012).

CdLS on the other hand is an autosomal dominant disorder that arises from heterozygous or X-linked mutations in the cohesion subunits *SMC1A*, *SMC3*, *RAD21*, as well as in the auxiliary factors *NIPBL* and *HDAC8* (Krantz et al., 2004; Tonkin et al., 2004; Musio et al., 2006; Deardorff et al., 2007; Deardorff et al., 2012a; Deardorff et al., 2012b). CdLS occurs approximately 1 in 10,000 live births (Opitz, 1985; Krantz et al., 2004), and around 65% of the reported cases arise from mutations in the *NIPBL* gene (Krantz et al., 2004; Tonkin et al., 2004; Zakari et al., 2015).

1.5 Mechanisms posited to produce RBS and CdLS

Intriguingly, the mechanisms through which mutations contribute to cohesinopathies are thought to vary widely. Cells isolated from RBS patients exhibit chromosomal segregation defects, premature centromere separation (PCS), heterochromatin repulsion (HR), lagging chromosomes, aneuploidy, elevated levels of apoptosis and reduced cell proliferation which is consistent with the role of Esco2 (Figure 1.5) (Schule et al., 2005; Vega et al., 2005; Gordillo et al., 2008; Mehta et al., 2013 and Horsfield et al., 2012). In contrast, cells from CdLS patients do not exhibit PCS/HR cellular morphology or mitotic defects (Krantz et al., 2004). Because of the distinct cellular phenotypes, defects in *trans*-DNA tethering events were initially believed to be the underlying cause of RBS. Whereas due to the lack of overt defects in *trans*-DNA tethering and early studies that linked Drosophila *Nipped B* (*NIPBL* homolog) to transcription regulation, the underlying cause of CdLS is largely modeled as occurring through defects in *cis* DNA-tethering (Figure 1.6). Analyses of various model systems reveal that multiple mechanisms within each syndrome may be at work (discussed in

review article, Banerji et al., 2017, in revision). Below, I discuss in detail the suggested mechanisms underlying both RBS and CdLS.

(1) Apoptosis is activated in both RBS and CdLS

Currently the mechanism of RBS pathogenesis is unclear. To date, *ESCO2* mutations are the only etiologic genetic agent known to produce RBS. The popular model of RBS suggests reduced progenitor cell proliferation and increased mitotic failure accompanied by apoptosis as the underlying mechanism (Monnich et al., 2011). Studies using *ESCO2* knockout mice report both cohesion defects and roughly two-fold increase in apoptotic cells, similar to RBS patient cells (Whelan et al., 2012; Gordillo et al., 2008, van der Lelij et al., 2009). Similar findings are observed in studies using both zebrafish and medaka embryos, establishing teleosts as a powerful model from which to study the molecular pathologies that underlie RBS (Monnich et al., 2011; Morita et al., 2012). In zebrafish, *esco2* morpholinos (MO) cause lethality by 72 hours post ferlilization (hpf), but reducing the dosage permits bone and cartilage development (Monnich et al., 2011). These *esco2* morphants exhibited craniofacial cartilage defects, under-developed jaws and shorter pectoral fins, characteristic of RBS phenotypes. They found RBS to arise through reduced progenitor cell proliferation and increased incidences of both mitotic failure and apoptosis.

Similar findings are observed in *esco2* mutants (Morita et al., 2012; Percival et al., 2015). By using Targeted Induced Local Lesions in Genomics (TILLING) approach one group found a missense mutation (R80S) that was responsible for the RBS-like phenotypes in the medaka (Morita et al., 2012). Interestingly, the phenotypes of the

homozygous *esco2*^{*R80S*} mutants are very similar to the *esco2* morphants. *esco2*^{*R80S*}

mutants have a variety of clinical phenotypes arising from a single mutation. Recently, a

study using zebrafish *esco2*^{*hi2865*} mutant (with a retroviral insertion in intron 1 of a gene

which has homology with *ESCO2* gene) reported the apoptotic response to be p53-

dependent, consistent with mitotic failure. However, a subset of mutant cells exhibits

normal mitoses, suggesting the potential for multiple mechanisms underlying RBS

phenotypes (Percival et al., 2015).

Apoptosis may be an under-appreciated phenotype of CdLS, since there are reports

that CdLS cells do not exhibit mitotic defects and apoptosis (Krantz et al., 2004). It is

important to point out that there are reports however, of mitotic defects occurring in

CdLS patient cell lines (Kaur et al., 2005). Moreover, there are reports of increased levels

of apoptosis in zebrafish morphants for the cohesin subunits (*smc3*, *smc1a*, *rad21a*,) and

the cohesin loading factor (*nipblb*) that give rise to CdLS in humans (Ghiselli, 2006;

Fazio et al., 2016, Schuster et al., 2015; Pistocchi et al., 2013). Knockdown of cohesin

subunits also exhibit p53-dependent apoptosis, consistent with cell death due to mitotic

failure (Ghiselli, 2006; Schuster et al., 2015).

(2) Transcriptional deregulation underlie both RBS and CdLS

There is strong evidence that suggests that CdLS arises from misregulation of

developmental genes (Bose et al., 2012; Dorsett, 2010; Dorsett and Merkenschlager,

2013). It is now well established that cohesins regulate transcriptional processes

involving transcription termination, enhancer-promoter registration, CTCF-insulator

recruitment and RNAPII transitioning (Dorsett and Krantz, 2009; Cucco and Musio,

2016; Dorsett and Merkenschlager, 2013). But the extent to which cohesin and its auxiliary factors function through a single common mechanism or through multiple mechanisms remains an important developmental issue.

One mechanism includes long- distance DNA looping which plays an important part in cohesin-mediated gene regulation (Ball et al., 2014; Kagey et al., 2010). Cohesin recruitment to these loops involves the CCCTC-binding factor (CTCF) insulator. CTCF binds to specific DNA motifs and in turn recruits cohesins to these specific loci (Wendt and Peters, 2009; Hadjur et al., 2009; Hou et al., 2010; Kagey et al., 2010; Ball et al., 2014; Parelho et al., 2008; Rubio et al., 2008). In fact, studies from numerous model systems suggest that CTCF both precludes enhancer-promoter interactions through DNA looping and recruits cohesins for loop stabilization (Wendt and Peters, 2009; Degner et al., 2011; Nativio et al., 2011; Majumder and Boss, 2011; Guo et al., 2012). In mammalian cells, there is more than 50% overlap between cohesin and CTCF binding sites (Wendt et al., 2008). In zebrafish, cohesin both positively (i.e. CTCF independent) and negatively (i.e. CTCF-dependent) regulates transcription factor *runx1* expression (Rhodes et al., 2010). Intriguingly, Drosophila CTCF and cohesin colocalization appears reduced (Misulovin et al., 2008; Pauli et al., 2008; Van Bortle et al., 2014). In combination these findings suggest that while defects in CTCF recruitment of cohesin may contribute to cohesinopathies, additional mechanisms must be at play (Mourad and Cuvier, 2016).

In addition to CTCF, the transcription co-activator Mediator is implicated in cohesin-dependent transcription. Mediator is a large complex that recruits RNAPII to the promoter (Kagey et al., 2010; Conaway et al., 2005; Kornberg, 2005; Taatjes, 2010;

Malik and Roeder, 2005; Roeder, 1998). Mutations in the Drosophila *NIPBL* ortholog, *Nipped-B,* are linked to long-distance enhancer-mediated transcriptional changes that occur during development (Rollins et al., 1999; Dorsett, 2016). Evidence from embryonic stem cells suggests that Mediator participates in this cohesin-dependent DNA looping (Kagey et al., 2010), consistent with similar findings regarding transcription factor *hoxd* in zebrafish *nipbla/b* morphants (Muto et al., 2014). Changes in nuclear architecture in both *nipbla/b* and *med12* single morphants, suggesting that expression of these genes is indeed mediated through chromatin looping (Muto et al., 2014).

New studies provide a growing body of evidence that RBS models, similar to CdLS, exhibit significant changes in gene expression (Banerji et al., 2016; Choi et al., 2010; Leem et al., 2011; 288 Monnich et al., 2011; Xu et al., 2013; Xu et al., 2016; Rahman et al., 2015). Support for a transcriptional role of ESCO2 comes from studies using human cell lines that ESCO2 represses *Notch* transcription to promote neuronal differentiation (Leem et al., 2011). Interestingly, the study using $esco2^{R80S}$ medaka mutants show evidence of Esco2 functioning during embryogenesis by upregulating certain genes in the Notch pathway (Morita et al., 2012). Additionally, there is evidence that ESCO factors act as transcription repressors by recruiting chromatin modifiers (Choi et al., 2010; Kim et al., 2008). Additional evidence comes from the comparison of gene expression profiles from cohesin subunit, *rad21* null mutants ($rad21^{nz171}$) and *esco2* morphants that show a number of overlapping genes with altered expression profiles (Rhodes et al., 2010; Monnich et al., 2011). Intriguingly, this common gene pool exhibited opposing directions in gene expression: genes upregulated in the $rad21^{nz171}$ mutant were downregulated in *esco2* morphant embryos, and vice versa. An explanation

for such opposing transcriptional effects is likely due to differences in the loss of structural components (cohesin) verses enzymatic activities (Esco2). For instance, cohesins may remain chromatin bound and/or CTCF associated in *esco*2 morphants. Alternatively, opposing transcriptional effects between $rad21^{nz171}$ mutants and *esco2* morphants may reflect direct verses indirect roles in transcription.

Based on the findings from various model systems, it is certain that the etiologies of RBS and CdLS (or in general all cohesinopathies) are not straightforward, but rather quite complex. Reports of transcriptional deregulation and apoptosis in both syndromes suggest that multiple mechanisms are at play. This unifying model may appear to be challenged by disparate findings regarding NIPBL, cohesin and CTCF residency on chromatin (Misulovin et al., 2008; Kagey et al., 2010; Muto et al., 2011; Zuin et al., 2014; Minamino et al., 2015; Rahman et al., 2015). It is tempting to speculate that disparities in cohesin recruitment to DNA, as well as identified binding partners, reflect unique cohesin complexes that occur in different tissues and mediate different functions (i.e. transcriptional repression vs. activation). Further efforts in testing a unifying transcriptional basis for all cohesinopathies include identifying the mechanisms through which cohesins are deposited on specific loci, elucidating how chromatin-associated cohesins mediate *trans* versus *cis* conformations, and assessing how those complexes impact gene expression profiles.

1.6 Using the zebrafish caudal fin to distinguish between different RBS models

The zebrafish regenerating fin is a powerful model system, which could provide valuable evidence to distinguish between different RBS models. For instance, the

zebrafish CNS, heart, gut, and cephalic structures appear exquisitely sensitive to cohesins and Nipbl levels (Muto et al., 2011; Pistocchi et al., 2013; Muto et al., 2014; Fazio et al 2016). Similar to humans, the zebrafish genome harbors orthologues of most cohesion genes (*nipbla* and *nipblb*, *esco1* and *esco2*, *smc1a* and *smc1al*, *smc3*, *rad21a* and *rad21b*, *stag1a/b* and *stag2a/b* and *stag3*; *pds5a* and *pds5b*). Gene function may be examined through generation of mutant alleles using genome editing (Hwang et al., 2013; Seruggia and Montoliu, 2014) or by the use of gene targeting MOs (Nasevicius and Ekker, 2000). Our lab uses the zebrafish caudal fin to study skeletal morphogenesis. Because of its simple structure, easy accessibility, rapid regeneration following amputation, limited cell type composition, and the ability to knock down gene expression through gene-specific MOs, this is emerging as an excellent model system to elucidate tissue and bone growth pathways (Iovine et al., 2005). Investigating how Esco2 levels are affected in the zebrafish skeleton will provide new insights into the cohesinopathy field.

1.7 The fascinating process of zebrafish epimorphic fin regeneration

The caudal fin is composed of 16 to 18 segmented bony fin rays or lepidotrichia with new growth occurring by the distal addition of bony segments and associated fin ray joints (Figure 1.7) (Haas, 1962; Goss et al., 1957). Each bony fin ray is made up of two concave hemirays that surrounds mesenchymal cells (Santamaria et al., 1992). These hemirays are lined by osteoblasts that secrete the bone matrix and primarily enclose the mesenchymal compartment, which consists of mesenchymal cells, blood vessels, nerves, melanocytes and fibroblasts. A layer of epithelial cells covers the entire fin and ontogenic

15

fin growth occurs by successive addition of bony segments to the distal tip of the fin (Haas, 1962).

Zebrafish are capable of impressive epimorphic regeneration in a variety of tissues such as caudal fin, skin, retina and heart. The process can be defined as a post-traumatic morphogenetic event where a specialized compartment of highly proliferating cells (blastemal) are formed at the wound site by the aggregation of mesenchymal cells (Akimenko et al., 2003; Schebesta et al., 2006). Regeneration of the adult caudal fin is a fascinating process by which the lost tissue is restored in approximately 2 weeks following amputation (Figure 1.8). The 3 phases of the regeneration process consists of wound healing, blastema formation and regenerative outgrowth (Nechiporuk and Keating, 2002). The process of regeneration starts 12-24 hours post amputation (hpa) by wound healing by sealing the wound with migrating epithelial cells. After 12 hours there is thickening of the epidermis and the disorganized cells migrate towards the amputation plane to the blastema. It is important that a multilayered epidermis is formed during blastema formation and proliferation (Lee et al, 2009). The blastema consists of highly proliferative and undifferentiated cells that express different molecular markers such as *msxb* and *msxe* that label undifferentiated cells (Barker and Beck, 2009; Han et al., 2003). During the final regenerative outgrowth phase after 48-72 hpa, the blastema compartmentalizes into proximal and distal zones. After 72 hpa and later, outgrowth process takes place where cells migrate in both proximal and lateral directions (Nechiporuk and Keating, 2002).

1.8 CX43 is important for growth and development of vertebrate skeleton

Our lab uses the zebrafish regenerating fin as a tool to understand the molecular mechanisms regulating skeletal morphogenesis in vertebrates. Previously, our lab has established that homozygous mutations in a gap junction gene, *connexin43* (*cx43*) cause the short fin (*sof*^{b123}) phenotype. The *sof*^{b123} mutant is characterized by short bony fin ray segments, short fins, and reduced cell proliferation (Figure 1.9; Iovine et al., 2005 and Hoptak-Solga et al., 2008). Importantly, MO-mediated Cx43 knockdown in wild type regenerating fins also result in reduction in fin length, segment length and cell proliferation, recapitulating the phenotypes observed in *sof*^{b123} mutants (Hoptak-Solga et al., 2008).

Gap junctions are intracellular channels that are formed by the docking of two connexons of neighboring cells and freely permit direct exchange of small ions, second messengers and low molecular weight metabolites (<1000Da) (Figure 1.10). The connexons or hemichannels are made up of six four-pass transmembrane spanning proteins called connexins. Gap junctions play a vital role in developmental processes, tissue function, homeostasis maintenance, morphogenesis, cell differentiation, and growth control in multicellular organisms and during the process of skeletogenesis (Oyamada et al., 2005). In order to understand the role of Cx43 during skeletal development I utilize a zebrafish short fin mutant (*sof*^{b123}).

Cx43 exhibits conserved functions in the vertebrate skeleton. Mutations in *CX43* cause skeletal defects in human, mouse, chick and zebrafish. For example, pleiotropic developmental disorder, Occulodentodigital dysplasia (ODDD, Paznekas et al, 2003, Figure 1.11) is associated with missense mutations in human *CX43* gene. ODDD patients

17

exhibit skeletal and craniofacial abnormalities along with additional pleiotropic phenotypes such as eye and dental deformities. Also, a dominant mouse mutation in *CX43* exhibits various skeletal and pleiotropic phenotypes similar to human ODDD (Flenniken et al., 2005). Additional studies show that targeted gene knockdown of CX43 in adult chicks and in chick embryos results in facial abnormalities (Makarenkova and Patel, 1999) and limb malformation (McGonnell et al., 2001). Thus, the regenerating fin provides clinically relevant insights into highly conserved pathways critical for human skeletal development.

1.9 Hypothesis and Research objective

RBS and CdLS are pleiotropic developmental disorders exhibiting severe growth retardation resulting in limbs and craniofacial abnormalities. They are collectively termed cohesinopathies since both disorders comprise overlapping phenotypes and the causative genes for both syndromes perform common activities. It is therefore surprising that CdLS and RBS are considered separate syndromes. A consensus regarding underlying molecular mechanisms obtained from various model systems remains elusive. Due to distinct cellular morphology exhibited by RBS and CdLS patient cells, at present the molecular mechanisms through which cells and developing organisms respond to cohesion still remain unclear (Mehta et al., 2013; Horsfield et al., 2012; Dorsett and Merkenschlager, 2013). But certainly, the etiology of these disorders is much more complex, and does not fall into the categories typically defined by the different syndrome names. Analyses of various model systems reveal that multiple mechanisms within each syndrome may be at work. It is now well established that cohesins play a direct role in

gene expression and the developmental defects in CdLS patients arise due to transcriptional deregulation. But the role of apoptosis in CdLS cannot be completely ruled out. For instance, there are reports of cohesion defects and elevated levels of apoptosis in CdLS patient cells and zebrafish morphants (Kaur et al., 2005; Ghiselli et al., 2006; Fazio et al., 2016; Schuster et al., 2015). Currently, the role of apoptosis in CdLS is either underappreciated or not tested. On the other hand, mitotic failure and elevated levels of apoptosis is currently the popular model underlying RBS. Similar to cohesins, role of Esco2 has been reported in various *cis*-DNA tethering processes such as ribosome maturation and assembly, DNA repair and transcriptional regulation (Skibbens et al., 1999; Skibbens et al., 2010; Gard et al., 2009; Bose et al., 2012; Terret et al., 2009; Unal et al., 2004; Zakari et al., 2015; Leem et al., 2011). The growing bodies of evidence suggest a transcriptional mechanism underlying RBS, similar to CdLS. Considering the complexity in the mechanisms underlying these disorders, it is important to investigate the role of apoptosis and transcriptional deregulation underlying both diseases.

My research objective is to understand if CdLS and RBS occur as a result from a similar mechanism. Particularly I am interested to test the transcriptional mechanism underlying RBS using the zebrafish regenerating fin. Prior work on the regenerating fin revealed that Cx43 is required for both cell proliferation and joint formation during fin regeneration (Iovine et al., 2005). Since human *CX43* mutations cause a pleiotropic skeletal disorder Oculodentodigital dysplasia (ODDD) that overlap with those of both RBS and CdLS (Paznekas et al., 2003), I posit that ODDD is linked to cohesinopathies and that transcriptional deregulation of developmental genes such as *CX43* may contribute to RBS phenotypes. My findings (discussed in the next chapters) suggest that

Esco2 and the cohesin subunit Smc3 function together to regulate *cx43* expression during skeletal development. My work sheds light on a unified underlying mechanism of RBS and CdLS and in general all cohesinopathies.

1.10 Figures and Tables
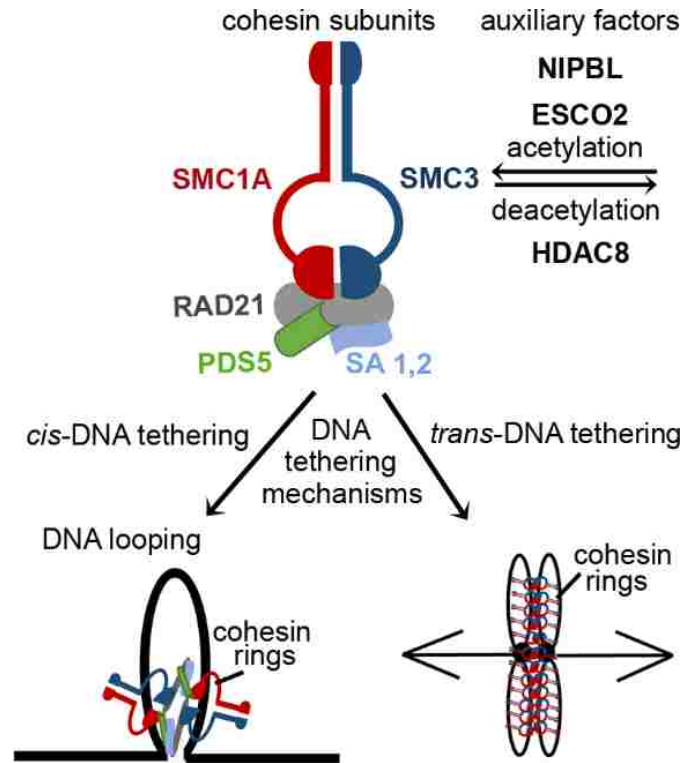
Figure 1.1: DNA tethering mechanisms of cohesins and auxiliary factors.
Schematic representation of the cohesin ring structure (composed of the 5 subunits; SMC1A, SMC3, RAD21, SA1,2 and PDS5) and auxiliary factors, NIPBL (loader), ESCO2 (acetyltransferase) and HDAC8 (deacetylase). Cohesins and auxiliary factors regulate both *cis* and *trans*-DNA tethering events. *Cis*-DNA tethering processes include DNA looping mechanisms during transcription, condensation and ribosome biogenesis. *Trans*-DNA tethering processes include sister chromatid segregation during S phase of cell cycle and DNA repair events

Source: Review article, Banerji et al., 2017 (in press, Developmental Dynamics)
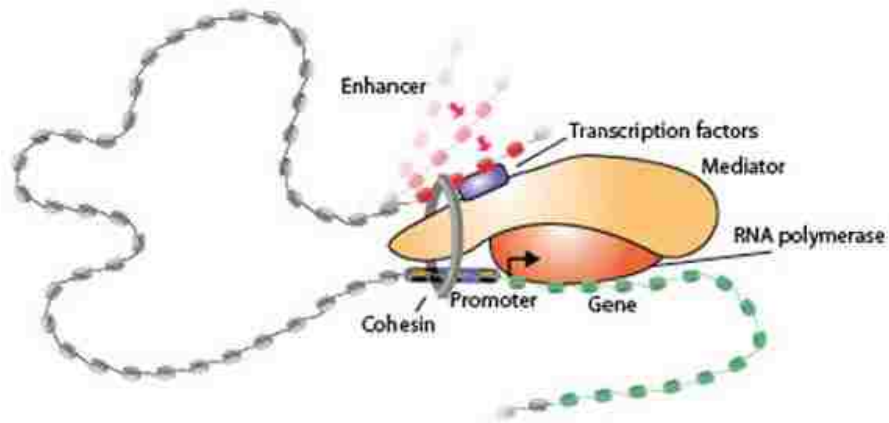
Figure 1.2: Transcription-based DNA looping model. A model depicting the physical association of the mediator and cohesin complex, functionally connecting enhancers and core promoter of actively transcribing genes in murine embryonic stem cells. The formation of DNA loops between enhancer-bound transcription factors and the transcription apparatus at the core promoter resulting in gene activation. Nipbl, the cohesin-loader is associates with mediator-cohesin complexes, providing a mean to load cohesin at promoters (Kagey et al., 2010).

Source: Surprise in genome structure linked to developmental diseases, Image: Tom DiCesare/Whitehead Institute (2010)

Figure 1.3: Multifaceted developmental disorders: RBS and CdLS. Characteristic features of RBS patients shown in left panel. Patients are characterized by skeletal deformities in limbs, missing digits, small head, cleft lip and palate. RBS limb reduction is mesomelic and symmetric in which the arms are more severely affected than the legs. Characteristic features of CdLS patients are shown in right panel. Patients are characterized by craniofacial abnormalities, organ defects and limb deformities. Variability of upper limb abnormalities and with missing and fused digits are commonly seen in CdLS patients.

Source: Photographs of RBS patients (left, Vega et al., 2005) and CdLS patients (right, Krantz et al., 2004)
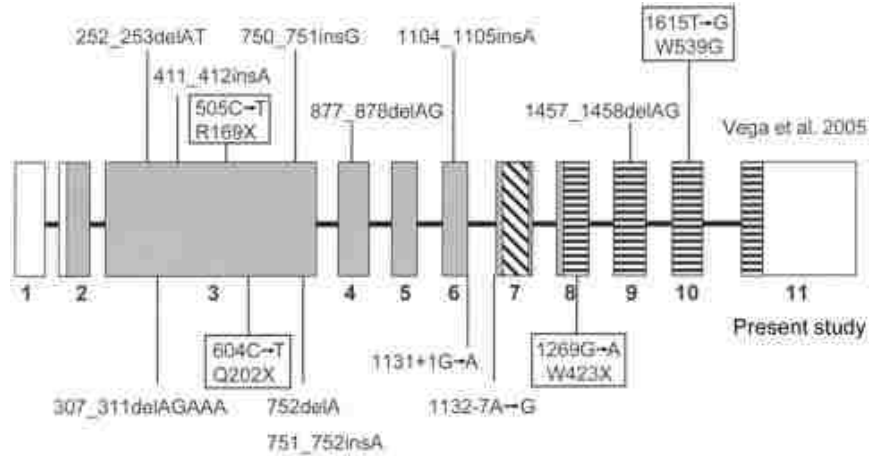
Figure 1.4: *ESCO2* gene structure with location of identified mutations. Eight mutations identified in 15 families with RBS reported by Vega et al., 2005 (shown at the top). Seven mutations found in 5 families with RBS reported by Schule et al., 2005 (shown at the bottom). White boxes -UTR, gray boxes - coding regions of exons 2–11. Location of the functional domains—the C2H2 zinc finger-like domain (diagonal stripes) and the acetyltransferase domain (horizontal stripes) are shown.

Source: Schule et al., 2005.

Figure 1.5: Cellular morphology of RBS patient cells. The RBS patient cells exhibit characteristic railroad-track morphology (indicated with arrows), which is indicative of premature centromere separation (PCS) and heterochromatin repulsion. The arrowhead indicates the Y chromosome splitting in the heterochromatin region. Normal chromosomes are shown with open arrows.

Source: Vega et al., 2005
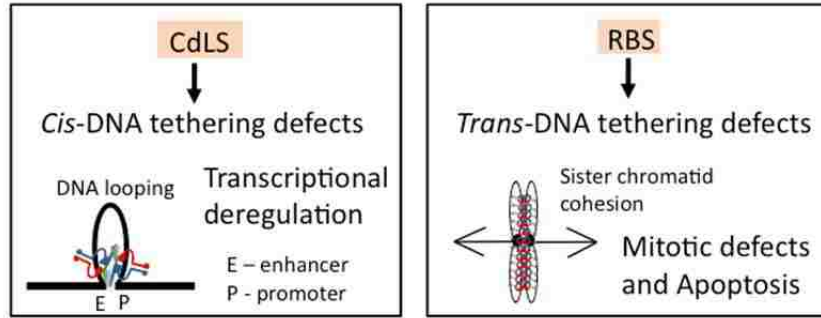
Figure 1.6: Suggested models of cohesinopathies. Currently the suggested models of CdLS and RBS are distinct. CdLS arises due to *cis*-DNA tethering defects resulting in transcriptional deregulation. In contrast, RBS arises due to defects in *trans*-DNA tethering resulting in mitotic defects and elevated levels of apoptosis.
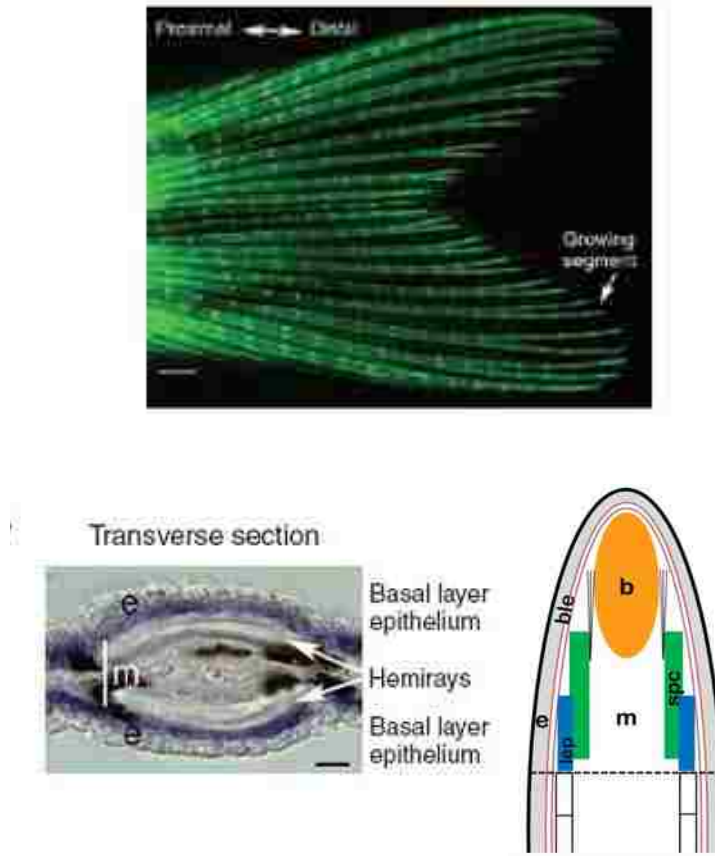
Figure 1.7: The zebrafish regenerating caudal fin is a model system for skeletal morphogenesis. (Top) A caudal fin is stained with calcein that detects bone matrix, revealing 16-17 bony fin rays comprised of bony segments separated by joints. (Bottom left) Representative image of a transverse section through a single fin ray is shown. White arrows indicate hemirays that are visible as crescents of bone surrounding mesenchymal tissue (m). The bony rays are surrounded by the epithelium (e) and basal layer of epithelium is the region with purple stain. (Bottom right) Schematic of a longitudinal section of the fin showing the different compartments as follows: Blastema (b), mesenchyma (m), epidermis (e), skeletal precursor cells (spc) and lepidotrichia (lep). The amputation plane is indicated by a black dotted line.

Source: Iovine, 2007 (Top and bottom left panels); Govindan et al., 2016.
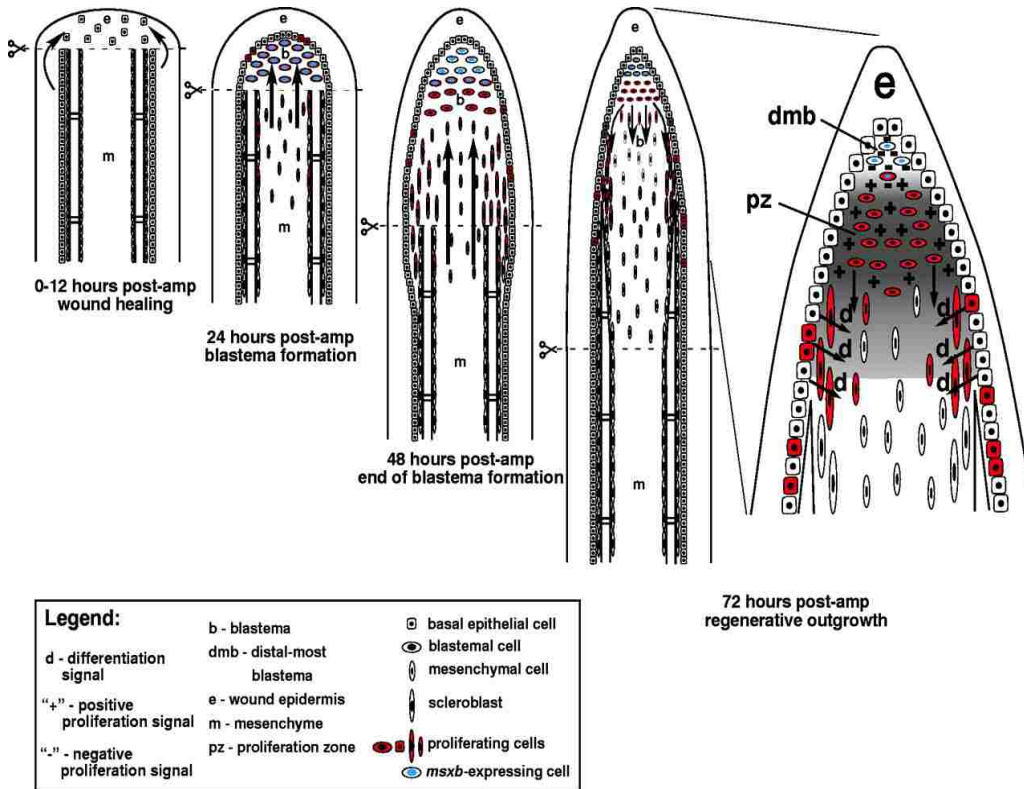
Figure 1.8: Stages of Fin regeneration. The three stages of epimorphic regeneration consist of (1) wound healing, (2) blastema formation and (3) the regenerative outgrowth phase. During wound healing, epithelial cells migrate distally to cover the wound by forming an apical epithelial cap. The blastema is a specialized compartment of the regenerating fin, consisting of highly proliferative cells. Cells in the blastema are divided into two subsets: distal most blastema cells and cells that is highly proliferative. During the final regenerative outgrowth phase, the gradient of *msxb* expression and proliferation is maintained, controlling the direction of outgrowth. Cells in the proliferative zone (pz) move in the proximal direction to differentiate. A zone of negative proliferation in the distal most blastema (dmb) maintains the directionality of the outgrowth by inhibiting proliferation.

Source: Nechiporuk and Keating, 2002.
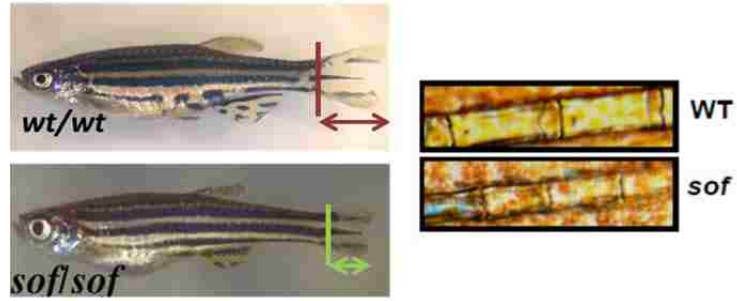
Figure 1.9: Fin length mutant (*sof* [b123]) exhibits defects in skeletal morphogenesis. (Top) Regenerate length (red arrows) and segment length indicated in wild-type zebrafish. (Bottom) *sof* [b123] mutant zebrafish exhibits shorter regenerate length (green arrows) and shorter segment length (Iovine et al., 2005).
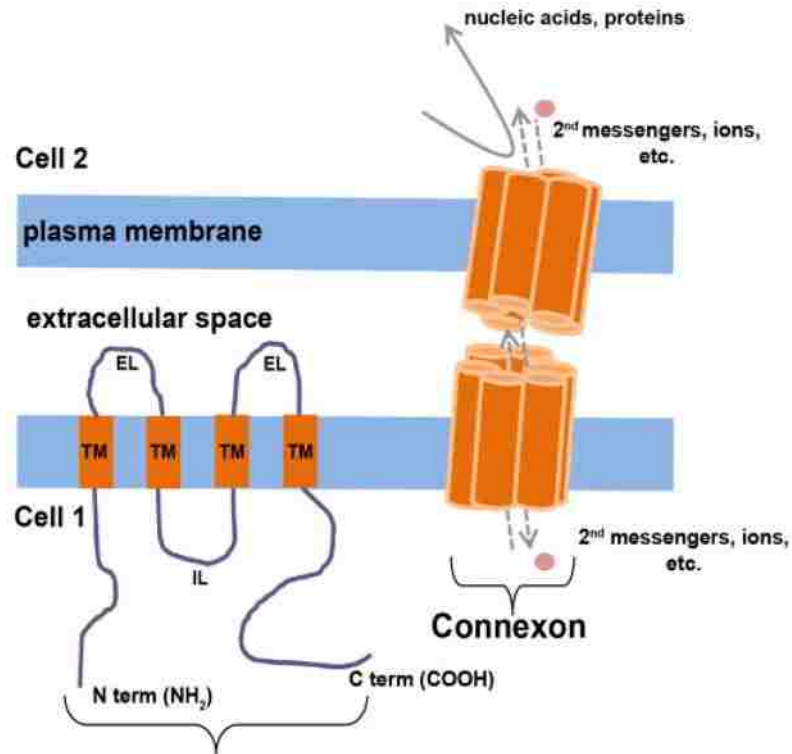
Figure 1.10: Gap junction channels function in direct cell-to-cell communications. Schematic representation of a single gap juction channel (connexin) containing four transmembrane-spanning domains, with both the amino and carboxy ends located in the cytoplasm. Six connexins comprise a connexon, or hemichannel. Two such connexons, from two neighbouring cells, dock together at the plasma membrane to make a functional gap junction channel. IL, intracellular loop; EL, extracellular loop.

Source: Ton and Iovine, 2013
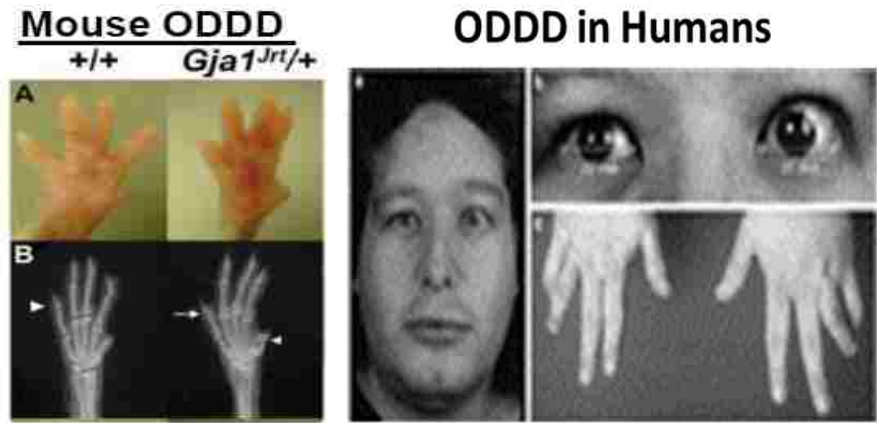
Figure 1.11: Cx43 is clinically relevant in vertebrates. (Left) Skeletal defects in the mouse model of Oculodentodigital Dysplasia (ODDD) are shown. (Right) ODDD phenotypes in humans are shown. These include craniofacial abnormalities, missing digits and problems in eye and teeth.

Source: (Left) Flenniken et al., 2005; (Right) Musa et al., 2009

Chromosome cohesion regulator	S. cerevisiae	S. pombe	D. melanogaster	X. laevis	D. rerio	H. sapiens	Function
SMC subunits	Smc1	Psm1	SMC1	smc1a[1]	Smc1al, Smc1a[2]	SMC1A	Core cohesin subunit
				smc1b[1]	Smc1b	SMC1B	Cohesin subunit (meiosis)
	Smc3	Psm3	Cap/SMC3	smc3/cspg6[1]	Smc3	SMC3/CSPG6/Bamacan	Core cohesin subunit
α-Kleisin subunit	Mcd1/Scc1	Rad21	Vtd/Rad21	rad21/mcd1/nxp1/scc1[1]	Rad21a, Rad21b[2]	RAD21	Core cohesin subunit
	Rec8	Rec8	C(2)M	rec8	Rec8/zgc:136888[1,3]	REC8	Cohesin subunit (meiosis)
	–	–	–		Rad21l1	RAD21L1/RAD21L	
Stromalin/SA subunit		Psc3	SA (stromalin)	stag1/sa1	Stag1[1,3]	STAG1/SA1/SCC3A	Cohesin subunit
			SA2 (stromalin-2)	stag2/sa2[1]	Stag2[1,3]	STAG2/SA2/SCC3B	
–		Rec11	–	stag3/sa3[1]	Stag3l3[1]	STAG3/SA3	Cohesin subunit (meiosis)
Interactors of α-kleisin and SA	Pds5	Pds5	Pds5	pds5a	Pds5a/zgc:66331	PDS5A	Balancing cohesion establishment with cohesin dissociation
				pds5b/as3/aprin[1]	Pds5b[1]	PDS5B/APRIN/AS3	
	?	?	Dmt (Dalmatian)	cdca5/sororin[1]	Cdca5	CDCA5/SORORIN	
	Rad61/Wpl1	Wapl	Wapl	wapal	Wapl/KIAA0261[1,3]	WAPAL/WAPL	
Kollerin	Scc2	Mis4	Nipped-B	nipbl/scc2/delangin	Nipbla/Scc2a, Nipblb/Scc2b	NIPBL/SCC2/DELANGIN	Cohesin loading
	Scc4	Ssl3		mau2/scc4[1]	Mau2/zgc:112338[1]	MAU2/SCC4	
Cohesin acetyl transferase (CoAT)	Eco1/Ctf7	Eso1	Eco/Deco San	esco1	Esco1[1]	ESCO1	Establishment of cohesion
				esco2/rbs/efo2[1]	Esco2	ESCO2	
Cohesin deacetylase (CoDAC)	Hos1	?	?	hdac8	Hdac8	HDAC8	Recycling of cohesin

[1] Predicted/in silico annotated only.

[2] No functional data available.

[3] Duplicated (EnsemblZv9, release 68).

?, protein not yet identified.

Table 1.1: Nomenclature and function of cohesin subunits and its auxiliary factors in various model systems.

Source: Horsfield et al., 2012

1.11 References

Akimenko, M. A., Marí-Beffa, M., Becerra, J., & Géraudie, J. 2003. Old questions, new tools, and some answers to the mystery of fin regeneration. *Developmental dynamics*, 226(2), 190-201.

Ball, A. R., Jr., Chen, Y. Y. & Yokomori, K. 2014. Mechanisms of cohesin-mediated gene regulation and lessons learned from cohesinopathies. *Biochim Biophys Acta,* 1839, 191-202.

Banerji, R., Eble, D.M., Iovine, M.K. and Skibbens, R.V., 2016. Esco2 regulates cx43 expression during skeletal regeneration in the zebrafish fin. *Developmental Dynamics*, 245(1), pp.7-21.

Banerji, R., Iovine, M.K. and Skibbens, R.V., 2016. How many roads lead to cohesinopathies? *Developmental Dynamics*, (In press).

Barker, D. M., & Beck, C. W. 2009. Overexpression of the transcription factor Msx1 is insufficient to drive complete regeneration of refractory stage Xenopus laevis hindlimbs. *Developmental Dynamics*, 238(6), 1366-1378.

Beckouet, F., Hu, B., Roig, M. B., Sutani, T., Komata, M., Uluocak, P., Katis, V. L., Shirahige, K. & Nasmyth, K. 2010. An Smc3 acetylation cycle is essential for establishment of sister chromatid cohesion. *Mol Cell,* 39, 689-99.

Berg, D. J., & Francke, U. (1993). Roberts syndrome: a review of 100 cases and a new rating system for severity. *American journal of medical genetics*, *47*(7), 1104-1123.

Bellows, A. M., Kenna, M. A., Cassimeris, L. & Skibbens, R. V. 2003. Human EFO1p exhibits acetyltransferase activity and is a unique combination of linker histone and Ctf7p/Eco1p chromatid cohesion establishment domains. *Nucleic Acids Res,* 31, 6334-43.

Borges, V., Lehane, C., Lopez-Serra, L., Flynn, H., Skehel, M., Rolef Ben-Shahar, T. & Uhlmann, F. 2010. Hos1 deacetylates Smc3 to close the cohesin acetylation cycle. *Mol Cell,* 39, 677-88.

Bose T, Lee KK, Lu S, Xu B, Harris B, et al. 2012. Cohesin proteins promote ribosomal RNA production and protein translation in yeast and human cells. *PLoS Genet* 8(6): e1002749.

Choi, H. K., Kim, B. J., Seo, J. H., Kang, J. S., Cho, H. & Kim, S. T. 2010. Cohesion establishment factor, Eco1 represses transcription via association with histone demethylase, LSD1. *Biochem Biophys Res Commun,* 394, 1063-8.

Ciosk, R., Shirayama, M., Shevchenko, A., Tanaka, T., Toth, A., Shevchenko, A. & Nasmyth, K. 2000. Cohesin's binding to chromosomes depends on a separate complex consisting of Scc2 and Scc4 proteins. *Mol Cell,* 5, 243-54.

Ciosk, R., Zachariae, W., Michaelis, C., Shevchenko, A., Mann, M. & Nasmyth, K. 1998. An ESP1/PDS1 complex regulates loss of sister chromatid cohesion at the metaphase to anaphase transition in yeast. *Cell,* 93, 1067-76.

Conaway, R. C., Sato, S., Tomomori-Sato, C., Yao, T. & Conaway, J. W. 2005. The mammalian Mediator complex and its role in transcriptional regulation. *Trends Biochem Sci,* 30, 250-5.

Cucco, F. and Musio, A., 2016, June. Genome stability: What we have learned from cohesinopathies. *American Journal of Medical Genetics Part C: Seminars in Medical Genetics* Vol. 172, No. 2, pp. 171-178.

Deardorff, M. A., Bando, M., Nakato, R., Watrin, E., Itoh, T., Minamino, M., Saitoh, K., Komata, M., Katou, Y., Clark, D., et al. 2012a. HDAC8 mutations in Cornelia de Lange syndrome affect the cohesin acetylation cycle. *Nature,* 489, 313-7.

Deardorff, M. A., Kaur, M., Yaeger, D., Rampuria, A., Korolev, S., Pie, J., Gil-Rodriguez, C., Arnedo, M., Loeys, B., Kline, A. D., et al. 2007. Mutations in cohesin complex members SMC3 and SMC1A cause a mild variant of cornelia de Lange syndrome with predominant mental retardation. *Am J Hum Genet,* 80, 485-94.

Deardorff, M. A., Wilde, J. J., Albrecht, M., Dickinson, E., Tennstedt, S., Braunholz, D., Monnich, M., Yan, Y., Xu, W., Gil-Rodriguez, M. C., et al. 2012b. RAD21 mutations cause a human cohesinopathy. *Am J Hum Genet,* 90, 1014-27.

Degner, S. C., Verma-Gaur, J., Wong, T. P., Bossen, C., Iverson, G. M., Torkamani, A., Vettermann, C., Lin, Y. C., Ju, Z., Schulz, D., et al. 2011. CCCTC-binding factor (CTCF) and cohesin influence the genomic architecture of the Igh locus and antisense transcription in pro-B cells. *Proc Natl Acad Sci U S A,* 108, 9566-71.

Dorsett, D. 2016. The Drosophila melanogaster model for Cornelia de Lange syndrome: Implications for etiology and therapeutics. *Am J Med Genet C Semin Med Genet,* 172, 129-37.

Dorsett, D. 2010. Gene regulation: the cohesin ring connects developmental highways. *Current Biology*, 20(20), R886-R888.

Dorsett D, Merkenschlager M. (2013) Cohesin at active genes: A unifying theme for cohesin and gene expression from model organisms to humans. *Curr Opin Cell Biol* 25(3): 327-333.

Dorsett, D. and Krantz, I.D., 2009. On the molecular etiology of Cornelia de Lange syndrome. *Annals of the New York Academy of Sciences*, 1151(1), pp.22-37.

Fazio, G., Gaston-Massuet, C., Bettini, L. R., Graziola, F., Scagliotti, V., Cereda, A., Ferrari, L., Mazzola, M., Cazzaniga, G., Giordano, A., et al. 2016. CyclinD1 Down-Regulation and Increased Apoptosis Are Common Features of Cohesinopathies. *J Cell Physiol,* 231, 613-22.

Flenniken, A. M., Osborne, L. R., Anderson, N., Ciliberti, N., Fleming, C., Gittens, J. E., & Rossant, J. 2005. A Gja1 missense mutation in a mouse model of oculodentodigital dysplasia. *Development*, 132(19), 4375-4386.

Funabiki, H., Yamano, H., Kumada, K., Nagao, K., Hunt, T. & Yanagida, M. 1996. Cut2 proteolysis required for sister-chromatid seperation in fission yeast. *Nature,* 381, 438-41.

Gard S, Light W, Xiong B, Bose T, McNairn AJ, et al. 2009. Cohesinopathy mutations disrupt the subnuclear organization of chromatin. J Cell Biol 187(4): 455-462.

Ghiselli, G. 2006. SMC3 knockdown triggers genomic instability and p53-dependent apoptosis in human and zebrafish cells. *Mol Cancer,* 5, 52.

Gordillo, M., Vega, H., Trainer, A. H., Hou, F., Sakai, N., Luque, R., Kayserili, H., Basaran, S., Skovby, F., Hennekam, R. C., et al. 2008. The molecular mechanism underlying Roberts syndrome involves loss of ESCO2 acetyltransferase activity. *Hum Mol Genet,* 17, 2172-80.

Goss RJ, Stagg MW. 1957. The regeneration of fins and fin rays in *fundulus heteroclitus*. J Exp Zool 136(3): 487-507.

Govindan, J., Tun, K.M. and Iovine, M.K., 2016. Cx43-Dependent Skeletal Phenotypes Are Mediated by Interactions between the Hapln1a-ECM and Sema3d during Fin Regeneration. *PloS one*, 11(2), p.e0148202.

Guo, Y., Monahan, K., Wu, H., Gertz, J., Varley, K.E., Li, W., Myers, R.M., Maniatis, T. and Wu, Q., 2012. CTCF/cohesin-mediated DNA looping is required for protocadherin α promoter choice. *Proceedings of the National Academy of Sciences*, 109(51), pp.21081-21086.

Hadjur, S., Williams, L. M., Ryan, N. K., Cobb, B. S., Sexton, T., Fraser, P., Fisher, A. G. & Merkenschlager, M. 2009. Cohesins form chromosomal cis-interactions at the developmentally regulated IFNG locus. *Nature,* 460, 410-3.

Han, M., Yang, X., Farrington, J. E., & Muneoka, K. 2003. Digit regeneration is regulated by Msx1 and BMP4 in fetal mice. *Development*, *130*(21), 5123-5132.

Haas HJ. 1962. Studies on mechanisms of joint and bone formation in the skeleton rays of fish fins. *Dev Biol* 5: 1-34.

Heidinger-Pauli, J. M., Mert, O., Davenport, C., Guacci, V. & Koshland, D. 2010. Systematic reduction of cohesin differentially affects chromosome segregation, condensation, and DNA repair. *Curr Biol,* 20, 957-63.

Hoptak-Solga, A. D., Nielsen, S., Jain, I., Thummel, R., Hyde, D. R. & Iovine, M. K. 2008. Connexin43 (GJA1) is required in the population of dividing cells during fin regeneration. *Dev Biol,* 317, 541-8.

Horsfield, J. A., Print, C. G. & Monnich, M. 2012. Diverse developmental disorders from the one ring: distinct molecular pathways underlie the cohesinopathies. *Front Genet,* 3, 171.

Hou, C., Dale, R. & Dean, A. 2010. Cell type specificity of chromatin organization mediated by CTCF and cohesin. *Proc Natl Acad Sci U S A,* 107, 3651-6.

Hou, F. & Zou, H. 2005. Two human orthologues of Eco1/Ctf7 acetyltransferases are both required for proper sister-chromatid cohesion. *Mol Biol Cell,* 16, 3908-18.

Hwang, W. Y., Fu, Y., Reyon, D., Maeder, M. L., Tsai, S. Q., Sander, J. D., Peterson, R. T., Yeh, J. R. & Joung, J. K. 2013. Efficient genome editing in zebrafish using a CRISPR-Cas system. *Nat Biotechnol,* 31, 227-9.

Iovine, M. K. 2007. Conserved mechanisms regulate outgrowth in zebrafish fins. *Nature chemical biology*, 3(10), 613-618.

Iovine, M. K., Higgins, E. P., Hindes, A., Coblitz, B. & Johnson, S. L. 2005. Mutations in connexin43 (GJA1) perturb bone growth in zebrafish fins. *Dev Biol,* 278, 208-19.

Ivanov, D., Schleiffer, A., Eisenhaber, F., Mechtler, K., Haering, C.H. and Nasmyth, K., 2002. Eco1 is a novel acetyltransferase that can acetylate proteins involved in cohesion. *Current biology*, 12(4), pp.323-328.

Jeppsson, K., Kanno, T., Shirahige, K. & Sjogren, C. 2014. The maintenance of chromosome structure: positioning and functioning of SMC complexes. *Nat Rev Mol Cell Biol,* 15, 601-14.

Kagey, M. H., Newman, J. J., Bilodeau, S., Zhan, Y., Orlando, D. A., van Berkum, N. L., Ebmeier, C. C., Goossens, J., Rahl, P. B., Levine, S. S., et al. 2010. Mediator and cohesin connect gene expression and chromatin architecture. *Nature,* 467, 430-5.

Kaur, M., DeScipio, C., McCallum, J., Yaeger, D., Devoto, M., Jackson, L. G., Spinner, N. B. & Krantz, I. D. 2005. Precocious sister chromatid separation (PSCS) in Cornelia de Lange syndrome. *Am J Med Genet A,* 138, 27-31.

Kim, B. J., Kang, K. M., Jung, S. Y., Choi, H. K., Seo, J. H., Chae, J. H., Cho, E. J., Youn, H. D., Qin, J. & Kim, S. T. 2008. Esco2 is a novel corepressor that associates with various chromatin modifying enzymes. *Biochem Biophys Res Commun,* 372, 298-304.

Kornberg, R. D. 2005. Mediator and the mechanism of transcriptional activation. *Trends Biochem Sci,* 30, 235-9.

Krantz, I. D., McCallum, J., DeScipio, C., Kaur, M., Gillis, L. A., Yaeger, D., Jukofsky, L., Wasserman, N., Bottani, A., Morris, C. A., et al. 2004. Cornelia de Lange syndrome is caused by mutations in NIPBL, the human homolog of Drosophila melanogaster Nipped-B. *Nat Genet,* 36, 631-5.

Lee, Y., Hami, D., De Val, S., Kagermeier-Schenk, B., Wills, A.A., Black, B.L., Weidinger, G. and Poss, K.D., 2009. Maintenance of blastemal proliferation by functionally diverse epidermis in regenerating zebrafish fins. *Developmental biology*, 331(2), pp.270-280.

Leem, Y. E., Choi, H. K., Jung, S. Y., Kim, B. J., Lee, K. Y., Yoon, K., Qin, J., Kang, J. S. & Kim, S. T. 2011. Esco2 promotes neuronal differentiation by repressing Notch signaling. *Cell Signal,* 23, 1876-84.

Liu, J. & Krantz, I. D. 2009. Cornelia de Lange syndrome, cohesin, and beyond. *Clin Genet,* 76, 303-14.

Majumder, P. & Boss, J. M. 2011. Cohesin regulates MHC class II genes through interactions with MHC class II insulators. *J Immunol,* 187, 4236-44.

Makarenkova, H., & Patel, K. 1999. Gap junction signalling mediated through connexin-43 is required for chick limb development. *Developmental biology*, 207(2), 380-392.

Malik, S. & Roeder, R. G. 2005. Dynamic regulation of pol II transcription by the mammalian Mediator complex. *Trends Biochem Sci,* 30, 256-63.

Mannini, L., Liu, J., Krantz, I. D. & Musio, A. 2010. Spectrum and consequences of SMC1A mutations: the unexpected involvement of a core component of cohesin in human disease. *Hum Mutat,* 31, 5-10.

Marston, A. L. 2014. Chromosome segregation in budding yeast: sister chromatid cohesion and related mechanisms. *Genetics,* 196, 31-63.

McGonnell, I. M., Green, C. R., Tickle, C., & Becker, D. L. 2001. Connexin43 gap junction protein plays an essential role in morphogenesis of the embryonic chick face. *Developmental Dynamics*, 222(3), 420-438.

Mehta GD, Kumar R, Srivastava S, Ghosh SK. 2013. Cohesin: Functions beyond sister chromatid cohesion. *FEBS Lett* 587(15): 2299-2312.

Minamino, M., Ishibashi, M., Nakato, R., Akiyama, K., Tanaka, H., Kato, Y., Negishi, L., Hirota, T., Sutani, T., Bando, M., et al. 2015. Esco1 Acetylates Cohesin via a Mechanism Different from That of Esco2. *Curr Biol,* 25, 1694-706.

Mishiro, T., Ishihara, K., Hino, S., Tsutsumi, S., Aburatani, H., Shirahige, K., & Nakao, M. 2009. Architectural roles of multiple chromatin insulators at the human apolipoprotein gene cluster. *The EMBO journal*, 28(9), 1234-1245.

Misulovin, Z., Schwartz, Y. B., Li, X. Y., Kahn, T. G., Gause, M., MacArthur, S., Fay, J. C., Eisen, M. B., Pirrotta, V., Biggin, M. D., et al. 2008. Association of cohesin and Nipped-B with transcriptionally active regions of the Drosophila melanogaster genome. *Chromosoma,* 117, 89-102.

Monnich, M., Kuriger, Z., Print, C. G. & Horsfield, J. A. 2011. A zebrafish model of Roberts syndrome reveals that Esco2 depletion interferes with development by disrupting the cell cycle. *PLoS One,* 6, e20051.

Morita, A., Nakahira, K., Hasegawa, T., Uchida, K., Taniguchi, Y., Takeda, S., Toyoda, A., Sakaki, Y., Shimada, A., Takeda, H., et al. 2012. Establishment and characterization of Roberts syndrome and SC phocomelia model medaka (Oryzias latipes). *Dev Growth Differ,* 54, 588-604.

Mourad, R. & Cuvier, O. 2016. Computational Identification of Genomic Features That Influence 3D Chromatin Domain Formation. *PLoS Comput Biol,* 12, e1004908.

Musa, F.U., Ratajczak, P., Sahu, J., Pentlicky, S., Fryer, A., Richard, G. and Willoughby, C.E., 2009. Ocular manifestations in oculodentodigital dysplasia resulting from a heterozygous missense mutation (L113P) in GJA1 (connexin 43). *Eye*, 23(3), pp.549-555.

Musio, A., Selicorni, A., Focarelli, M. L., Gervasini, C., Milani, D., Russo, S., Vezzoni, P. & Larizza, L. 2006. X-linked Cornelia de Lange syndrome owing to SMC1L1 mutations. *Nat Genet,* 38, 528-30.

Muto, A., Calof, A. L., Lander, A. D. & Schilling, T. F. 2011. Multifactorial origins of heart and gut defects in nipbl-deficient zebrafish, a model of Cornelia de Lange Syndrome. *PLoS Biol,* 9, e1001181.

Muto, A., Ikeda, S., Lopez-Burks, M. E., Kikuchi, Y., Calof, A. L., Lander, A. D. & Schilling, T. F. 2014. Nipbl and mediator cooperatively regulate gene expression to control limb development. *PLoS Genet,* 10, e1004671.

Nasevicius, A. & Ekker, S. C. 2000. Effective targeted gene 'knockdown' in zebrafish. *Nat Genet,* 26, 216-20.

Nativio, R., Sparago, A., Ito, Y., Weksberg, R., Riccio, A. & Murrell, A. 2011. Disruption of genomic neighbourhood at the imprinted IGF2-H19 locus in Beckwith-Wiedemann syndrome and Silver-Russell syndrome. *Hum Mol Genet,* 20, 1363-74.

Nechiporuk, A., & Keating, M. T. 2002. A proliferation gradient between proximal and msxb-expressing distal blastema directs zebrafish fin regeneration. *Development*, 129(11), 2607-2617.

Opitz, J. M. 1985. The Brachmann-de Lange syndrome. *Am J Med Genet,* 22, 89-102.

Parelho, V., Hadjur, S., Spivakov, M., Leleu, M., Sauer, S., Gregson, H. C., Jarmuz, A., Canzonetta, C., Webster, Z., Nesterova, T., et al. 2008. Cohesins functionally associate with CTCF on mammalian chromosome arms. *Cell,* 132, 422-33.

Oyamada, M., Oyamada, Y., & Takamatsu, T. 2005. Regulation of connexin expression. *Biochimica et Biophysica Acta (BBA)-Biomembranes*, 1719(1), 6-23.

Pauli, A., Althoff, F., Oliveira, R. A., Heidmann, S., Schuldiner, O., Lehner, C. F., Dickson, B. J. & Nasmyth, K. 2008. Cell-type-specific TEV protease cleavage reveals cohesin functions in Drosophila neurons. *Dev Cell,* 14, 239-51.

Paznekas, W. A., Boyadjiev, S. A., Shapiro, R. E., Daniels, O., Wollnik, B., Keegan, C. E., Innis, J. W., Dinulos, M. B., Christian, C., Hannibal, M. C., et al. 2003.

Connexin 43 (GJA1) mutations cause the pleiotropic phenotype of oculodentodigital dysplasia. *Am J Hum Genet,* 72, 408-18.

Percival, S. M., Thomas, H. R., Amsterdam, A., Carroll, A. J., Lees, J. A., Yost, H. J. & Parant, J. M. 2015. Variations in dysfunction of sister chromatid cohesion in esco2 mutant zebrafish reflect the phenotypic diversity of Roberts syndrome. *Dis Model Mech,* 8, 941-55.

Pistocchi, A., Fazio, G., Cereda, A., Ferrari, L., Bettini, L. R., Messina, G., Cotelli, F., Biondi, A., Selicorni, A. & Massa, V. 2013. Cornelia de Lange Syndrome: NIPBL haploinsufficiency downregulates canonical Wnt pathway in zebrafish embryos and patients fibroblasts. *Cell Death Dis,* 4, e866.

Rahman, S., Jones, M. J. & Jallepalli, P. V. 2015. Cohesin recruits the Esco1 acetyltransferase genome wide to repress transcription and promote cohesion in somatic cells. *Proc Natl Acad Sci U S A,* 112, 11270-5.

Rhodes, J. M., Bentley, F. K., Print, C. G., Dorsett, D., Misulovin, Z., Dickinson, E. J., Crosier, K. E., Crosier, P. S. & Horsfield, J. A. 2010. Positive regulation of c-Myc by cohesin is direct, and evolutionarily conserved. *Dev Biol,* 344, 637-49.

Roeder, R. G. 1998. Role of general and gene-specific cofactors in the regulation of eukaryotic transcription. *Cold Spring Harb Symp Quant Biol,* 63, 201-18.

Rolef Ben-Shahar, T., Heeger, S., Lehane, C., East, P., Flynn, H., Skehel, M. & Uhlmann, F. 2008. Eco1-dependent cohesin acetylation during establishment of sister chromatid cohesion. *Science,* 321, 563-6.

Rollins, R. A., Korom, M., Aulner, N., Martens, A. & Dorsett, D. 2004. Drosophila nipped-B protein supports sister chromatid cohesion and opposes the stromalin/Scc3 cohesion factor to facilitate long-range activation of the cut gene. *Mol Cell Biol,* 24, 3100-11.

Rollins, R. A., Morcillo, P. & Dorsett, D. 1999. Nipped-B, a Drosophila homologue of chromosomal adherins, participates in activation by remote enhancers in the cut and Ultrabithorax genes. *Genetics,* 152, 577-93.

Rubio, E. D., Reiss, D. J., Welcsh, P. L., Disteche, C. M., Filippova, G. N., Baliga, N. S., Aebersold, R., Ranish, J. A. & Krumm, A. 2008. CTCF physically links cohesin to chromatin. *Proc Natl Acad Sci U S A,* 105, 8309-14.

Santamaria, J. A., Marí-Beffa, M., & Becerra, J. 1992. Interactions of the lepidotrichial matrix components during tail fin regeneration in teleosts. *Differentiation*, 49(3), 143-150.

Schebesta, M., Lien, C. L., Engel, F. B., & Keating, M. T. 2006. Transcriptional profiling of caudal fin regeneration in zebrafish. *The Scientific World Journal*, 6, 38-54.

Schule, B., Oviedo, A., Johnston, K., Pai, S. & Francke, U. 2005. Inactivating mutations in ESCO2 cause SC phocomelia and Roberts syndrome: no phenotype-genotype correlation. *Am J Hum Genet,* 77, 1117-28.

Schuster, K., Leeke, B., Meier, M., Wang, Y., Newman, T., Burgess, S. & Horsfield, J. A. 2015. A neural crest origin for cohesinopathy heart defects. *Hum Mol Genet,* 24, 7005-16.

Seitan, V. C., Banks, P., Laval, S., Majid, N. A., Dorsett, D., Rana, A., Smith, J., Bateman, A., Krpic, S., Hostert, A., et al. 2006. Metazoan Scc4 homologs link sister chromatid cohesion to cell and axon migration guidance. *PLoS Biol,* 4, e242.

Seruggia, D. & Montoliu, L. 2014. The new CRISPR-Cas system: RNA-guided genome engineering to efficiently produce any desired genetic alteration in animals. *Transgenic Res,* 23, 707-16.

Shintomi, K. & Hirano, T. 2010. Sister chromatid resolution: a cohesin releasing network and beyond. *Chromosoma,* 119, 459-67.

Skibbens, R. V. 2016. Of Rings and Rods: Regulating Cohesin Entrapment of DNA to Generate Intra- and Intermolecular Tethers. *PLoS Genet,* 12, e1006337.

Skibbens, R.V., 2010. Buck the establishment: reinventing sister chromatid cohesion. *Trends in cell biology*, 20(9), pp.507-513.

Skibbens, R. V., Corson, L. B., Koshland, D. & Hieter, P. 1999. Ctf7p is essential for sister chromatid cohesion and links mitotic chromosome structure to the DNA replication machinery. *Genes Dev,* 13, 307-19.

Skibbens, R.V., 2009. Establishment of sister chromatid cohesion. *Current Biology*, 19(24), pp.R1126-R1132.

Taatjes, D. J. 2010. The human Mediator complex: a versatile, genome-wide regulator of transcription. *Trends Biochem Sci,* 35, 315-22.

Terret ME, Sherwood R, Rahman S, Qin J, Jallepalli PV. (2009) Cohesin acetylation speeds the replication fork. *Nature* 462(7270): 231-234.

Ton QV, Iovine MK. 2013. Determining how defects in *connexin43* cause skeletal disease. *Genesis* 51(2): 75-82.

Tonkin, E. T., Wang, T. J., Lisgo, S., Bamshad, M. J. & Strachan, T. 2004. NIPBL, encoding a homolog of fungal Scc2-type sister chromatid cohesion proteins and fly Nipped-B, is mutated in Cornelia de Lange syndrome. *Nat Genet,* 36, 636-41.

Toth, A., Ciosk, R., Uhlmann, F., Galova, M., Schleiffer, A. & Nasmyth, K. 1999. Yeast cohesin complex requires a conserved protein, Eco1p(Ctf7), to establish cohesion between sister chromatids during DNA replication. *Genes Dev,* 13, 320-33.

Uhlmann, F., Lottspeich, F. and Nasmyth, K., 1999. Sister-chromatid separation at anaphase onset is promoted by cleavage of the cohesin subunit Scc1. *Nature*, 400(6739), pp.37-42.

Unal E, Arbel-Eden A, Sattler U, Shroff R, Lichten M, et al. 2004. DNA damage response pathway uses histone modification to assemble a double-strand break-specific cohesin domain. *Mol Cell* 16(6): 991-1002.

Van Bortle, K., Nichols, M. H., Li, L., Ong, C. T., Takenaka, N., Qin, Z. S. & Corces, V. G. 2014. Insulator function and topological domain border strength scale with architectural protein occupancy. *Genome Biol,* 15, R82.

Van den Berg, D. J. & Francke, U. 1993. Sensitivity of Roberts syndrome cells to gamma radiation, mitomycin C, and protein synthesis inhibitors. *Somat Cell Mol Genet,* 19, 377-92.

van der Lelij, P., Godthelp, B. C., van Zon, W., van Gosliga, D., Oostra, A. B., Steltenpool, J., de Groot, J., Scheper, R. J., Wolthuis, R. M., Waisfisz, Q., et al. 2009. The cellular phenotype of Roberts syndrome fibroblasts as revealed by ectopic expression of ESCO2. *PLoS One,* 4, e6936.

Vega, H., Waisfisz, Q., Gordillo, M., Sakai, N., Yanagihara, I., Yamada, M., van Gosliga, D., Kayserili, H., Xu, C., Ozono, K., et al. 2005. Roberts syndrome is caused by mutations in ESCO2, a human homolog of yeast ECO1 that is essential for the establishment of sister chromatid cohesion. *Nat Genet,* 37, 468-70.

Wendt, K. S. & Peters, J. M. 2009. How cohesin and CTCF cooperate in regulating gene expression. *Chromosome Res,* 17, 201-14.

Wendt, K. S., Yoshida, K., Itoh, T., Bando, M., Koch, B., Schirghuber, E., Tsutsumi, S., Nagae, G., Ishihara, K., Mishiro, T., et al. 2008. Cohesin mediates transcriptional insulation by CCCTC-binding factor. *Nature,* 451, 796-801.

Whelan, G., Kreidl, E., Wutz, G., Egner, A., Peters, J. M. & Eichele, G. 2012. Cohesin acetyltransferase Esco2 is a cell viability factor and is required for cohesion in pericentric heterochromatin. *EMBO J,* 31, 71-82.

Xiong, B., Lu, S. & Gerton, J. L. 2010. Hos1 is a lysine deacetylase for the Smc3 subunit of cohesin. *Curr Biol,* 20, 1660-5.

Xu, B., Gogol, M., Gaudenz, K. & Gerton, J. L. 2016. Improved transcription and translation with L-leucine stimulation of mTORC1 in Roberts syndrome. *BMC Genomics,* 17, 25.

Xu, B., Lee, K. K., Zhang, L. & Gerton, J. L. 2013. Stimulation of mTORC1 with L-leucine rescues defects associated with Roberts syndrome. *PLoS Genet,* 9, e1003857.

Zakari, M., Yuen, K. & Gerton, J. L. 2015. Etiology and pathogenesis of the cohesinopathies. *Wiley Interdiscip Rev Dev Biol,* 4, 489-504.

Zhang, J., Shi, X., Li, Y., Kim, B. J., Jia, J., Huang, Z., Yang, T., Fu, X., Jung, S. Y., Wang, Y., et al. 2008. Acetylation of Smc3 by Eco1 is required for S phase sister chromatid cohesion in both human and yeast. *Mol Cell,* 31, 143-51.

Zakari, M., Yuen, K. & Gerton, J. L. 2015. Etiology and pathogenesis of the cohesinopathies. *Wiley Interdiscip Rev Dev Biol,* 4, 489-504.

Zuin, J., Dixon, J. R., van der Reijden, M. I., Ye, Z., Kolovos, P., Brouwer, R. W., van de Corput, M. P., van de Werken, H. J., Knoch, T. A., van, I. W. F., et al. 2014. Cohesin and CTCF differentially affect chromatin architecture and gene expression in human cells. *Proc Natl Acad Sci U S A,* 111, 996-1001.

CHAPTER 2

Esco2 regulates *cx43* expression during skeletal regeneration in the zebrafish

2.1 Abstract

Roberts syndrome (RBS) is a rare genetic disorder characterized by craniofacial abnormalities, limb malformation and often severe mental retardation. RBS arises from mutations in *ESCO2* that encodes an acetyltransferase and modifies the cohesin subunit SMC3. Mutations in *SCC2/NIPBL* (encodes a cohesin loader), *SMC3* or other cohesin genes (*SMC1*, *RAD21/MCD1*) give rise to a related developmental malady termed Cornelia de Lange Syndrome (CdLS). RBS and CdLS exhibit overlapping phenotypes, but RBS is thought to arise through mitotic failure and limited progenitor cell proliferation while CdLS arises through transcriptional deregulation. Here, I use the zebrafish regenerating fin model to test the mechanism through which RBS-type phenotypes arise. *esco2* is upregulated during fin regeneration and specifically within the blastema. Esco2 knockdown adversely affects both tissue and bone growth in regenerating fins – consistent with a role in skeletal morphogenesis. Esco2 knockdown significantly diminishes *cx43/gja1* expression, which encodes the gap junction connexin subunit required for cell-cell communication. *cx43/CX43* mutations cause the *short fin* (*sof^{b123}*) phenotype in zebrafish and oculodentodigital dysplasia (ODDD) in humans. Importantly, *cx43* overexpression rescues *esco2*-dependent growth defects. These results conceptually link ODDD to cohesinopathies and provide evidence that ESCO2 may play a transcriptional role critical for human development.

2.2 Introduction

The skeleton supports soft tissues, provides for muscle attachment and protects internal organs from risk of injury. Additional functions include calcium and phosphorus storage, blood cell production and immune response. Given this diverse array of functionality, mutations that affect skeletal functions exhibit pleiotropic defects that include osteoporosis, osteoarthritis, hematopoietic and immunity deficiencies. Aberrations in skeletal development, especially long bone growth and morphogenesis, are also components of a number of multi-spectrum developmental abnormalities such as Roberts syndrome (RBS) and Cornelia de Lange Syndrome (CdLS). In addition to severe long-bone growth defects and missing digits, both RBS and CdLS patients may exhibit craniofacial abnormalities, cleft palate, syndactyly, organ defects and severe mental retardation (Liu & Krantz, 2009; Mannini et al, 2010).

Recent genetic mapping studies reveal that mutations in cohesion pathways are responsible for RBS and CdLS disorders – as well as a host of related diseases collectively termed cohesinopathies (Schule et al, 2005; Gordillo et al, 2008; Krantz et al, 2004; Musio et al, 2006; Tonkin et al, 2004; Vega et al, 2005; Deardorff et al, 2007; Deardorff et al, 2012a,b; Van der Lejij et al, 2010; Yuan et al, 2015). Elucidating the molecular basis of these disorders span topics of both chromosome segregation and transcriptional regulation (Rudra and Skibbens, 2013). For instance, RBS arises from mutations in *ESCO2*. High fidelity chromosome segregation requires that sister chromatids be identified from DNA synthesis (S-phase) to anaphase onset during mitosis (M-phase). Identity is achieved by cohesin complexes that tether together sister chromatids. ESCO2 is an acetyltransferase that converts chromatin-bound cohesins to a

tether-competent state (Skibbens et al, 1999; Toth et al, 1999; Ivanov et al, 2002; Zhang et al, 2008; Unal et al, 2008; Ben-Shahar et al, 2008). Thus, it is not surprising that cells isolated from RBS patients exhibit mitotic failure, elevated levels of apoptosis, reduced proliferation and genotoxic hypersensitivities (Mehta et al, 2013; Horsfield et al, 2012). On the other hand, CdLS arises from mutations in the cohesin genes *SMC1A, SMC3* and *RAD21*, the cohesin deposition factor encoded by *NIPBL*, and the de-acetylase encoded by *HDAC8* that targets SMC3 (Krantz et al, 2004; Musio et al, 2006; Tonkin et al, 2004; Deardorff et al., 2007; Deardorff et al, 2012a,b). Intriguingly, CdLS patient cells typically exhibit normal mitosis and retain a euploid genomic state, revealing that CdLS instead arises mainly through transcriptional deregulation (Liu & Krantz, 2009; Dorsett & Merkenschlager, 2013). A transcriptional basis of CdLS is supported by findings that cohesins are critical for 1) transcription termination, 2) enhancer-promoter registration, 3) CTCF-insulator recruitment and 4) RNAPII transitioning from a paused to elongating state (Dorsett & Merkenschlager, 2013). Despite the phenotypic similarities between RBS and CdLS, the role for ESCO2 in transcription remains undefined.

The zebrafish caudal fin contains 16 to 17 segmented bony fin rays with new growth occurring by the distal addition of bony segments and associated fin ray joints (Goss & Stagg, 1957; Haas, 1962). Because of its simple structure, rapid regeneration following amputation, and the ability to knockdown gene expression through gene-specific morpholinos, the zebrafish fin is emerging as an excellent model system from which to elucidate tissue and bone growth pathways. For instance, mutations in *connexin43* (*cx43*) cause the *short fin* (*sof*[b123]) phenotype, which is characterized by defects in bony fin ray growth and joint formation (Iovine et al, 2005; Hoptak-Solga et

al, 2008). Missense mutations in human *CX43* cause Oculodentodigital dysplasia (ODDD) - a genetic disorder that effects both craniofacial and distal skeleton limb development (Paznekas et al, 2003). Thus, the regenerating fin provides clinically relevant insights into highly conserved pathways critical for human skeletal development.

Esco2 knockdown studies in zebrafish and medaka embryos produce severe developmental defects – in part recapitulating RBS phenotypes (Monnich et al, 2011; Morita et al, 2012). Large-scale cell death and subsequent indirect or downstream effects, however, complicate interpreting the effects of Esco2 knockdown in these studies. Here, I report on the role of *esco2* during fin regeneration, in the absence of embryonic complications. The regenerating fin is an ideal system to study the effects of reduced *esco2* on the skeleton in that it avoids the possible confounding effects of reduced *esco2* during development previously reported (Monnich et al., 2011; Whelan et al., 2012). In this chapter, sI provide details of results that reveal that *esco2* expression is upregulated in regenerating fins, particularly in the blastema, which is a specialized compartment that contains the majority of proliferative cells. Moreover, Esco2 knockdown results in defects in both fin regeneration and bony segment length. Importantly, the results reveal that Esco2 knockdown reduces *cx43* expression and diminishes Cx43 signaling pathways but does not globally reduce other gene expression pathways. In combination, these results suggest the possibility that Esco2 may act as a specific transcriptional regulator with targets that include *cx43*.

2.3 Materials and methods

Statement on the ethical treatment of animals

This work was carried out in strict accordance with the recommendations in the Guide for the Care and Use of Laboratory Animals of the National Institutes of Health. Lehigh's Institutional Animal Care and Use Committee (IACUC) (Protocol identification # 128, approved 11/16/2014) approved the protocols used for this manuscript. Lehigh University's Animal Welfare Assurance Number is A-3877-01. All experiments were performed to minimize pain and discomfort.

Housing and husbandry

Zebrafish (*Danio rerio*) are housed in a re-circulating system built by Aquatic Habitats (now Pentair). Both 3L tanks (up to 12 fish/tank) and 10L tanks (up to 30 fish/tank) are used. The fish room has a 14:10 light:dark cycle. Room temperature (RT) is tightly regulated and varies from 27-29°C (Westerfield, 1993). Water quality is monitored automatically and dosed to maintain conductivity (400-600 µs) and pH (6.95-7.30). Nitrogen levels are maintained by a biofilter. A 10% water change occurs daily. Recirculating water is filtered sequentially through pad filters, bag filters, and a carbon canister before circulating over UV lights for sterilization. Fish are fed three times daily, once with brine shrimp (hatched from INVE artemia cysts) and twice with flake food (Aquatox AX5) supplemented with 7.5 % micropellets (Hikari), 7.5 % Golden Pearl (300-500 micron, Brine Shrimp direct), and 5 % Cyclo-Peeze (Argent).

Zebrafish strains and surgical procedures

The zebrafish strains used were wild-type (C32), *sof*[b123] (Iovine & Johnson, 2000), and *Tg(hsp70:miR-133sp*[pd48]*)* (Yin et al, 2012). Caudal fin amputations, fin regeneration and harvesting were done as previously described (Sims et al, 2009; Ton & Iovine, 2013; Govindan & Iovine, 2014). Briefly, fish were first anaesthetized in 0.1% tricaine solution and their caudal fin rays amputated to the 50% level uisng a sterile razor blade and visualized using a dissecting scope. Fin regeneration proceeded until the desired time period depending on the type of experiment. At the required time point, the regenerated fins were harvested and fixed in 4% paraformaldehyde (PFA) in PBS overnight at 4°C. The fins were then dehydrated in 100% methanol and stored at 20°C until further use.

Gene knockdown by morpholino injection and electroporation

All morpholinos (MOs) used were fluorescein-tagged and purchased from Gene Tools, LLC. The MOs were reconstituted in sterile water to a final concentration of 1mM. The sequences for MOs used are as follows: MO targeted against *esco2* (*esco2*-MO: 5'-CTCTTTCGGGATAACATCTTCAATC-3', from Monnich et al., 2011), *esco2* -5-base mismatch control MO (*esco2*-MM: 5'-CTCTTTCCGCATAAGATGTTGAATC-3', and Gene Tools standard control MO (5'-CCTCTTACCTCAGTTACAATTTATA-3'). Microinjection and electroporation procedures were carried out as described previously (Thummel et al, 2006; Hoptak-Solga et al, 2008; Sims et al, 2009). Briefly, caudal fins were amputated at 50% level. At 3 days post amputation (3 dpa), fish were anaesthetized and MOs injected using a Narishige IM 300 Microinjector. Approximately 50 nl of MO

was injected per ray into either the dorsal or ventral side of the regenerating fin tissue (approximately first 5 - 6 bony fin rays), keeping the other side uninjected. The uninjected side served as the internal control. Immediately after injection, both sides of the fin were electroporated using a CUY21 Square Wave electroporator (Protech International Inc). To minimize non-specific effects of the electroporation procedure, both sides of the fin were electroporated. The following parameters were used during electroporation: ten 50-ms pulses of 15 V with a 1 s pause between pulses. These fish were returned back to the system water for regeneration to proceed. After 24 hours (i.e. 1 day post electroporation (1 dpe), which is equivalent to 4 dpa, the injected side of the fins were evaluated by fluorescence using a Nikon Eclipse 80i Microscope (Diagnostic Instruments) to confirm MO uptake. The MO injected fins were evaluated for regenerate length, segment length, cell proliferation, cell death, *in situ* hybridization, and protein levels by western blots and RNA levels by qRT-PCR. For fins used for lysate preparation or for qRT-PCR, all fins were injected and electroporated prior to harvesting.

Regenerate length and segment length measurement and analysis

At 4 dpe/7 dpa, MO injected (*esco2*-MO or *esco2*-MM) fins were calcein stained prior to measuring regenerate length and segment length (Du et al, 2001; Sims et al, 2009). Briefly, fish were allowed to swim for 10 minutes in 0.2% calcein (pH 7) at room temperature followed by swimming in fresh system water for another 10 minutes. The fish were anaesthetized and imaged using Nikon Eclipse 80i Microscope equipped with a SPOT-RTKE digital camera (Diagnostic Instruments) and SPOT software (Diagnostic Instruments). All measurements were performed on the longest fin ray (3rd fin ray) from

48

the ventral or dorsal most lobe of the caudal fin, as previously established (Iovine &
Johnson, 2000). Images used to measure regenerate length and bone segment length were
analyzed using Image Pro software. For fin regenerate length, measurements were based
on amputation site to the distal tip of the 3rd fin ray. For bone segment length, the
distance between the first two joints formed following regeneration was measured. For
each experiment at least 6-8 fish were used per trial and at least 3 independent trials were
performed. Student's t-test ($P < 0.05$) was used for statistical analysis.

**RNA probe preparation and in situ hybridization on whole mount and
cryosectioned fins**

RNA probes were made using linear PCR product as template, where the T7 RNA
polymerase-binding site was included in the reverse primer. The *cx43* template was made
as described (Iovine et al, 2005). The *esco2* product was generated using gene-specific
primers (forward primer- 5'AGCAGGGACCTTCTACAGCA3'and reverse primer
5'TAATACGACTCACTATAGGGGGGATCATCTGGAAGAACG3'). RNA probes
were labeled with digoxygenin (DIG) following manufacturer instructions (Roche). *In
situ* hybridization (ISH) was performed on wild-type (WT) fins of different time points
(1, 3, 5 and 8 dpa) and 5 dpa *sof*[b123] fins. Briefly, fins were amputated at 50% level and
harvested at the appropriate time point. For ISH on knockdown fins, MO (*esco2*-MO or
esco2-MM) was injected and electroporated on WT-3 dpa fins and harvested after 24
hours (1 dpe/4 dpa). For ISH on whole mount fins the standard protocol was followed
(Ton & Iovine, 2013; Govindan & Iovine, 2014). Note that for ISH on *transgenic
hsp70:miR-133sp*[pd48]- positive and negative fins, at 3 dpa fish were heat shocked at 37˚C

for 1 hour and harvested after 24 hours (1 dpe/4 dpa). For all ISH experiments, approximately 6-8 fins were used per trial and 3 independent trials were performed. A Nikon Eclipse 80i Microscope equipped with a SPOT-RTKE digital camera (Diagnostic Instruments) and SPOT software (Diagnostic Instruments) was used to acquire images.

ISH on sections was done as described with the following modifications (Smith et al, 2008). WT-5 dpa fins were first rehydrated sequentially by methanol-PBS washes, cryosectioned and stored at -20°C. Slides were defrosted for approximately 1 hour prior to hybridization and section locations marked with a hydrophobic barrier pen (ImmEdge Pen; PAP pen, VWR Laboratories). RNA probe was mixed with hybridization buffer: 1X salt solution (NaCl, Tris HCl, Tris Base, Na_2HPO_4, and 0.5 M EDTA), 50% deionized formamide (Sigma), 10% dextran sulfate, 1 mg/ml tRNA, and 1X Denhart's (Fisher) and denatured by incubating at 70°C for 5 minutes. The denatured probe mix was added to the sections and hybridized overnight at 65°C. Slides were washed at 65°C with a 1X SSC, 50% formamide and 0.1% Tween-20 solution, rinsed with MABT (100mM Maleic acid, 150mM NaCl, and 0.1% Tween-20) and incubated in a blocking solution (MABT, goat serum and 10% milk) for 2 hours. Anti- DIG antibody (1:5000) was diluted in MABT and the slides were incubated overnight at 4°C. Slides were washed 4X in MABT, 2X in Alkaline Phosphatase staining buffer (100mM Tris, pH 9.5, 50mM MgCl2, 100mM NaCl, and 0.1% Tween-20), then incubated overnight at 37°C in 10% polyvinyl alcohol staining solution and NBT/BCIP stock solution (Roche). The reaction was stopped by washing extensively with PBST. Sections were mounted in 100% glycerol and images acquired using a Nikon Eclipse 80i Microscope equipped with a SPOT-

RTKE digital camera (Diagnostic Instruments) and SPOT software (Diagnostic Instruments).

Immunoblotting and Esco2 antibody

Escherichia coli lysates from cells expressing either GST or GST-Esco2 fusion protein (protein expression was induced using 0.3mM IPTG for 4 hours) were prepared as described (Gerhart et al, 2012). Briefly, cells from 1 ml of culture were pelleted and lysed using 50µg/ml lysozyme in lysis buffer (100mM Tris- HCl pH 7.5, 50 mM NaCl, 10mM EDTA pH 8, complete protease inhibitor cocktail, Roche). To this mixture, 2.2 N NaOH and 8% BME were added. Protein precipitation was carried out using 55% TCA followed by wash with 0.5% TCA. The protein pellets were resuspended in 2X SDS buffer. GST or GST-Esco2 were detected by western blot using anti-GST antibody (Santa Cruz, 1:5000) or affinity-purified anti-Esco2 (1:1000). Affinity purified polyclonal Anti-Esco2 was generated in rabbit against the N-terminal peptide LSRKRKHGSPDAESC (Genscript) and used at a concentration of 1:1000 for the non-competed western blot. For anti-Esco2 antibody specificity assay, identical gels were loaded with decreasing volumes of the GST-Esco2 protein samples. For the competed blot, the anti-Esco2 antibody was pre-incubated with the Esco2 peptide (100µM). The blots were incubated with primary antibody overnight at 4°C.

Fin lysates were prepared as previously described (Hoptak-Solga et al, 2008; Gerhart et al, 2012; Govindan & Iovine, 2014). Briefly, approximately 9-10 MO-injected (*esco2* MO or *esco2* MM) 1 dpe/4 dpa regenerating fins were pooled, and then suspended in incubation buffer (136.8 mM NaCl, 5.36 mM KCl, 0.34 mM Na$_2$HPO$_4$, 0.35 mM

KH_2PO_4, 0.8 mM $MgSO_4$, 2.7 mM $CaCl_2$, 20 mM HEPES with pH adjusted to 7.5)

supplemented with protease inhibitor (Thermo scientific, Halt[TM] Protease and

Phosphatase Inhibitor Cocktail, 100X). The harvested fin tissue was homogenized by a

tissue homogenizer (Bio-Gen, PRO 200) at high speed (3X) for 5 seconds with 10 second

cooling intervals. Homogenized samples were centrifuged at 200g for 10 min at 4°C and

supernatant protein levels normalized according to Bradford assays. Note that for

preparation of proteins lysate from heat shocked $Tg(hsp70:miR-133sp^{pd48})$ – positive and

$Tg(hsp70:miR-133sp^{pd48})$ –negative fish, 37˚C heat shock was performed for 1 hour at 3

dpa and fins harvested at 1 dpe/4dpa as previously described.

GST, Esco2, Cx43 or tubulin was detected using anti-GST (1:5000) (Santa Cruz),

anti- Esco2 (1:1000), anti-Cx43 (1:1000) or anti-α-tubulin (1:1000) (Sigma), followed by

exposure to peroxidase-conjugated goat anti-rabbit IgG (GST, Esco2 and Cx43) or goat

anti-mouse IgG (tubulin) (Pierce Rockford, IL) at a concentration of 1:20,000. Signal

detection was performed using ECL chemiluminescent reagent (SuperSignal West Femto

Maximum Sensitivity Substrate, Pierce Rockford, IL) and X-ray film.

Image J software was used to calculate the band intensities and the percent change

was calculated. Relative pixel densities of gel bands were measured using a gel analysis

tool in ImageJ software as described (Bhadra and Iovine, 2015). The density of each band

was obtained as the area under the curve using the gel analysis tool. For relative density

calculation, the density of the Esco2, Cx43 or tubulin bands for the experimental sample

was first normalized against the density of the Esco2, Cx43 or tubulin bands from the

control sample. Relative pixel density was calculated as the ratio of Esco2 and tubulin or

Cx43 and tubulin, where tubulin is the loading control.

Cell proliferation and cell death assay*s*

For detection of proliferating cells in S-phase, bromodeoxyuridine (5-bromo-2'-deoxyuridine, BrdU) labeling was performed with few modifications (Nechiporuk & Keating, 2002, Iovine et al, 2005). Briefly, 3 dpa MO injected (*esco2*-MO or *esco2*-MM) fish were allowed to swim for 5 minutes in 50μg/ml of BrdU (Roche) mixed in system water at 1 dpe/4 dpa and harvested on the same day. The BrdU-labeled fins were fixed in 4% PFA overnight at 4°C and then dehydrated by keeping in 100% methanol overnight. Before use, the fins were rehydrated gradually in a series of methanol solutions containing 0.1% Triton X-100 in PBS (PBTx). Next, fins were treated for 30 minutes in a solution containing 2N HCl in PBTx. Following that, the fins were blocked for 2 hours (0.25% BSA in PBTx). The primary antibody against BrdU (Roche) is a mouse monoclonal and used at a 1:50 dilution and incubated overnight at 4°C. Extensive washes (4 hours) in the PBTx solution were performed the next day and fins incubated overnight at 4°C in 1:200 dilution of anti-mouse antibody conjugated to Alexa-546 (Invitrogen). The next day extensive washes (4 hours) were performed and the fins mounted in 100% glycerol and visualized under a Nikon Eclipse 80i Microscope equipped with a SPOT-RTKE digital camera (Diagnostic Instruments) and SPOT software (Diagnostic Instruments). For measuring BrdU labeled cells the Image Pro software was used. A ratio of distance migrated by BrdU positive cells from the regenerating tip in μm (a) and the regenerating length in μm (b) was calculated. BrdU labeling was then obtained by measuring a/b ratio of the uninjected and injected (*esco2*-MO and *esco2*-MM) side of the fin.

For both histone-3-phosphate (H3P) and Terminal deoxynucleotidyl transferase dUTP nick end labeling (TUNEL) assays, 3 dpa MO-injected (*esco2*-MO or *esco2*-MM) fins were harvested at 1 dpe/4 dpa and fixed in 4% PFA overnight at 4°C. These fins were then dehydrated in 100% methanol overnight before use. In order to detect mitotic cells, H3P staining and the number of H3P positive cells per unit area were carried out as described previously (Ton & Iovine, 2013). The primary and secondary antibodies used for H3P assay are as follows: rabbit anti-histone-3-phosphate (1:200) (anti-H3P, Millipore) and anti-rabbit Alexa 546 (1:200) (Invitrogen). H3P- positive cells were counted without software from within the distal-most 250μm of the 3rd fin ray as previously established (Iovine et al, 2005; Hoptak-Solga et al, 2008).

TUNEL assay (ApopTag Kit, Chemicon) was performed as described in the manufacturer's instructions with the following modifications. The fins were rehydrated by successive washes in methanol/PBST, treated with proteinase K at a concentration of 5μg/ml for 45 minutes at room temperature, and then re-fixed in 4% PFA in PBS for 20 minutes. After extensive PBST washes, fins were incubated in ethanol: acetic acid (2:1, v: v) at -20°C for 10 minutes. Following extensive PBST washes, fins were incubated in equilibrium buffer (from ApopTag Kit) for 1 hour at room temperature, and then incubated overnight in 37°C water bath in TdT solution. The enzymatic reaction was stopped by extensive washes in stop/wash buffer for 3 hours in 37°C water bath, briefly rinsed in PBST and blocked with blocking solution (from ApopTag Kit) for 1 hour. The fins were incubated overnight at 37° in Rhodamine antibody solution (from ApopTag Kit). Fins were washed extensively in PBST and then mounted in 100% glycerol. Image acquisition was performed using a Nikon Eclipse 80i microscope equipped with a SPOT-

RTKE digital camera (Diagnostic Instruments) and SPOT software (Diagnostic Instruments). Cell death was analyzed by counting the number of TUNEL-positive cells without software from the distal-most 250 μm of the 3rd fin ray, similar to the H3P-positive cell counting analysis. For all the experiments at least 6-8 fins were used per trial and at least 3 independent trials were performed. Student's t-test ($P < 0.05$) was used for statistical analysis.

Quantitative real- time PCR analysis

Quantitative real- time PCR analysis (qRT-PCR) was completed on total mRNA extracted from 1 dpe/4 dpa harvested fins (3 dpa *esco2*-MO and standard control-MO injected). Total RNA extraction was carried out by following the standard protocol (Sims et al, 2009). Briefly, Trizol reagent (Gibco) was used to extract mRNA from minimum of 10 fins. For making cDNA, 1μg of total RNA was reverse transcribed with SuperScript III reverse transcriptase (Invitrogen) using oligo (dT) primers. The following primers (2.5μM) for *keratin, cx43* (Sims et al, 2009), *sema3d* (Ton & Iovine, 2013), *hapln1a* (Govindan & Iovine, 2014), and *mps1* (Bhadra & Iovine, 2015) were used for qRT-PCR analysis. The primers for *shh* and *spry4* were designed using Primer express software (*shh*: forward primer: 5'-GGCTCATGACACAGAGATGCA-3', reverse primer: 5'-CATTACAGAGATGGCCAGCGA-3' and *spry4*: forward primer: 5'-CGCAACGACCTGTTCATCTGA-3', reverse primer: 5'-GCACTCTTGCATTCGAAAGCA-3'). Data from three independent Esco2 knockdown RNA samples were used, with qRT-PCR for each gene performed in duplicate, for comparison between experimental treatments. RNA and subsequent cDNA synthesized

from standard control MO injected fins served as the control. The standard control MO does not target any zebrafish genes. Analyses of the samples were done using Rotor-Gene 6000 series software (Corbette Research) and the average cycle number (C_T) determined for each amplicon. *Keratin* was used as a housekeeping gene, and the delta C_T (ΔC_T) values represent expression levels normalized to *keratin* values. $\Delta\Delta C_T$ values represent the relative level of gene expression and the fold difference was determined using the $\Delta\Delta C_T$ method ($2^{-\Delta\Delta C_T}$) as described (Ton and Iovine, 2013). Standard deviation was calculated using the comparative method described in User Bulletin 2 # ABI PRISM 7700 Sequence Detection System

(http://www3.appliedbiosystems.com/cms/groups/mcb_support/documents/generaldocuments/cms_040980.pdf).

Heat shock induction of *cx43* expression

Tg(*hsp70:miR-133sp*[pd48]) are denoted as transgene-positive (Tg+) and their siblings denoted as transgene-negative (Tg-) were used in the heat shock experiment (Yin et al, 2012). For all the experiments at least 6-8 fish were used per trial and at least 3 independent trials were performed. Esco2 knockdown was performed on 3dpa Tg+ and Tg- fish as described above. After 4 hours both groups were heat shocked at 37ºC for 1 hour and returned to the system water for recovery. Tg+HS+ and Tg-HS+ denoted these groups respectively. To confirm that rescue depended on *cx43*, we also examined phenotypes in the transgenic line without heat shock (Tg+HS-). Induction of the transgene expression upon heat shock was confirmed after 24 hours by screening for GFP-positive fins in the Tg+HS+ group. The control groups (Tg-HS+ and Tg+HS-) were

negative for GFP expression after heat shock. For measurement of regenerate length and segment length fins were harvested at 4 dpe/7 dpa and calcein stained as previously described (Du et al, 2001; Sims et al, 2009). The measurement and data analysis were done as described below. Image acquisition was carried out by using the Nikon Eclipse 80i microscope equipped with a SPOT-RTKE digital camera (Diagnostic Instruments) and SPOT software (Diagnostic Instruments). Image Pro software was used for regenerate and segment length measurements.

To evaluate the regenerate length and segment length of $Tg(hsp70:miR-133sp^{pd48})$ fins, the *esco2*-MO injected side of each fin was compared to its un-injected side by % similarity method as described (Bhadra and Iovine, 2015). Briefly, the length of the injected side and uninjected sides were measured in μm and denoted as A and B respectively. The % similarity for each fin was calculated by using the formula: [(A/B) x 100]. Values close to 100% indicate that the *esco2*-MO has no effect on the phenotype whereas a value less than 100% indicate that the MO has an effect on the observed phenotype. The mean of % similarity for the Esco2 knockdown experimental group (Tg+HS+) and the corresponding Esco2 knockdown control groups (Tg-HS+ and Tg+HS-) were estimated and compared, and the statistical significance between the groups was determined using two-tailed unpaired student's *t*-test (P < 0.05). Segment length analysis was performed on calcein stained fins. Briefly, for segment length, the distance between the first two newly formed joints following amputation was measured (in the 3rd fin ray from either the dorsal or ventral end) since that was previously established as a standard (Iovine & Johnson, 2000). To evaluate the phenotypic effect of segment length, the % similarity method was used as described above.

2.4 Results

esco2 mRNA is upregulated in the blastema of regenerating fins

Despite the fact that *ESCO2* is critical for proper human development (Schule et al, 2005; Vega et al, 2005), little information exists regarding its expression or the molecular basis through which mutations in *ESCO2* result in skeletal disorders. Here, I exploit the adult zebrafish regenerating fin to address both of these fundamental issues in the absence of confounding effects due to embryonic death. To ascertain the temporal regulation of *esco*2 expression in regenerating fins, fins were amputated at the 50% level and regenerating tissue harvested at 1, 3, 5 and 8 days post amputation (dpa). The expression of *esco2* was then assessed by whole mount *in situ* hybridization (Figure 2.1). At 1 dpa, *esco2* was not detectable. *esco2* was readily apparent at both 3 and 5 dpa with levels starting to diminish at this later time point. By 8 dpa, *esco2* expression was significantly reduced. High *esco2* expression at 3 dpa is consistent with previous studies that map this period as the peak rate of regeneration in the zebrafish fin (Hoptak-Solga et al, 2008; Lee et al, 2005) and suggest that the localization of *esco2* expression might similarly correlate with the highly proliferative blastemal compartment. To test this possibility, 5 dpa fins stained for *esco2* expression by *in situ* hybridization were cryosectioned. The results reveal that *esco2* expression is specifically upregulated in the blastemal compartment (Figure 2.2). To establish that the probe had access to all *esco2*-positive tissue, 5 dpa fins were cryosectioned prior to hybridization (Smith et al, 2008). Results from this regimen confirm that *esco2* is expressed specifically within the blastema (Figure 2.2). In summary, *esco2* expression is temporally regulated and occurs specifically in the blastemal compartment of the zebrafish regenerating fin.

esco2 is a critical regulator of fin regeneration and specifically of bone growth

Esco2 is likely essential (Monnich et al, 2011), requiring knockdown strategies to ascertain function in the adult regenerating fin. Therefore, I depleted Esco2 using morpholino (MO)-mediated knockdown methodologies (Hoptak-Solga et al, 2008; Sims et al, 2009) using one of the two validated MOs for Esco2 (Monnich et al, 2011). As a control I used either a custom mismatch morpholino (5MM) containing five mismatches compared with the *esco2* targeting MO or the 'standard control' MO from Gene Tools that does not recognize target genes in zebrafish. Uptake is accomplished by first injecting the MO into the blastema of the regenerating fin, followed by electroporation across the fin. All MOs are modified with fluorescein, permitting validation of cellular uptake. Only fins positive for MOs at 1 day post electroporation (dpe) are kept for further analysis. Procedural details for all knockdown experiments are outlined in Figure 2.3.

Regenerate length and segment length were evaluated at 4 dpe/7 dpa. All fin regenerate and segment length measurements were obtained from the 3rd fin ray and results compared between injected (*esco2*-MM or *esco2*-MO) and uninjected portions of the same fin, a strategy previously documented as providing for both internal controls and standardized analyses (Hoptak-Solga et al, 2008; Iovine & Johnson, 2000). Uninjected control fins regenerated in a robust fashion. *esco2*-MM injected regenerating fins exhibited identical growth to the uninjected control (Figure 2.4). In contrast, regenerating fins injected with the *esco2*-MO exhibited a significant decrease in regenerate length compared to uninjected controls within the same fins (Figures 2.4), documenting that *esco2* is critical for fin regeneration.

Roberts syndrome patients exhibit significant bone growth deficiencies -

especially in the arms and legs (Mehta et al, 2013; Horsfield et al, 2012). Thus, it became

important to quantify the extent that *esco2* depletion may specifically impact bone

segment growth in regenerating fins. To address this question, segment length was

measured in uninjected, *esco2*-MM and *esco2*-MO injected fins. The results show that

segment length in uninjected fish was nearly identical to that of *esco2*-MM injected fish

(Figure 2.4). However, segment length was significantly reduced in *esco2*-MO injected

fish compared to the uninjected side of the same fish fins (Figure 2.4). Thus, *esco2* is

critical for bone growth in regenerating fin, consistent with its role in skeletal

development in humans.

To confirm that the *esco2*-MO was effective in reducing Esco2 protein levels, I

generated an antibody against Esco2 and verified its specificity using bacterial lysates

expressing GST-Esco2. The results show that anti-Esco2 antibody recognizes GST-

Esco2, which migrates at the predicted size of 94 kDa. The anti-GST antibody also

recognizes the GST-Esco2 band at the predicted size of 94 kDa and a 26 kDa band in the

GST alone lane (Figure 2.5). The anti-Esco2 antibody does not recognize GST alone. To

confirm the specificity of the anti-Esco2 antibody, a peptide competition assay was

performed. Esco2-directed antibody was pre-incubated with the peptide that the antibody

was generated against. The resulting competed antibody produced a greatly reduced

signal, compared to non-competed antibody, when used to detect GST-Esco2, confirming

antibody specificity (Figure 2.5). Upon validating the specificity of the Esco2-directed

antibody, I tested the effectiveness of the *esco2*-MO to knockdown Esco2 levels in vivo.

At 3 dpa, fins were injected with either *esco2*-MM or *esco2*-MO and harvested the next

day (1 dpe/4 dpa) to prepare fin lysate (see also Figure 2.3). The lysates were used to test for Esco2 reduction by western blot. Quantification of the resulting western blots shows that the *esco2*-MO reduces Esco2 protein levels by approximately 70% while robust levels of Esco2 persist in MM injected fins (Figure 2.5). The results of the Western blot analyses document the efficacy of the *esco2*-MO to significantly reduce Esco2 protein levels.

Role of *esco2* in cell proliferation and programmed cell death

Reduced tissue and bone segment growth in regenerating fins could be due to decreased cell proliferation, increased programmed cell death (PCD), or both. In order to address possible changes in the level of cell proliferation, I evaluated both 5-bromo-2'-deoxyuridine (BrdU) as a marker for S-phase (Iovine et al, 2005) and histone-3-phosphate (H3P) as a marker for M phase (Wei et al, 1999). Morpholino-injected fish (where half of the fin was injected with either *esco2*-MO or *esco2*-MM, see also Figure 2.3) were allowed to swim in water supplemented with BrdU at 1 dpe/4 dpa and harvested on the same day. To quantify BrdU staining through which BrdU incorporation could be directly compared between the two fin halves, I compared the ratio of the BrdU-positive domains in the regenerating tip to the total regenerate length. As expected, *esco2*-MM injected and uninjected fins exhibited nearly identical ratios of BrdU labeled cells to regenerate fin length. In contrast, *esco2*-MO injected and uninjected sides produced a significant decrease in the ratio of BrdU labeled cells to regenerate length (Figure 2.6). Next I evaluated H3P-positive cells at 1 dpe/4 dpa (see also Figure 2.3). To compare H3P-positive cells between *esco2*-MM and MO injections in fin halves of the

61

same fine, I counted the total number of H3P-positive cells in the 250 mm area that defines the proliferative blastema, normalizing for the area (Nechiporuk et al, 2003). Regenerating fins in which one fin half was uninjected and the other half injected with *esco2*-MM exhibited nearly identical numbers of H3P-positive cells within this defined area (Figure 2.6). In contrast, the *esco2* MO-injected side exhibited a statistically significant reduced level of H3P-staining cells compared to the uninjected sides of the fins (Figure 2.6). Thus, cell proliferation appears to play a critical role in skeletal regrowth defects that occur in regenerating fins depleted of Esco2.

To address the possibility that PCD is increased in Esco2 depleted fins, fins were injected with either *esco2*-MM or *esco2*-MO on one half of the fin, the other half uninjected, and the fins were harvested 1 dpe/4 dpa for TUNEL staining (see also Figure 2.3). Importantly, I did not detect a noticeable difference in the number of TUNEL-positive cells between the *esco2*-MO injected side and the uninjected side of the same fins (Figure 2.7). Statistical analysis confirms that similar numbers of apoptotic cells are present in Esco2 knockdown and uninjected sides of the same fins (Figure 2.7). Thus, it appears, that regenerate and bone growth defects that occur upon Esco2 knockdown can be separated from increased levels of PCD.

esco2 and *cx43* appear to function in a common pathway

The pattern of *esco2* expression and localization during fin regeneration, coupled with impact of *esco2* depletion on bone segment regrowth, are strikingly similar to those previously reported for *cx43* mutations that cause the *short fin* (*sof*[b123]) phenotype (Iovine et al, 2005; Hoptak-Solga et al, 2008). Could Esco2 and Cx43 function in a common pathway to influence

bone segment growth? To address this possibility, I first tested whether Esco2 function is

downstream of Cx43. If true, then *esco2* expression might be reduced in *sof*^{*b123*} mutant fins.

Whole mount *in situ* hybridization was performed to monitor *esco2* message levels in wild type

(WT) and *sof*^{*b123*} regenerating fins. The results show that *esco2* expression levels are nearly

identical in regenerating WT and *sof*^{*b123*} fins (Figure 2.8), suggesting that *esco2* is not

downstream of *cx43*. An alternate possibility is that *cx43* is downstream of *esco2*. Whole mount

in situ hybridization was performed on Esco2 knockdown fins (1 dpe/4 dpa, see also Figure 2.3)

to determine if *cx43* expression is reduced in the half of the fin injected with *esco2*-MO (Figure

2.9). Indeed, *cx43* was reduced in fin rays injected with *esco2*-MO and not reduced in either

MM control or uninjected controls (Figure 2.9). To independently test for *cx43* dependency on

esco2, I performed qRT- PCR at 1 dpe/4 dpa (see also Figure 2.3). The results from 3

independent Esco2 knockdown samples show that *cx43* is significantly down regulated in Esco2

knockdown regenerating fins (Table 2.1; Figure 2.10). Since reduced cell proliferation is not

sufficient to cause reduced *cx43* expression (Govindan & Iovine, 2014; Bhadra & Iovine, 2015),

the observed reduction of *cx43* expression is not likely the result of reduced cell proliferation in

Esco2 knockdown fins. In combination, these findings support a model where Cx43 acts

downstream of, and may be regulated by, Esco2.

  To further examine the possibility that Esco2 and Cx43 function in a common

pathway, I next evaluated expression of both *semaphorin3d* (*sema3d*) and *hyaluronan*

and proteoglycan link protein 1a (*hapln1a*), two genes recently found to function

downstream of *cx43* (Ton & Iovine, 2013; Govindan & Iovine, 2014). If *esco2* is required

for *cx43* expression, then *esco2* depletion should also repress these *cx43* targets. I

examined the expression levels of *sema3d* and *hapln1a* using qRT-PCR on 3 dpa

regenerating fins injected with *esco2*-MO compared to the standard control morpholino. The results show that both *sema3d* and *hapln1a* are significantly down regulated in MO-injected regenerating fins (Table 2.1; Figure 2.10), consistent with the model that Esco2 regulates Cx43 signaling pathways that are critical for development. To exclude the possibility that Esco2 depletion represses all gene expression, I evaluated expression levels of three genes not known to be *cx43*-dependent, *sonic hedgehog* (*shh*), *sprouty 4* (*spry4*) and *mono polar spindle* (*mps1*) (Laforest et al, 1998; Lee et al, 2005; Poss et al, 2002). Expression levels of these genes are not reduced, demonstrating that Esco2 depletion does not lead to global gene repression. Both *shh* and *spry4* appear to be modestly upregulated, which could suggest either that Esco2 antagonizes these genes or that Esco2-dependent disruption of cell proliferation indirectly affects gene expression in these pathways. In combination, these results reveal that Esco2 acts as a transcriptional regulator with targets that include *cx43*.

If *cx43* truly acts downstream of Esco2 and *cx43* reduction in part mediate the bone growth defects observed upon Esco2 knockdown, then I reasoned that *cx43* overexpression might attenuate the regenerate and bone segment growth defects in regenerating fins. To test this prediction, I next attempted to rescue *esco2*-dependent skeletal growth defects by overexpression of *cx43*. I utilized the *Tg*(*hsp70:miR-133sp* [pd48]) line that harbors an EGFP cDNA followed by three miR-133 binding sites (Ebert et al, 2007; Loya et al, 2009). Prior studies found that miR-133 knockdown via this "sponge" transgene increases *cx43* levels during zebrafish heart regeneration (Yin et al, 2012). I confirmed upregulation of both *cx43* mRNA and Cx43 protein in regenerating fins of this transgenic line treated for heat shock (Figure 2.11). Moreover, to rule out the

possibility that increased Cx43 leads to an increase in Esco2, I further confirmed that the levels of *esco2* mRNA and Esco2 protein are not upregulated in this transgenic line treated for heat shock (Figure 2.11).

Either transgenic-positive (Tg+) or transgenic-negative (control siblings, Tg-) fins were treated for Esco2 knockdown (Figure 2.12). Four hours post electroporation, Tg+ and Tg- fish were both heat shocked (HS+) at 37°C for 1 hour. These fish are denoted as Tg+HS+ and Tg-HS+, respectively. Alternatively, a second group of Esco2 knockdown Tg+ fish was not heat shocked and thus denoted as Tg+HS-. To demonstrate that heat shock alone does not rescue *esco2*-dependent phenotypes, I performed Esco2 knockdown in Tg-HS+. Results from 3 independent trials show that Esco2 knockdown in Tg-HS+ exhibited the predicted growth defects for regenerate fin and bone segment lengths (i.e. the percent similarity between the Esco2 knockdown side and the uninjected side is low) (Figure 2.12). In contrast, Esco2 knockdown followed by induction of the transgene (causing *cx43* over-expression) in Tg+HS+, exhibited increased regenerate length and segment length, demonstrating Cx43-dependent rescue of the Esco2 knockdown phenotypes (i.e. the percent similarity between the Esco2 knockdown side and the uninjected side is significantly increased when *cx43* is overexpressed). I performed the same experiment using *esco2*-MM construct as a negative control. As expected, I did not observe skeletal phenotypes in these fins (data not shown). In order to demonstrate that the rescue of phenotype is heat shock dependent and therefore requires overexpression of *cx43*, I performed the same Esco2 knockdown experiment in the absence of heat shock in Tg+ fish (Tg+HS-). Importantly, I did not observe rescue of skeletal phenotypes in fish that carry the transgene but in which I do not induce its expression via the heat pulse

(Figure 2.12). The combination of these experiments provide compelling evidence that

Esco2 and Cx43 function in a common pathway, and that the observed *esco2*-dependent

skeletal phenotypes are at least partially mediated by reduced *cx43* expression.

2.5 Discussion

Cohesinopathies are a growing collection of severe and phenotypically pleiotropic developmental maladies, but at present the molecular mechanisms through which cells and developing organisms respond to cohesion mutations remains unclear (Mehta et al, 2013; Horsfield et al, 2012; Dorsett & Merkenschlager, 2013; Barbero, 2013). For instance, CdLS appears to arise through transcriptional deregulation that occurs in response to heterozygous or X-linked mutations in *NIPBL*, *SMC1*, *SMC3, RAD21, HDAC8 or PDS5* (Krantz et al, 2004; Musio et al, 2006; Tonkin et al, 2004; Deardorff et al, 2007; Deardorff et al, 2012a,b; Gillis et al, 2004; Zhang et al, 2009). In contrast, the sister cohesinopathy RBS, which arises through homozygous mutation of *ESCO2* (Schule et al, 2005; Gordillo et al, 2008; Vega et al, 2005), is thought to arise instead through reduced progenitor cell proliferation and increased mitotic failure and apoptosis (Mehta et al, 2013; Horsfield et al, 2012; Whelan et al, 2012). My current studies suggest that Esco2 is a critical and specific transcription regulator – leading us to speculate that RBS is most likely a transcriptional deregulation malady. Support for this model is three-fold. First, Esco2 knockdown reduces transcription of specific cell signaling pathways such as *cx43*, mutations in which disrupt proper development (Paznekas et al, 2003; Musa et al, 2009; Iovine et al, 2005), but not other developmentally relevant signaling pathways such as *shh* (Table 2.1; Figure 2.10). Second, recent evidence reveals that Esco2 regulates Notch signaling through binding/sequestration of the intracellular Notch domain (Leem et al, 2011). Notch is required for neuronal differentiation, skeletal development and hematopoietic lineages – consistent with pleiotropic phenotypes that result in both *esco2* and *notch* mutations (Zanotti & Canalis, 2013). Third, my results reveal no significant

increase in the incidence of apoptotic cells following Esco2 knockdown in the blastemal compartment of regenerating fins. At present, I cannot exclude the possibility that a small increase in apoptotic cells is masked by a low but consistent background level required for remodeling in the regenerating fin, but the fact that elevated levels were not discernible in MO-injected fins compared to MM-injected and uninjected matched-fin controls suggests instead that the effects on fin and bone segment regeneration can occur independent of apoptosis. These findings contrast studies involving Esco2 knockdown in zebrafish and medaka embryos and mice in which reproducible elevations in apoptotic cells were reported (Monnich et al, 2011; Morita et al, 2012; Whelan et al, 2012). However, the effects in those studies are modest. ESCO2 knockdown in mice neuroeptihelium, for instance, produced severe microcephaly but succeeded in inducing only a 2-fold increase in the number of apoptotic cells (Whelan et al, 2012). In zebrafish embryos, *esco2* depletion resulted in Caspase 8 activation that was temporally limited (Monnich et al, 2011). Esco2 depletion also resulted in a 4-fold increase in the number of apoptotic cells in zebrafish embryos and global induction of apoptosis in medaka embryos, but such increases that occur in inviable or failing embryos are plausibly downstream events indirectly coupled to *esco2* effects (Monnich et al, 2011; Morita et al, 2012). Thus, it remains possible that apoptosis is not the major clinically relevant etiologic effect of *esco2* mutation in RBS patients, especially since apoptosis is not a feature of CdLS cells (Tonkin et al, 2004; Castronovo et al, 2009; Revenkova et al, 2009). I hypothesize that the transcriptional deregulation that arises from *ESCO2* mutations may be the underlying etiologic basis for the developmental abnormalities of RBS - upon which are overlaid cohesion defects, mitotic failure and apoptosis.

Currently, mutation of *ESCO2* represents the sole etiologic agent of the severe developmental disorder Roberts Syndrome (RBS) in humans (Vega et al, 2005). I posit that a second revelation from this work is that Esco2 may be an upstream regulator of Cx43 function in zebrafish regenerating fins. For instance, *esco2* depletion not only reduces *cx43* expression, but also expression of *sema3d* and *hapln1a,* two genes in the bone growth signaling pathways that rely upon Cx43. Conversely, genes that appear independent of Cx43, such as *shh*, *spry4* and *mps1* were not reduced in Esco2 knockdown regenerating fins. Notably, the spatial and temporal expressions of *esco2* and *cx43* are nearly identical within the regenerating fin (Iovine et al, 2005). Moreover, the demonstration that overexpression of *cx43* rescues *esco2*-dependent skeletal phenotypes strongly suggests that Esco2 and Cx43 function in a common pathway. If this model is correct that Esco2-dependent expression of Cx43 is an important factor in human development, then *cx43* mutation should similarly manifest developmental abnormalities. In fact, mutations of human *CX43* cause Oculodentodigital dysplasia (ODDD), a malady that includes craniofacial dysmorphias, distal limb skeletal growth defects and abnormal eye and teeth development (Paznekas et al, 2003; Musa et al, 2009). I note prior studies in which mutation/depletion of either *esco2*, *nipbl* or *rad21* were found to impact a plethora of developmentally relevant genes, including *CX43/GJA1* – observations that helped to inform the current work (Monnich et al, 2011; Kawauchi et al, 2009). My findings suggest that Esco2 function may be coupled to a Cx43-dependent signaling pathway previously shown to directly promote proper development. Based on these results, I suggest that ODDD could be a mild form of cohesinopathies.

Conservatively, this work is consistent with a model that Esco2 regulates the expression of *cx43* and its downstream targets (i.e. *sema3d* and *hapln1a*), thereby influencing growth and skeletal patterning (Figure 2.13). Future experiments to test this model include measuring *cx43* expression level in RBS patient cells and directly assessing *esco2* localization/regulation of the *cx43* promoter. Alternatively, the impact of Esco2 on the skeleton may occur through its roles in DNA damage repair, DNA replication fork progression, chromosome compaction or ribosome maturation/assembly (Skibbens et al, 1999; Skibbens et al, 2010; Gard et al, 2009; Bose et al, 2012; Terret et al, 2009; Unal et al, 2004; Strom et al, 2004; Gerton, 2012; Skibbens et al, 2013).
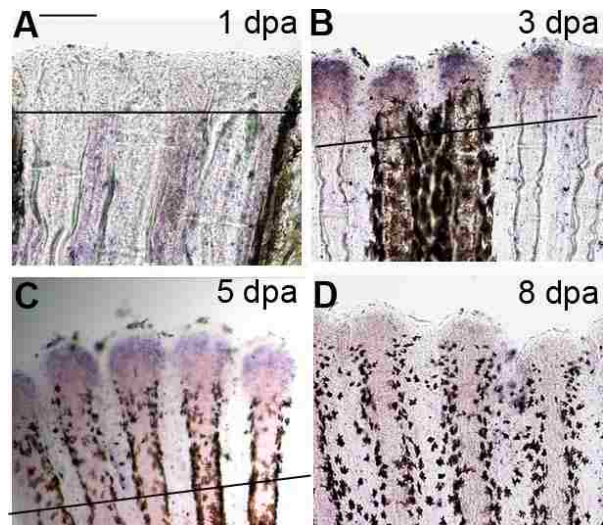
Figure 2.1: Time course *in situ* hybridization of *esco2* in whole mount regenerating fins. (A) *esco2* expression in 1 day post amputated (dpa) regenerating fin was largely not detectable. (B) *esco2* expression in 3 dpa regenerating fin was strongly detected at the distal end and (C) began to gradually decline in 5 dpa regenerating fin. (D) Expression of *esco2* was reduced in regenerating fin by 8 dpa. The amputation plane is indicated by a solid line except in 8 dpa regenerating fin (panel D), where it is out of the field of view. Scale bar is 50 µm.
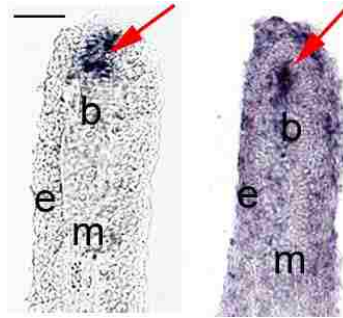
Figure 2.2: *In situ* **hybridization of** *esco2* **in fin cryosections.** (Left) Cryosection from a whole mount wild-type (WT)-5 dpa *in situ* hybridized fin showing tissue specific expression of *esco2* mRNA within the blastema compartment. (Right) *In situ* hybridization was completed on a WT-5 dpa fin cryosection showing a similar pattern of *esco2* expression localized specifically at the blastemal region. Arrows indicate *esco2* expression at blastema. b- blastema, e- epidermis, m- mesenchyme. Scale bar is 50 μm.
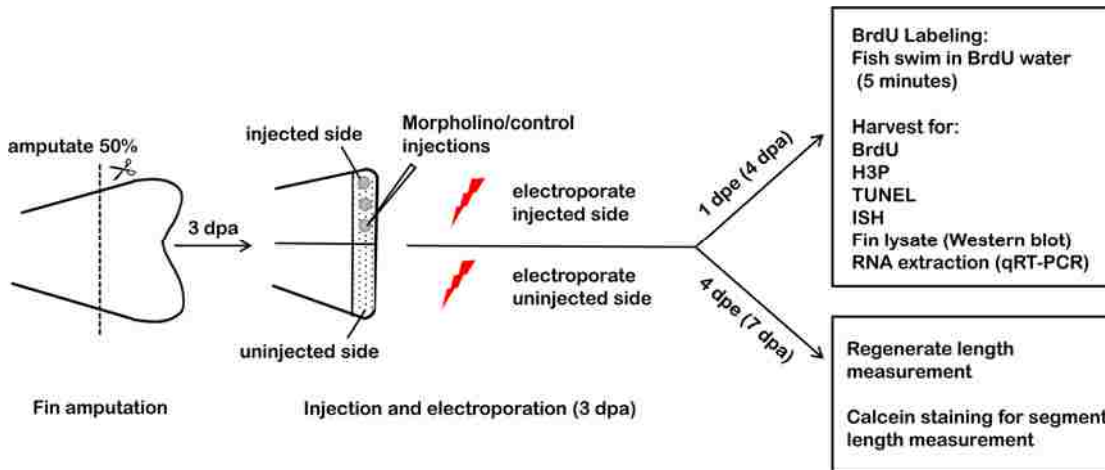
Figure 2.3: Timeline of experimental procedure. Fins were amputated at 50% level and allowed to regenerate for 3 days. At 3 dpa, either gene-targeted morpholino or a control morpholino (MO) was injected to one half of the regenerating fin, immediately followed by electroporation on both sides. After 24 hours,1 day post electroporation (1 dpe/4 dpa), the fins were evaluated by fluorescence microscopy to confirm MO uptake. The fins were harvested at 1 dpe/4 dpa for histone-3-phosphate (H3P) assay, Terminal deoxynucleotidyl transferase dUTP nick end labeling (TUNEL) assay, in situ hybridization (ISH), and fin lysate preparation for protein expression by western blot and RNA extraction for quantitative real time PCR (qRT-PCR). Note that for protein lysates and for qRT-PCR, all fin rays across the fin were injected with morpholino and electroporated prior to harvesting at 1 dpe/4 dpa. For 5-bromo-2'-deoxyuridine (BrdU) labeling the MO-injected fins were allowed to swim in 50µg/ml of BrdU water for 5 minutes at 1 dpe/4 dpa and harvested on the same day. For regenerate length and segment length analysis fins were allowed to regenerate longer and were calcein stained at 4 dpe/7 dpa. For each experiment at least 6-8 fish were used per trial and at least 3 independent trials were performed.
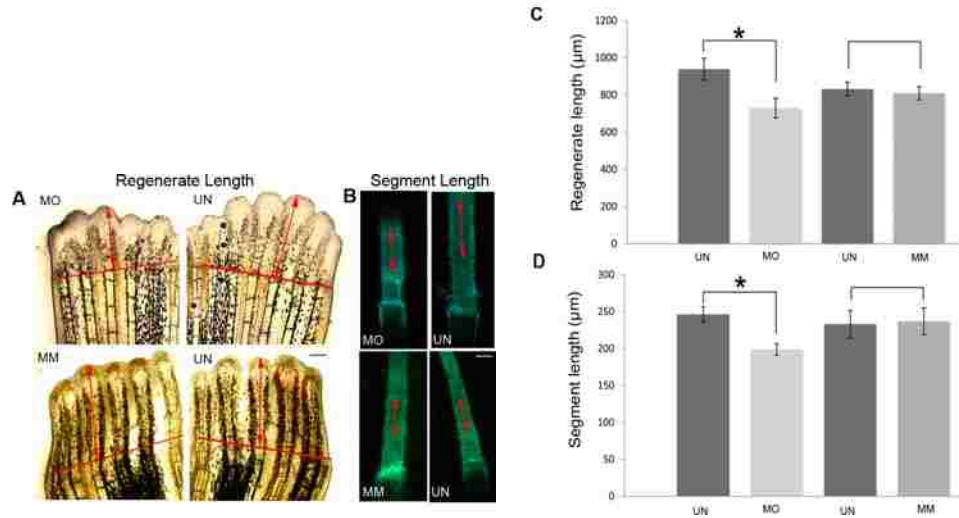
Figure 2.4: Morpholino mediated Esco2 knockdown phenotypes include reduction in regenerate length and bone segment length. (A) Representative images showing decreased regenerate length in *esco2* morpholino (MO) injected half compared to the uninjected (UN) half of the same fin. (B) Representative images showing similar levels of regeneration in fins injected with *esco2* mismatch (MM) MO compared to the UN half of the same fin. The red line indicates the amputation plane. Arrows indicate the distance from the amputation plane to the distal end of the 3rd fin ray. (C) Representative images of calcein stained segments of the 3rd fin ray show shorter bone segments in MO-injected fin half compared to the UN half of the same fin. (D) Representative images of calcein stained segments of the 3rd fin ray of MM-injected and UN fins reveal bone segments of similar lengths. For all experiments 6-8 fish were used per trial and at least 3 independent trials were performed. The MO/MM was injected/electroporated in 3 dpa fins and was allowed to regenerate for 4 days. For regenerate length and segment length measurements the fins were calcein stained at 4 dpe/7 dpa. For calcein staining, fish were allowed to swim for 10 minutes in 0.2% calcein (pH 7) at room temperature followed by fresh system water for another 10 minutes. (E) Graph reveals significant reduction (*) in regenerate length in MO treated fins compared to UN fins. Regenerate length of MM treated fins and UN fins show no significant differences in length. (F) Graph shows significant reduction (*) in segment length between MO treated fins and UN fins. The segment length of MM treated fins and UN fins show no significant difference. Student's t-test was used for determining statistical significance where $p < 0.05$. Error bars represent standard error. Scale bar is 50 µm.

74
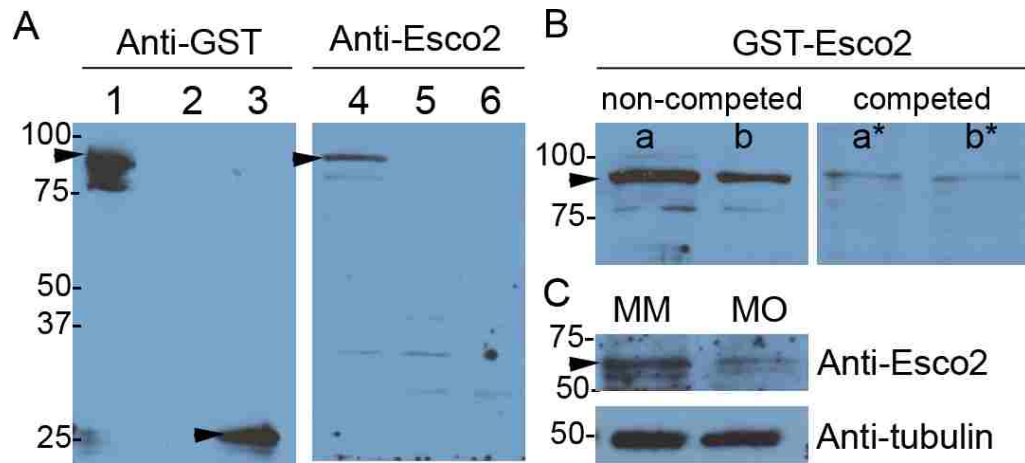
Figure 2.5: The Esco2 antibody is specific and MO-mediated Esco2 knockdown results in decreased levels of Esco2 protein. (A) Western blot of bacterial lysates expressing either GST-Esco2 or GST. Lanes 1 and 4 are lysates of induced GST-Esco2. Lanes 2 and 5 are lysates of uninduced GST-Esco2. Lanes 3 and 6 are lysates of induced GST. When probed with either the anti-Esco2 antibody or an anti-GST antibody, a major protein band of the predicted size of 94 kDa (indicated by an arrowhead) is detected in the induced GST-Esco2 lysates (lanes 1 and 4), and not in the uninduced GST-Esco2 lysates (lanes 2 and 5). Additional bands below 94 kD likely represent proteolysis of GST-Esco2. The anti-Esco2 antibody does not detect GST alone, which has a molecular weight of 26 kD (compare lanes 3 and 6). (B) Two volumes of bacterial lysates expressing GST-Esco2 were loaded in two identical gels. Pre-incubation of the anti-Esco2 antibody with the Esco2 peptide (competed lanes a* and b*) significantly reduced the antibody binding compared to non-competed antibody (lanes a and b). The 94 kDa bands are marked (arrowhead). (C) Western blot reveals that anti-Esco2 antibody detects a major protein band at 68 kDa from fin lysate prepared from mismatch (MM) control morpholino injected fins and Esco2 knockdown (MO) fins (1 dpe/4 dpa). The blot confirms the reduction of Esco2 protein in the knockdown lysate (MO) compared to the control lysate (MM). The presence of additional bands in the fin lysates may be due to modification or degradation. Tubulin was used as a loading control. The single band marked was used for relative band intensity analysis using the gel analysis tool (ImageJ software). Similar findings were observed in each of three trials.
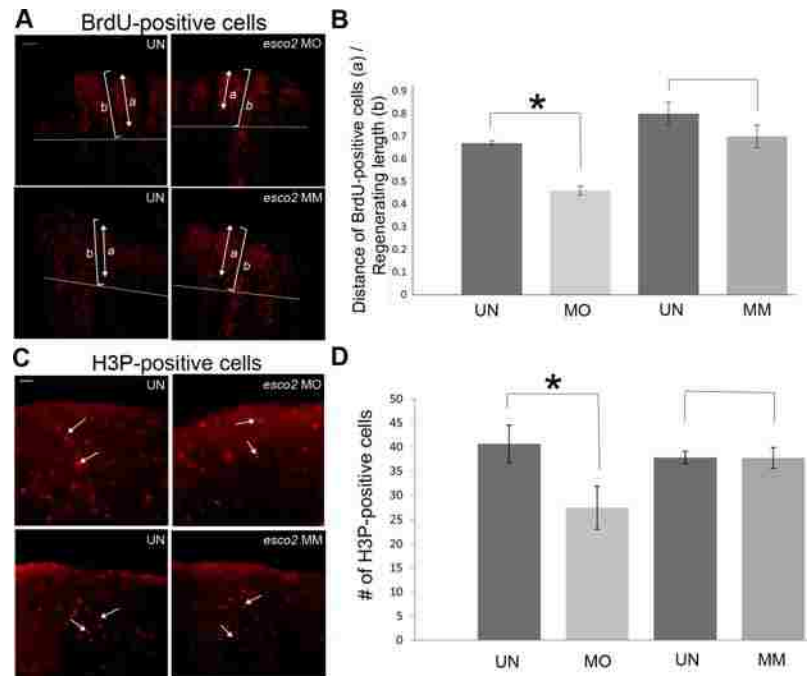
Figure 2.6: Role of *esco2* in cell proliferation. (A) (Top) Representative images of BrdU-positive cells in uninjected (UN) and *esco2*-MO injected (MO) fins. (Bottom) Representative images of BrdU-positive cells in uninjected (UN) and MM injected fins. Briefly, the MO/MM was injected/electroporated in 3 dpa fins and the next day (1 dpe/4 dpa) the fish were allowed to swim in 50µg/ml BrdU water for 5 mins and then harvested. For all the experiments at least 6-8 fins were used per trial and at least 3 independent trials were performed. The arrow indicates the span of the BrdU-positive cells from the tip of the 3rd fin ray (a) and the bracket indicates total regenerate length of the 3rd fin ray (b) The amputation plane is shown by a horizontal line. (B) Graph shows the significant reduction (*) in a/b ratio of BrdU-positive cells in MO injected fins compared to the UN fins. The difference between the MM treated fins and the UN fins is not significantly different. Student's t-test was used for determining statistical significance where $p < 0.05$. Error bars represent standard error. Scale bar is 100 µm. (C) (Top) Representative images of H3P-positive cells in uninjected (UN) and *esco2*-MO injected (MO) fins. (Bottom) Representative images of H3P-positive cells in uninjected (UN) and MM injected fins. The arrows indicate single H3P-positive cells. At least 6-8 fins were used per trial and 3 independent trials were performed. The MO/MM was injected in 3 dpa fins and harvested at 1 dpe/4 dpa. H3P- positive cells were counted by eye from within the distal-most 250µm of the 3rd fin ray as previously established. (D) Graph shows the significant reduction (*) in the average number of H3P-positive cells in MO injected fins compared to the UN fins. The difference between the MM treated fins and the UN fins is not significantly different. Student's t-test was used for statistical analysis where $p < 0.05$. Error bars represent standard error. Scale bar is 50 µm.
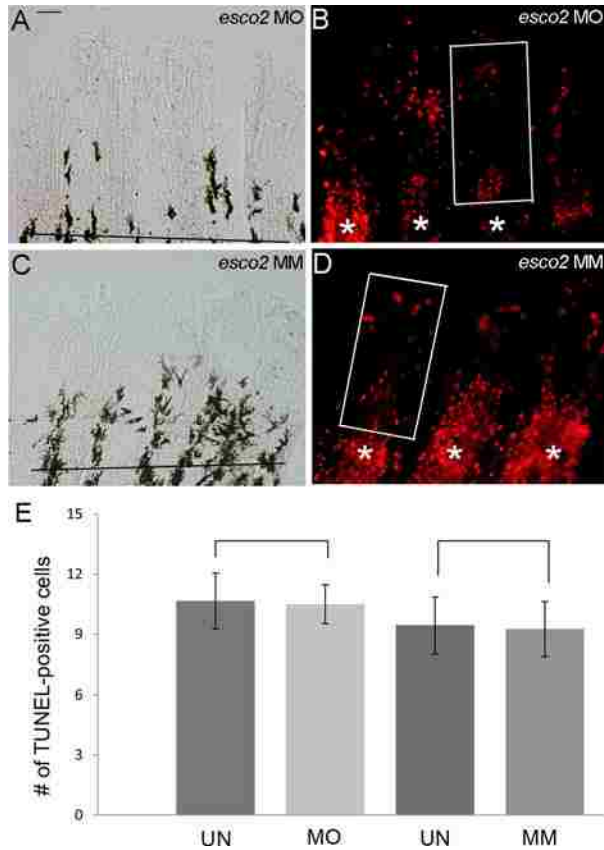
Figure 2.7: Role of *esco2* in programmed cell death. Representative bright-field image (A) and TUNEL-positive cells (B) in *esco2*-MO injected fin. Representative bright-field image (C) and TUNEL-positive cells (D) in MM injected fins. At least 6-8 fins were used per trial and 3 independent trials were performed. The MO/MM was injected in 3 dpa fins and harvested at 1 dpe/4 dpa. TUNEL- positive cells were counted by eye from within the distal-most 250μm of the 3rd fin ray. The amputation plane is shown by a horizontal line and * indicates the individual fin rays. High levels of TUNEL-positive cells located at the amputation plane serve as an internal control for staining. The box represents the area used to count the cells. (E) Graph shows similar average numbers of TUNEL-positive cells in either MO injected fins or the MM injected fins, compared to the UN fins. Student's t-test was used for determining statistical significance where $p < 0.05$. Error bars represent standard error. Bracketed comparisons were not significant. Scale bar is 50 μm.
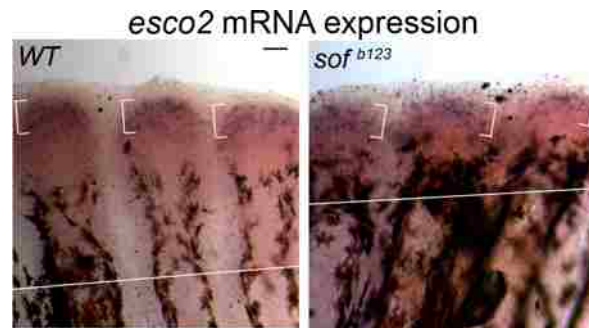
**Figure 2.8: Expression of *esco2* mRNA in wild-type (WT) and *short fin* (*sof* [b123])
fins by whole mount *in situ* hybridization.** WT and *sof* [b123] fins were amputated at
50% level and allowed to regenerate for 5 days. At 5 dpa the fins were harvested. At
least 6-8 fins were used per trial and 3 independent trials were performed. (Left)
Whole mount *in situ* hybridization (ISH) on WT-5 dpa regenerating fin showing
esco2 expression. (Right) Whole mount ISH on *sof* [b123] -5 dpa regenerating fins
shows similar expression levels of *esco2*. The brackets represent the zone of *esco2*
expression. Scale bar is 50 µm.
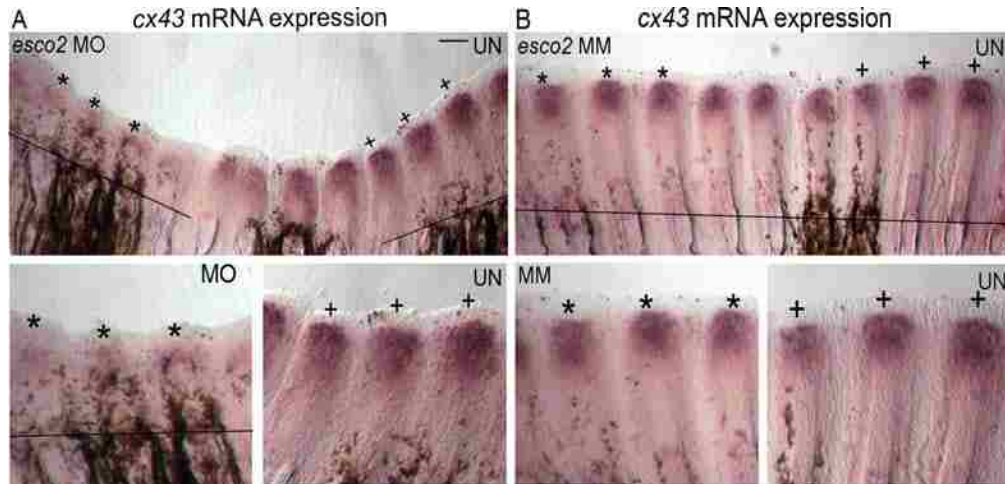
Figure 2.9: *In situ* **hybridization on morpholino mediated Esco2 knockdown fins shows reduced levels of *cx43* expression.** The MO/MM was injected in 3 dpa fins and fins were harvested at 1 dpe/4 dpa. Black lines identify the amputation plane unless it is out of the field of view (i.e. as occurs in most of the higher magnification images). The fin in panel A appears curved since there was less growth on the Esco2 knockdown side compared with the uninjected side. (A) (Top) Representative image of a fin with Esco2 knockdown side (*esco2* MO) showing decreased staining of *cx43*, compared to the uninjected side (UN). Bottom left- Higher magnification of the knockdown side (MO) of the same fin (fin rays from top image marked by *) showing reduced *cx43* expression. (Bottom right) Higher magnification of the uninjected side (UN) of the same fin (fin rays from top image marked by + showing robust *cx43* expression. (B) (Top) Representative image of a fin microinjected with *esco2*-MM in one half and the other side uninjected (UN) reveal similar levels of *cx43*. (Bottom left) Higher magnification of the *esco2*-MM injected side (MM) of the same fin (fin rays from top image marked by *) showing *cx43* expression. (Bottom right) Higher magnification of the uninjected side (UN) of the same fin (fin rays from top image marked by + showing similar *cx43* expression levels. Scale bar is 100 μm.
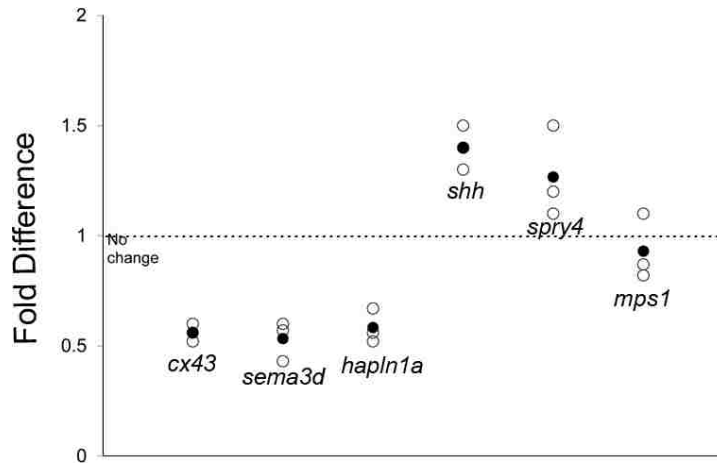
Figure 2.10: *cx43* and *cx43*-dependent target genes are reduced following Esco2 knockdown. The fold difference values from qRT-PCR are shown. A fold difference of 1 indicates no change with respect to standard MO treated fins. Three independent Esco2 knockdown (KD) samples were prepared. Each sample was tested in duplicate (trials 1-3) for *cx43, sema3d, hapln1a, shh, spry4* and *mps1*, and compared to the internal reference gene. Circles represent the individual trials and solid circles represent the averages.
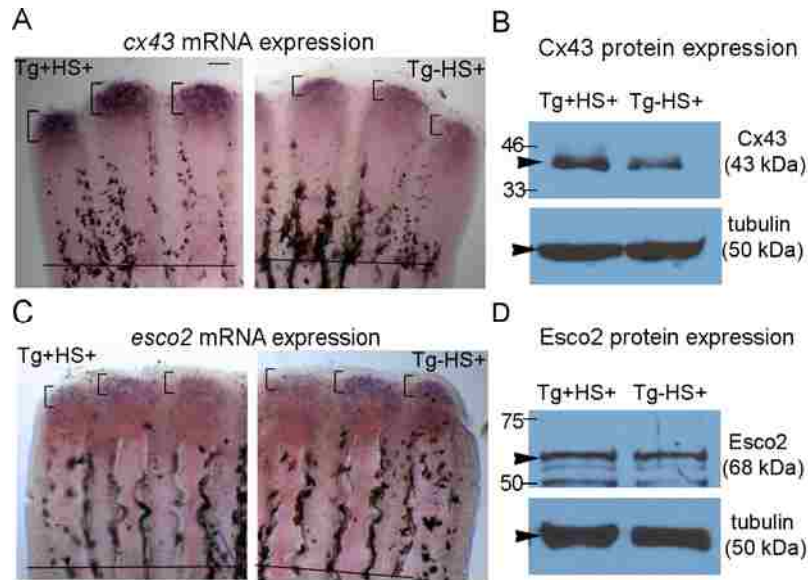
Figure 2.11: Upregulation of both *cx43* mRNA and Cx43 protein in regenerating fins of the transgenic line treated for heat shock. (A) Expression of *cx43* mRNA in transgenic *hsp70:miR-133sp^{pd48}*-positive (Tg+HS+) and *hsp70:miR-133sp^{pd48}*-negative (Tg-HS+) fins by whole mount ISH. The Tg+HS+ fins show a higher expression of *cx43* mRNA compared to Tg-HS+ fins. The brackets mark the zone of *cx43* expression in each fin ray and the horizontal line represents the amputation plane. Scale bar is 50 μm. (B) Western blot reveals a 50% upregulation of Cx43 protein levels in fin lysates of Tg+HS+ compared to Tg-HS+. Tubulin was used as a loading control. The bands marked were used for relative band intensity analysis using the gel analysis tool (ImageJ software). (C) Expression of *esco2* mRNA in transgenic *hsp70:miR-133sp^{pd48}*-positive (Tg+HS+) and *hsp70:miR-133sp^{pd48}*-negative (Tg-HS+) fins by whole mount ISH. Tg+HS+ and Tg-HS+ fins show similar expression level of *esco2* mRNA. The brackets mark the zone of *esco2* expression in each fin ray and the horizontal line represents the amputation plane. Scale bar is 50 μm. (D) Western blot reveals the Esco2 protein expression is nearly similar (90%) in fin lysates of Tg+HS+ and Tg-HS+. Tubulin was used as a loading control. The single band marked was used for relative band intensity analysis using the gel analysis tool (ImageJ software).
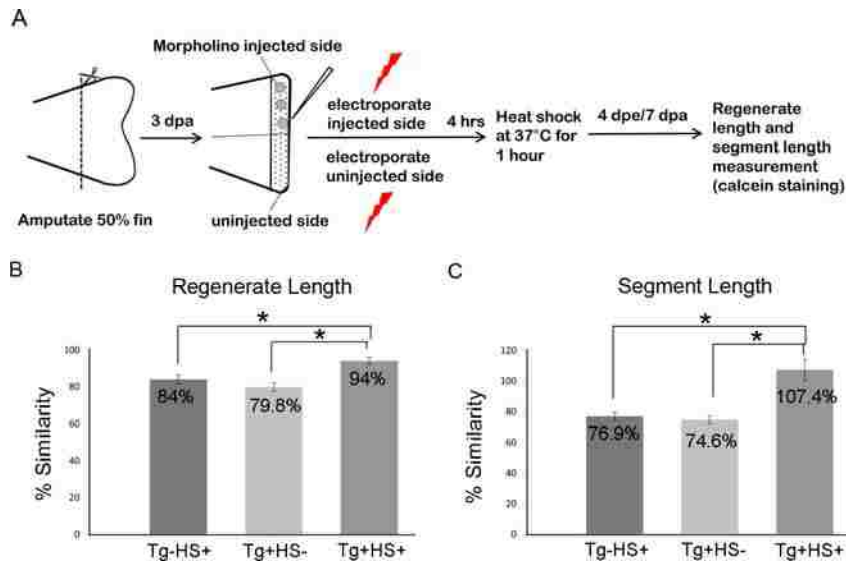
Figure 2.12: Overexpression of *cx43* rescues Esco2 knockdown phenotypes. (A) Figure depicting the timeline of fin amputation, morpholino injection and electroporation, heat shock, and data analysis. The 3 groups included in this experiment were Tg+HS- (transgenic *hsp70:miR-133sp^{pd48}*-positive, heat shocked), Tg-HS+ (transgenic *hsp70:miR-133sp^{pd48}*-negative, heat shocked) and Tg+HS- (transgenic *hsp70:miR-133sp^{pd48}*-positive, not heat shocked). Briefly, fins from all three groups were amputated at 50% level and allowed to regenerate for 3 days. At 3 dpa, morpholino was injected to one half of the regenerating fin tissue, immediately followed by electroporation on both sides. After an interval of 4 hours fish receiving heat shock were shifted to 37°C for 1 hour. Induction of the transgene expression upon heat shock was confirmed after 24 hours by screening for GFP-positive fins in the Tg+HS+ group. The control groups (Tg-HS+ and Tg+HS-) were negative for GFP expression. For ISH experiments, the fins were harvested at 1 dpe/4 dpa. For measurement of regenerate length and segment length fins were calcein stained at 4 dpe/7 dpa. For each experiment at least 6-8 fish were used per trial and at least 3 independent trials were performed (B) Graph reveals significant (*) rescue of *esco2*-dependent segment length defects in heat shocked *miR-133sp^{pd48}*-positive Esco2 knockdown fins (Tg+HS+) compared both to heat shocked transgene-negative (Tg-HS+) and to *miR-133sp^{pd48}*-positive with no heat shock (Tg+HS-). Measurements from the injected side and the uninjected side of the same fin were used to calculate percent similarity and the average was calculated for each group. Note that a percent similarity of 100% indicates no difference between the knockdown side and the control sides of the fin. Student's t-test was used for determining statistical significance where p < 0.05. Error bars represent standard error. (C) Graph reveals significant (*) rescue of *esco2*-dependent regenerate length defects in heat shocked *miR-133sp^{pd48}*-positive Esco2 knockdown fins (Tg+HS+) compared both to heat shocked transgene-negative (Tg-HS+) and to *miR-133sp^{pd48}*-positive in the absence of heat shock (Tg+HS-).
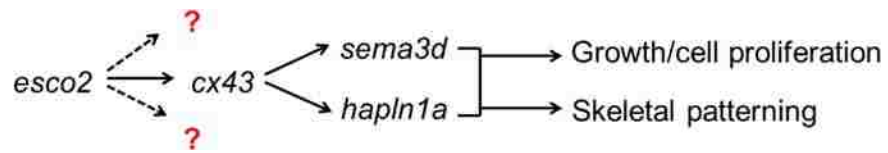
Figure 2.13: New model depicts the connection between Esco2 and Cx43 skeletal patterning pathway during fin regeneration. Proposed pathway for Esco2 regulation of *cx43* expression levels and genes downstream of *cx43*. Esco2 may have additional targets.

Gene	Average $C_{T(esco2\ KD)}$	Average C_T (keratin)	ΔC_T *esco2* KD -keratin[a]	ΔC_T *esco2* MM -keratin[a]	$\Delta\Delta C_T$ $\Delta C_{T(MO)}$- $\Delta C_{T\ (MM)}$[b]	Fold Difference relative to MM[c]
cx43	23.31 $\pm$ 0.11	17.14 $\pm$ 0.15	6.16 $\pm$ 0.19	5.21 $\pm$ 0.14	0.95 $\pm$ 0.24	0.51 (0.43 - 0.61)
sema3d	24.25 $\pm$ 0.15	17.25 $\pm$ 0.07	7.0 $\pm$ 0.16	6.05 $\pm$ 0.12	0.94 $\pm$ 0.21	0.52 (0.44 - 0.6)
hapln1a	24.43 $\pm$ 0.05	18.09 $\pm$ 0.04	6.34 $\pm$ 0.07	5.57 $\pm$ 0.42	0.85 $\pm$ 0.42	0.58 (0.43- 0.78)
mps1	22.27 $\pm$ 0.08	17.72 $\pm$ 0.08	4.55 $\pm$ 0.12	4.47 $\pm$ 0.34	-0.08 $\pm$ 0.36	0.94 (0.73 - 1.21)
shh	22.7 $\pm$ 0.1	19.51 $\pm$ 0.05	3.24 $\pm$ 0.11	3.53 $\pm$ 0.14	-0.28 $\pm$ 0.18	1.21 (1.07- 1.38)
spry4	23.3 $\pm$ 0.08	19.35 $\pm$ 0.1	3.91 $\pm$ 0.13	4.45 $\pm$ 0.31	-0.54 $\pm$ 0.34	1.45 (1.14- 1.85)

Table 2.1: Quantitative RT-PCR confirms changes in gene expression

a. The ΔC_T value is determined by subtracting the average Keratin C_T value from the average Gene C_T value. The standard deviation of the difference is calculated from the standard deviations of the gene and Keratin values using the Comparative Method.

b. The calculation of $\Delta\Delta C_T$ involves subtraction by the ΔC_T calibrator value. This is subtraction of an arbitrary constant, so the standard deviation of $\Delta\Delta C_T$ is the same as the standard deviation of the ΔC_T value.
c. The range given for gene relative to MM is determined by evaluating the expression: $2^\wedge -\Delta\Delta C_T$ with $\Delta\Delta C_T + s$ and $\Delta\Delta C_T - s$, where s = the standard deviation of the $\Delta\Delta C_T$ value.

2.7 References

Barbero JL. 2013. Genetic basis of cohesinopathies. Appl Clin Genet 6: 15-23.

Ben-Shahar TR, Heeger S, Lehane C, East P, Flynn H, Skehel M, Uhlmann F. 2008. Eco1- dependent cohesin acetylation during establishment of sister chromatid cohesion. Science 321(5888): 563-566.

Bhadra, J. and Iovine, M.K., 2015. Hsp47 mediates Cx43-dependent skeletal growth and patterning in the regenerating fin. *Mechanisms of development*, 138, pp.364-374.

Bose T, Lee KK, Lu S, Xu B, Harris B, Slaughter B, Gerton, JL. 2012. Cohesin proteins promote ribosomal RNA production and protein translation in yeast and human cells. PLoS genetics 8(6): e1002749.

Castronovo P, Gervasini C, Cereda A, Masciadri M, Milani D, Russo S, Larizza L. 2009. Premature chromatid separation is not a useful diagnostic marker for Cornelia de Lange syndrome. Chromosome research 17(6): 763-771.

Choi HK, Kim B J, Seo JH, Kang JS, Cho H, Kim ST. 2010. Cohesion establishment factor, Eco1 represses transcription via association with histone demethylase, LSD1. Biochemical and biophysical research communications 394(4): 1063-1068.

Deardorff MA, Kaur M, Yaeger D, Rampuria A, Korolev S, Pie J, Krantz ID. 2007. Mutations in cohesin complex members *SMC3* and *SMC1A* cause a mild variant of Cornelia de Lange syndrome with predominant mental retardation. Am J Hum Genet 80(3): 485-494.

Deardorff MA, Bando M, Nakato R, Watrin E, Itoh T, Minamino M, Shirahige K. 2012. *HDAC8* mutations in Cornelia de Lange syndrome affect the cohesin acetylation cycle. Nature 489(7415): 313-317.

Deardorff MA, Wilde JJ, Albrecht M, Dickinson E, Tennstedt S, Braunholz D, Kaiser FJ. 2012. *RAD21* mutations cause a human cohesinopathy. Am J Hum Genet 90(6): 1014-1027.

Dorsett D, Merkenschlager M. 2013. Cohesin at active genes: A unifying theme for cohesin and gene expression from model organisms to humans. Curr Opin Cell Biol 25(3): 327-333.

Du SJ, Frenkel V, Kindschi G, Zohar Y.2001. Visualizing normal and defective bone development in zebrafish embryos using the fluorescent chromophore calcein. Dev boil 238(2): 239-246.

Ebert MS, Neilson JR, Sharp PA. 2007. MicroRNA sponges: competitive inhibitors of small RNAs in mammalian cells. Nature methods 4(9): 721-726.

Gard S, Light W, Xiong B, Bose T, McNairn AJ, Harris B, Gerton, JL. 2009. Cohesinopathy mutations disrupt the subnuclear organization of chromatin. J Cell Biol 187(4): 455-462.

Gerhart SV, Eble DM, Burger RM, Oline SN, Vacaru A, Sadler KC, Iovine MK. 2012. The Cx43-like connexin protein Cx40. 8 is differentially localized during fin ontogeny and fin regeneration. PloS one 7(2): e31364-e31364.

Gerton JL. 2012. Translational mechanisms at work in the cohesinopathies. Nucleus 3(6): 520-525.

Gillis LA, McCallum J, Kaur M, DeScipio C, Yaeger D, Mariani A, Krantz, ID. 2004. *NIPBL* mutational analysis in 120 individuals with Cornelia de Lange syndrome

and evaluation of genotype-phenotype correlations. Am J Hum Genet 75(4): 610-623.

Gordillo M, Vega H, Trainer AH, Hou F, Sakai N, Luque R, Jabs EW. 2008. The molecular mechanism underlying Roberts syndrome involves loss of ESCO2 acetyltransferase activity. Hum Mol Genet 17(14): 2172-2180.

Goss RJ, Stagg MW. 1957. The regeneration of fins and fin rays in *fundulus heteroclitus*. J Exp Zool 136(3): 487-507.

Govindan J, Iovine MK. 2014. Hapln1a is required for Connexin43-dependent growth and patterning in the regenerating fin skeleton. PLoS One 9(2): e88574.

Haas HJ. 1962. Studies on mechanisms of joint and bone formation in the skeleton rays of fish fins. Dev Biol 5: 1-34.

Hoptak-Solga AD, Nielsen S, Jain I, Thummel R, Hyde DR, Iovine MK. 2008. *Connexin43* (*GJA1*) is required in the population of dividing cells during fin regeneration. Dev Biol 317(2): 541-548.

Horsfield JA, Print CG, Monnich M. 2012. Diverse developmental disorders from the one ring: Distinct molecular pathways underlie the cohesinopathies. Front Genet 3: 171.

Iovine MK, Higgins EP, Hindes A, Coblitz B, Johnson SL. 2005. Mutations in *connexin43* (*GJA1*) perturb bone growth in zebrafish fins. Dev Biol 278(1): 208-219.

Iovine MK, Johnson SL. 2000. Genetic analysis of isometric growth control mechanisms in the zebrafish caudal fin. Genetics 155(3): 1321-1329.

Ivanov D, Schleiffer A, Eisenhaber F, Mechtler K, Haering CH, Nasmyth K. 2002. Eco1 is a novel acetyltransferase that can acetylate proteins involved in cohesion. Current biology 12(4): 323-328.

Kawauchi S, Calof AL, Santos R, Lopez-Burks ME, Young CM, Hoang MP, Lander AD. 2009. Multiple organ system defects and transcriptional dysregulation in the *nipbl*(+/-) mouse, a model of Cornelia de Lange syndrome. PLoS Genet 5(9): e1000650.

Krantz ID, McCallum J, DeScipio C, Kaur M, Gillis LA, Yaeger D, Jackson LG. 2004. Cornelia de Lange syndrome is caused by mutations in *NIPBL*, the human homolog of *drosophila melanogaster nipped-B*. Nat Genet 36(6): 631-635.

Laforest L, Brown CW, Poleo G, Géraudie J, Tada M, Ekker M, Akimenko MA 1998. Involvement of the *sonic hedgehog*, *patched 1* and *bmp2* genes in patterning of the zebrafish dermal fin rays. Development 125(21): 4175-4184.

Lee Y, Grill S, Sanchez A, Murphy-Ryan M, Poss KD. 2005. Fgf signaling instructs position-dependent growth rate during zebrafish fin regeneration. Development 132(23): 5173-5183.

Leem YE, Choi HK, Jung SY, Kim BJ, Lee KY, Yoon K, Kim ST. 2011. Esco2 promotes neuronal differentiation by repressing Notch signaling. Cellular signalling 23(11): 1876-1884.

Liu J, Krantz ID. 2009. Cornelia de Lange syndrome, cohesin, and beyond. Clin Genet 76(4): 303-314.

Loya CM, Lu CS, Van Vactor D, Fulga TA. 2009. Transgenic microRNA inhibition with spatiotemporal specificity in intact organisms. Nature methods 6(12), 897-903.

Mannini L, Liu J, Krantz ID, Musio A. 2010. Spectrum and consequences of *SMC1A* mutations: The unexpected involvement of a core component of cohesin in human disease. Hum Mutat 31(1): 5-10.

Mehta GD, Kumar R, Srivastava S, Ghosh SK. 2013. Cohesin: Functions beyond sister chromatid cohesion. FEBS Lett 587(15): 2299-2312.

Monnich M, Kuriger Z, Print CG, Horsfield JA. 2011. A zebrafish model of Roberts syndrome reveals that Esco2 depletion interferes with development by disrupting the cell cycle. PLoS One 6(5): e20051.

Morita A, Nakahira K, Hasegawa T, Uchida K, Taniguchi Y, Takeda S, Yanagihara I. 2012. Establishment and characterization of Roberts syndrome and SC phocomelia model medaka (*Oryzias latipes*). Dev Growth Differ 54(5): 588-604.

Musa FU, Ratajczak P, Sahu J, Pentlicky S, Fryer A, Richard G, Willoughby CE. 2009. Ocular manifestations in oculodentodigital dysplasia resulting from a heterozygous missense mutation (L113P) in *GJA1* (*connexin43*). Eye (Lond) 23(3): 549-555.

Musio A, Selicorni A, Focarelli ML, Gervasini C, Milani D, Russo S, Larizza L. 2006. X-linked Cornelia de Lange syndrome owing to *SMC1L1* mutations. Nat Genet 38(5): 528-530.

Nechiporuk A, Keating MT. 2002. A proliferation gradient between proximal and msxb expressing distal blastema directs zebrafish fin regeneration. Development 129(11): 2607-2617.

Paznekas WA, Boyadjiev SA, Shapiro RE, Daniels O, Wollnik B, Keegan CE, Jabs EW. 2003. *Connexin 43* (*GJA1*) mutations cause the pleiotropic phenotype of oculodentodigital dysplasia. Am J Hum Genet 72(2): 408-418.

Poss KD, Nechiporuk A, Hillam AM, Johnson SL, Keating MT. 2002. *Mps1* defines a proximal blastemal proliferative compartment essential for zebrafish fin regeneration. Development 129(22): 5141-5149.

Revenkova E, Focarelli ML, Susani L, Paulis M, Bassi MT, Mannini L, Musio A. 2009. Cornelia de Lange syndrome mutations in *SMC1A* or *SMC3* affect binding to DNA. Hum Mol Genet 18(3): 418-427.

Rudra S, Skibbens RV. 2013. Chl1 DNA helicase regulates Scc2 deposition specifically during DNA-replication in. PLoS One 8(9): e75435.

Schule B, Oviedo A, Johnston K, Pai S, Francke U. 2005. Inactivating mutations in *ESCO2* cause SC phocomelia and Roberts syndrome: No phenotype-genotype correlation. Am J Hum Genet 77(6): 1117-1128.

Sims KJr, Eble DM, Iovine MK. 2009. Connexin43 regulates joint location in zebrafish fins. Dev Biol 327(2): 410-418.

Skibbens RV, Colquhoun JM, Green MJ, Molnar CA, Sin DN, Sullivan BJ, Tanzosh EE. 2013. Cohesinopathies of a feather flock together. PLoS Genet 9(12): e1004036.

Skibbens RV, Corson LB, Koshland D, Hieter P. 1999. Ctf7p is essential for sister chromatid cohesion and links mitotic chromosome structure to the DNA replication machinery. Genes Dev 13(3): 307-319.

Skibbens RV, Marzillier J, Eastman L. 2010. Cohesins coordinate gene transcriptions of related function within *Saccharomyces cerevisiae*. Cell Cycle 9(8): 1601-1606.

Smith A, Zhang J, Guay D, Quint E, Johnson A, Akimenko MA. 2008. Gene expression analysis on sections of zebrafish regenerating fins reveals limitations in the whole-mount *in situ* hybridization method. Dev Dyn 237(2): 417-425.

Strom L, Lindroos HB, Shirahige K, Sjogren C. 2004. Postreplicative recruitment of cohesin to double-strand breaks is required for DNA repair. Mol Cell 16(6): 1003-1015.

Terret ME, Sherwood R, Rahman S, Qin J, Jallepalli PV. 2009. Cohesin acetylation speeds the replication fork. Nature 462(7270): 231-234.

Thummel R, Bai S, Sarras MP, Song P, McDermott J, Brewer J, Godwin AR. 2006. Inhibition of zebrafish fin regeneration using in vivo electroporation of morpholinos against *fgfr1* and *msxb*. Dev Dyn 235(2): 336-346.

Ton QV, Iovine MK. 2013. Determining how defects in *connexin43* cause skeletal disease. Genesis 51(2): 75-82.

Tonkin ET, Wang TJ, Lisgo S, Bamshad MJ, Strachan T. 2004. *NIPBL*, encoding a homolog of fungal Scc2-type sister chromatid cohesion proteins and fly nipped-B, is mutated in Cornelia de Lange syndrome. Nat Genet 36(6): 636-641.

Toth A, Ciosk R, Uhlmann F, Galova M, Schleiffer A, Nasmyth K. 1999. Yeast cohesin complex requires a conserved protein, Eco1p (Ctf7), to establish cohesion between sister chromatids during DNA replication. Genes & development 13(3): 320-333.

Unal E, Arbel-Eden A, Sattler U, Shroff R, Lichten M, Haber JE, Koshland D. 2004. DNA damage response pathway uses histone modification to assemble a double-strand break-specific cohesin domain. Mol Cell 16(6): 991-1002.

Unal E, Heidinger-Pauli JM, Kim W, Guacci V, Onn I, Gygi SP, Koshland DE. 2008. A molecular determinant for the establishment of sister chromatid cohesion. Science 321(5888): 566-569.

Van der Lelij P, Chrzanowska KH, Godthelp BC, Rooimans MA, Oostra AB, Stumm M, de Winter JP. 2010. Warsaw breakage syndrome, a cohesinopathy associated with mutations in the XPD helicase family member DDX11/ChlR1. The American Journal of Human Genetics 86(2): 262-266.

Vega H, Waisfisz Q, Gordillo M, Sakai N, Yanagihara I, Yamada M, Joenje H. 2005. Roberts syndrome is caused by mutations in *ESCO2*, a human homolog of yeast *ECO1* that is essential for the establishment of sister chromatid cohesion. Nat Genet 37(5): 468-470.

Wei Y, Yu L, Bowen J, Gorovsky MA, Allis CD. 1999. Phosphorylation of histone H3 is required for proper chromosome condensation and segregation. Cell 97(1): 99-109.

Westerfield M. 1993. The Zebrafish Book. Eugene: University of Oregon Press.

Whelan G, Kreidl E, Wutz G, Egner A, Peters JM, Eichele G. (2012). Cohesin acetyltransferase Esco2 is a cell viability factor and is required for cohesion in pericentric heterochromatin. The EMBO journal 31(1): 71-82.

Yin VP, Lepilina A, Smith A, Poss KD. 2012. Regulation of zebrafish heart regeneration by miR-133. Developmental biology 365(2): 319-327.

Yuan B, Pehlivan D, Karaca E, Patel N, Charng WL, Gambin T, Lupski JR. 2015. Global transcriptional disturbances underlie Cornelia de Lange syndrome and related phenotypes. The Journal of clinical investigation 125(2): 636.

Zanotti S, Canalis E. 2013. Notch signaling in skeletal health and disease. Eur J Endocrinol 168(6): R95-103.

Zhang B, Chang J, Fu M, Huang J, Kashyap R, Salavaggione E, Milbrandt J. 2009. Dosage effects of cohesin regulatory factor PDS5 on mammalian development: Implications for cohesinopathies. PLoS One 4(5): e5232.

Zhang J, Shi X, Li Y, Kim BJ, Jia J, Huang Z, Qin J. 2008. Acetylation of Smc3 by Eco1 is required for S phase sister chromatid cohesion in both human and yeast. Molecular cell 31(1): 143-151.

CHAPTER 3

Cohesin mediates Esco2-dependent transcriptional regulation in zebrafish

regenerating fin model of Roberts Syndrome

3.1 Abstract

Robert syndrome (RBS) and Cornelia de Lange syndrome (CdLS) are human developmental disorders characterized by craniofacial deformities, limb malformation, and mental retardation. These birth defects are collectively termed cohesinopathies as both arise from mutations in cohesion pathway genes. The mechanism that underlies RBS, however, remains unknown. Previously, I used the clinically relevant *CX43* to demonstrate a transcriptional role for Esco2. In this chapter, I show that morpholino-mediated knockdown of Smc3 perturbs zebrafish bone and tissue regeneration, producing similar results to those previously reported for Esco2 knockdown. Additionally, Smc3 knockdown also reduces *cx43* expression. Importantly, Smc3-dependent bone and tissue regeneration defects are rescued by transgenic *cx43* overexpression, providing evidence that Smc3 directly contributes to RBS-type phenotypes in the regenerating fin model produced by Esco2 knockdown. Moreover, chromatin immunoprecipitation (ChIP) assays revealed that Smc3 binds to a discrete region of the *cx43* promoter, suggesting that Esco2 exerts transcriptional regulation of *cx43* through modification of Smc3 bound to the *cx43* promoter. These findings unify RBS and CdLS as transcription-based maladies.

3.1 Introduction

Roberts syndrome (RBS) is a multi-spectrum developmental disorder characterized by severe skeletal deformities resulting in craniofacial abnormalities, long-bone growth defects and mental retardation (Van den Berg and Francke, 1993; Vega et al., 2005). Infants born with severe forms of RBS are often stillborn and even modest penetrance of RBS phenotypes lead to significantly decreased life expectancy (Schule et al., 2005). Cornelia de Lange Syndrome (CdLS) patients exhibit similar phenotypes to RBS patients that include severe long-bone growth defects, missing digits, craniofacial abnormalities, organ defects and severe mental retardation (Liu and Krantz, 2009; Mannini et al., 2010). Collectively, RBS and CdLS are termed cohesinopathies as they arise due to mutations in cohesion genes, most of which were originally identified for their role in sister chromatid tethering reactions (termed cohesion) (Vega et al., 2005; Schule et al., 2005; Gordillo et al., 2008; Krantz et al., 2004; Musio et al., 2006; Tonkin et al., 2004; Deardorff et al., 2007;Deardorff et al., 2012a, Deardorff et al., 2012b). Cohesins are composed of two structural maintenance of chromosome (SMC) subunits, SMC1A and SMC3, and several non-SMC subunits that include RAD21 (Mcd1/Scc1), SA1, 2 (stromal antigen/Scc3/Irr1) and PDS5. At least a subset of cohesion subunits form rings that appear to topologically entrap DNA (Jeppsson et al., 2014; Dorsett, 2016; Marston, 2014).

RBS is an autosomal recessive disease that arises due to loss of function mutations in the *ESCO2* gene that encodes an N-acetyltransferase (Ivanova and Ivanov, 2002; Vega et al., 2005). *ESCO2/EFO2* (and *ESCO1/EFO1* paralog) are the human orthologues of the *ECO1/CTF7* first identified in budding yeast (Skibbens et al., 1999; Toth et al., 1999; Bellows et al., 2003; Hou and Zou, 2005). All ESCO/EFO family N-acetyltransferases

modifies the SMC3 cohesin subunit (Zhang et al., 2008; Unal et al., 2008; Rolef Ben-Shahar et al., 2008). ESCO2 plays an essential role in sister chromatid cohesion during S phase and ensures proper chromosome segregation during mitosis. In contrast, CdLS arises due to autosomal dominant mutations in cohesin subunits (*SMC1A*, *SMC3* and *RAD21*) and cohesin auxiliary factors (*NIPBL* and *HDAC8*) (Krantz et al., 2004; Tonkin et al., 2004; Schule et al., 2005; Musio et al., 2006; Deardorff et al., 2007;Deardorff et al., 2012a, Deardorff et al., 2012b; Gordillo et al., 2008; Yuan et al., 2015). NIPBL/Scc2 and MAU2/Scc4 heterodimer complex are required for cohesin ring opening/closing reactions that loads cohesins onto DNA (Dorsett and Merkenschlager, 2013; Skibbens, 2016).

Extensive research provides fascinating evidence that cohesin functions beyond sister chromatid cohesion (*trans*-tethering that brings together two DNA molecules). Cohesins also participate in various *cis*- tethering events such as transcriptional regulation via looping and chromosome condensation (Dorsett and Merkenschlager, 2013). Intriguingly, cohesins form both *cis* and *trans*- DNA tethers throughout the genome and throughout the cell cycle, a circumstance that has hampered efforts to understand the specific structures and functions, when mutated, which contribute to the molecular etiology of cohesinopathies. For instance, work from various model systems strongly suggest that CdLS arises through transcriptional deregulation that involves mostly *cis*-DNA tethers formed during G1 portion of the cell cycle. In contrast, a predominant view is that RBS arises through trans-tethering defects that result in mitotic failure and loss of progenitor stem cells through apoptosis (Monnich et al., 2011; Morita et al., 2012; Percival et al., 2015). More recent evidence, however, is consistent with an

emerging model that transcriptional deregulation may underlie RBS as well as CdLS (Banerji et al., 2016; Xu et al., 2013; Xu et al., 2014).

The zebrafish regenerating caudal fin is a valuable model system for studies related to skeletal morphogenesis (Iovine, 2007; Ton and Iovine, 2013). Advantages of the adult fin include its simple structure, accessibility, and its capacity for epimorphic regeneration. Furthermore, the regenerating fin eliminates any potentially confounding effects of embryonic lethality observed during development upon cohesin gene knockdown (Monnich et al., 2011; Morita et al., 2012). In the previous chapter (also published as Banerji et al., 2016), I report on a novel regenerating fin model of RBS and documented the role of *esco2* in skeletal and tissue regrowth. Importantly, I revealed that Esco2 is critical for Connexin43 (*cx43*) expression. Cx43 comprises gap junctions which confer direct communication between cells through channels that allows small signaling molecules (<1000 Da) to pass (Goodenough et al., 1996). CX43 function is conserved among vertebrates, is the most abundant connexin in bone cells, and is important for skeletal development such that *CX43* mutations lead to the skeletal disorder Oculodentodigital dysplasia (ODDD) in humans and mice (Paznekas et al., 2003; Flenniken et al., 2005; Jones et al., 1993). In zebrafish, mutations in *cx43* cause *short fin* (*sof*[b123]), phenotypes that include reduced fin length, reduced bone segment length, and reduced cell proliferation (Iovine et al., 2005). Here, I provide evidence that Smc3 knockdown recapitulates both Esco2 and Cx43 knockdown phenotypes (i.e. decreased bone segment and tissue regrowth). Critically, *smc3* is required for *cx43* expression. Moreover, I mapped Smc3 binding within the *cx43* promoter, consistent with the model that Smc3 directly impacts *cx43* expression. These findings provide new insight

regarding the underlying molecular mechanism of RBS, indicating that Esco2 activated

Smc3 binds to clinically relevant skeletal regulatory genes.

3.3 Materials and methods

Statement on the Ethical Treatment of Animals

This work was performed strictly according to the recommendations in the Guide for the Care and Use of Laboratory Animals of the National Institutes of Health. Lehigh's Institutional Animal Care and Use Committee (IACUC) approved the protocols performed in the manuscript (Protocol identification # 190, approved 05/19/16). Lehigh University's Animal Welfare Assurance Number is A-3877-01. All experiments were performed to minimize pain and discomfort.

Housing and Husbandry

Zebrafish (*Danio rerio*) were housed in a re-circulating system built by Aquatic Habitats (now known as Pentair). The fish room has a 14:10 light: dark cycle with tightly regulated room temperature ranging from 27 to 29°C (Westerfield, 1993). Monitoring of the water quality is done automatically to maintain conductivity of 400–600 µs and pH in the range of 6.95–7.30. A biofilter is used to maintain nitrogen levels and a 10% water change occurs daily. Sequential filtration of recirculating water was carried out using pad filters, bag filters, and a carbon canister before circulating over ultraviolet lights for sterilization. Fish feeding schedule was as follows: fed three times daily, once with brine shrimp (hatched from INVE artemia cysts) and twice with flake food (Aquatox AX5) supplemented with 7.5% micropellets (Hikari), 7.5% Golden Pearl (300–500 micron, Brine Shrimp direct), and 5% Cyclo-Peeze (Argent).

Zebrafish Strains and fin amputations

Both wild-type (C32) and *Tg* (*hsp70: miR-133sp^{pd48}*) (Yin et al., 2012) *Danio rerio* animals were used. Males and females from 6 months-1 year of age were included. All procedures involving caudal fin amputations, fin regeneration, and harvesting were done as previously described (Banerji et al., 2016). Briefly, 0.1% tricaine solution was used for fish anaesthetization and their caudal fin rays amputated at 50% level using a sterile razor blade. Regenerating fins were harvested at the required time points and fixed in 4% paraformaldehyde (PFA) overnight at 4°C. The fixed fins were dehydrated in methanol (100%) and stored at 20°C until further use.

Morpholino-mediated gene knockdown in regenerating fins

The morpholinos (MOs) used were all fluorescein-tagged and purchased from Gene Tools, LLC. The sequences for MOs are as follows: (MO1) *smc3*-ATG blocking MO: 5′-TGTACATGGCGGTTTATGC -3′, (MO2) *smc3*-splice blocking MO: 5′-GCGTGAGTCGCATCTTACCTGTTTA-3′, *esco2* –MO and Standard Control MO (Std-MO) from Banerji et al., 2016. MOs were reconstituted to a final concentration of 1 mM in sterile water. Microinjection and electroporation procedures were carried out as described in the previous studies (Banerji et al., 2016).

Regenerate Length, segment length, and H3P analyses

MO injected fins were calcein stained at 4 dpe/7 dpa and regenerate length and segment length was determined as described (Du et al., 2001; Banerji et al., 2016). For detection

of mitotic cells, histone-3-phosphate (H3P) assay was performed on fins harvested at 1 dpe/4 dpa as described (Banerji et al., 2016).

RNA extraction and RT-PCR analysis on regenerating fins

RT-PCR analysis was performed on total mRNA extracted from 1 dpe/4 dpa harvested fins that were either injected with *smc3* splice blocking MO (MO2) or Std-MO injected. Trizol reagent (Gibco) was used to extract mRNA from minimum of 8-10 fins. For making cDNA, 1 mg of total RNA was reverse transcribed with SuperScript III reverse transcriptase (Invitrogen) using oligo (dT) primers. Two pairs of primers were used for testing the splicing efficiency. The control primer pair (C1-C2) was designed to amplify a portion of the exon 1 of *smc3* mRNA whereas the targeting primer pair (P1-P2) was designed to amplify the exon1 along with a portion of the intron1. The sequences of the control primers are as follows: C1 (forward primer) 5'-GACTGTTATGTCTTTTGCGTG-3' and C2 (reverse primer) 5' GCGGTTTATGCACAAAACACT-3'. The sequences of the targeting primers are as follows: P1 (forward primer) 5'-GGAGGAGGGTGTTTAATTCAGC-3' and P2 (reverse Primer) 5'-GCTTCGAAAGCCTTGAATAATGAC-3'.

RNA probe preparation for in situ hybridization on whole-mount /cryosectioned fin

The *cx43* template was made as described (Iovine et al., 2005). The *smc3* template was generated using gene-specific primers (Forward primer 5'-CAAACTGTGGTCGATCCCTTCAGC and reverse primer 5-'**TAATACGACTCACTATAGGG**GCTTCTCTTCAATCTTCT-3'). The RNA

polymerase T7 (RT7) binding site is highlighted in bold for the reverse primer.

Digoxigenin-labelled RNA probes were generated and whole mount/cryosection in situ

hybridization was completed as previously described (Banerji et al., 2016).

Transgenic overexpression of *cx43*

Tg(*hsp70:miR-133sp pd48*) denoted as transgene-positive (Tg+) and their siblings

denoted as transgene-negative (Tg-) were used in the heat shock experiment as previously

described (Banerji et al., 2016). Knocking down miR-133 (which targets *cx43* for

degradation) via the 'sponge' transgene (three miR-133 binding sites) results in the

increase of *cx43* levels (Yin et al., 2012).

Morpholino-mediated protein knockdown via electroporation in AB9 cells

AB.9 (ATCC® CRL-2298™) is a primary fibroblast cell line originating from the

zebrafish caudal fins. Once the cells were at 80- 90% confluency in 100 mm dishes (28°C

with 5% CO_2) knockdown procedure was completed (Bhadra et al., 2015). Briefly, the

adherent cells were washed with 1X PBS and trypsinized in 0.05% Trypsin-EDTA 1X

(Gibco) for 5 min at 28˚C. DMEM media supplemented with 15% heat inactivated FBS,

antibiotics-antimycotics (Gibco) were added to inactivate the trypsin. The cells were

collected by centrifugation at 750 rpm for 5 minutes. The pellet was re-suspended in 1-

5ml of HEPES buffer (115mM NaCl, 1.2mM $CaCl_2$, 1.2mM $MgCl_2$, 2.4mM K_2PO_4 and

20mM HEPES with pH adjusted to 7.4) and put on ice. MOs were added to 400μl of re-

suspended cells in the cuvettes on ice and incubated for 5 minutes. The cells were

electroporated at 170V for 6-7 ms using an electroporater (BioRad Gene Pulser X Cell).

Electroporated cells were added to 1ml of fresh media in 60mm culture dishes and incubated at 28˚C for 24 hours.

Lysate preparation and immunoblotting

For cell lysate preparation for western blots, AB9 cells were washed in cold PBS and cold lysis buffer (5mM Tris-HCl, 5mM EDTA, 5mM EGTA with pH 7.5) with 100X Halt-TM protease and phosphatase inhibitor cocktail (Thermo Scientific) and 0.6% SDS buffer. A sterile rubber cell scraper (Corning Incorporated, Costar) was used for scraping. A 5ml syringe (Beckton Dickinson) with an 18G needle was used to collect the lysate in a fresh tube and was heated at 100˚C for 3 min. A 26G needle (Beckton Dickinson) was used to pass the lysate through at least 3 times. The cell lysates were stored in small aliquots in -80˚C. These cell lysates were used to run western blot as described (Hoptak-solga et al., 2008). Cx43, Esco2, Smc3 and Tubulin were detected using anti-Cx43 (1:1000, Hoptak-Solga et al., 2008), anti-Esco2 (1:1000, Banerji et al., 2016), anti-Smc3 (1:1000, Santa Cruz) and anti-α-Tubulin (1:1000, Sigma) respectively. The primary antibody step was followed by incubation in peroxidase-conjugated goat anti-rabbit IgG (1:10,000) for Cx43 and Esco2, peroxidase-conjugated rabbit anti-goat IgG (1:10,000) for Smc3 and peroxidase-conjugated goat anti-mouse IgG (1:10,000) for Tubulin. The ECL chemiluminescent reagent (SuperSignal West Femto Maximum Sentivity Substrate, Pierce Rockford, IL) and X-ray films were used for signal detection. For measurement of band intensities and the percent change calculation, the Image J software was used. Relative pixel densities of gel bands were measured using the gel analysis tool in ImageJ software as previously described (Bhadra and Iovine, 2015).

Immunofluorescence on AB9 cells

Poly-L-lysine cover glasses were used for seeding the cells as previously described (Bhadra et al., 2015). Once cells were 70 -80% confluent, they were washed cold PBS and fixed with 4% PFA for 30 min at room temperature. This was followed by washes in PBS (3X for 5 minutes each), permeabilization with 0.2% triton for 10 minutes, followed by multiple washes in PBS. Blocking was done using 1% BSA for 1 hr at room temperature. The cover slips were incubated with the primary antibody (see above) overnight at 4°C (in a covered chamber surrounded with damp Kim wipes). Cells were incubated with the secondary antibody for 1 hour at room temperature (protected from light). The secondary antibodies used were as follows: anti-rabbit Alexa 488 or 568 (1:200, Invitrogen), anti-mouse Alexa 488 or 568 (1:200, Invitrogen). DAPI (1:1000, MP Biomedicals, LLC.) labels the nucleus. Cells were mounted with Vectashield (Vector Laboratories) and examined with Nikon Eclipse TE2000-U at 40X or 60X.

Chromatin Immunoprecipitation (ChIP)

ChIP protocol was performed on AB9 cells using the High-Sensitivity ChIP kit (Abcam, ab185913) according to manufacturer's instruction. The procedure for monolayer or adherent cells was followed with few modifications. Briefly, cells were grown to 80%-90% confluence on 100 mm dishes (around 4-6 dishes per round of ChIP), trypsinized and centrifuged at 1000 rpm for 20 minutes. The pellet was washed with 10 mL of 1X PBS and again centrifuged at the same speed and time. For cross-linking, 9 ml DMEM medium-containing formaldehyde (final concentration of 1%) was added to the cells and incubated at room temperature for 10 minutes on a rocker. After 10 minutes 1.25 M

Glycine solution was added and centrifuged at 1000 rpm for 20 minutes followed by a washing step with 10 mL of ice cold 1X PBS. After another round of centrifugation, Lysis Buffer with protease inhibitor was used to re-suspend the cell pellet ($200\mu L/1x106$ cells) and incubated on ice for 30 minutes with periodic vortexing. The solution was centrifuged at 3000 rpm for 20 minutes and the chromatin pellet re-suspended with the ChIP Buffer supplied in the kit ($100\ \mu l/1x106$ cells). Chromatin was sheared using a tip sonicator (Branson sonfier cell disrupter 200) with a 2.4 mm tip diameter microprobe, (Qsonica P-3) set to 25% power output. Sonication was carried out in 3-4 pulses of 10-15 seconds each, followed by 30-40 seconds rest on ice between each pulse. The sonicated chromatin was centrifuged at 12,000 rpm at 4°C for 10 minutes and stored at -20°C. A small amount of chromatin solution was used for DNA extraction in order to verify the size of the sheared DNA before starting the immunoprecipitation procedure (100-700 bp with a peak size of 300 bp). Antibody binding to assay wells and ChIP reactions was performed according to the manufactures instructions. Antibodies used were anti-IgG (kit) and anti-Smc3 (Santa Cruz) with a concentration of 0.8 μg/well for both antibodies. The sealed strip wells with the respective antibodies and Antibody Buffer (kit) were incubated for 90 mins at room temperature on an orbital shaker. ChIP reaction was set up according to the low abundance target criteria (details provided in the protocol booklet) overnight at 4°C on an orbital shaker. Next day the wells were washed with Wash buffer (kit) and DNA release buffer and cross-links were reversed (according to the manual). The released DNA was used in PCR or qRT-PCR reactions.

ChIP primer design and qPCR

The zebrafish *cx43* promoter sequence was obtained from the BAC clone (DKEY-261A18). Overlapping 31 primer pairs were designed spanning the entire 6.7 kb region of the *cx43* promoter (Table S1). For qRT-PCR analysis, the primers were designed using the Primer Quest tool software from IDT (Table 3.2). Three independent samples were prepared for *ChIP*, and qRT-PCR reactions were performed in duplicate. ChIP DNA for non-immune IgG served as the negative control. The templates were a 1:10 dilution following ChIP using either IgG or Smc3 antibodies. PCR reactions were set up using SYBR green kit (Qiagen). Analyses of the amplified samples were done using Rotor-Gene 6000 series software (Corbette Research) and the average cycle number (C_T) determined for each amplicon. For fold enrichment calculation the *smc3* C_T values were normalized relative to IgG control values and were represented as delta C_T (ΔC_T). The fold enrichment was determined using the $\Delta\Delta C_T$ method ($2^{-\Delta\Delta C_T}$). Statistical significance was determined by one-way ANOVA test ($P<0.001$) using the MINITAB 17 software.

Statistical analysis

All graphs and error bars were generated using the Microsoft excel (2013) software. For statistical significance calculation, two-tailed unpaired *t*-test was performed using Graphpad software (La Jolla California USA, www.graphpad.com). Statistical significance was also determined by one-way ANOVA test ($P<0.001$) using the MINITAB 17 software.

3.4 Results

Expression of *smc3* in the regenerating fin

Esco2 is a critical regulator of fin skeletal and tissue regeneration that is required for expression of the developmental signaling factor *cx43* (Banerji et al., 2016). While Esco2 is essential for modifying the cohesin subunit Smc3 to produce sister chromatid tethering and high fidelity chromosome segregation, a role for Smc3 in mediating Esco2-dependent RBS-like skeletal and tissue defects remains unknown. To address this gap in knowledge I evaluated *smc3* expression and function during fin regeneration. First, I completed in situ hybridization to monitor the temporal expression of *smc3* mRNA in 1, 3, 5, 8 and 14 days post amputated (dpa) fins. The results reveal that *smc3* mRNA is strongly expressed 3 dpa, similar to *esco2* expression (Figure 3.1A). *smc3* expression decreased by 5 dpa fins and was negligible by 14 dpa (Figure 3.1A). Thus, the *smc3* expression mirrors that of *esco2* - both of which peak in expression at 3 dpa when regeneration is at its peak (Banerji et al., 2016; Lee et al., 2005; Hoptak-Solga et al., 2008).

Expression of *esco2* mRNA is localized to the highly proliferative blastemal compartment of the fin (Banerji et al., 2016). To test whether *smc3* expression is localized similarly to the blastema, I performed in situ hybridization on 3 dpa cryosectioned fins. The results reveal that the expression of *smc3* correlate with *esco2* localization (Figure 3.1B), but that *smc3* also extends to the epidermis, mesenchyme and skeletal precursor cells (Figure 3.1B, left panel). No staining was detected in 3 dpa cryosectioned fin in the absence of the *smc3* probe (Figure 3.1B, right panel). In combination, these studies reveal that *smc3* expression both temporally and spatially

coincides with that of *esco2* expression, consistent with a requirement during the early stage of regeneration specifically in the proliferative blastemal compartment of the regenerating fin.

Knockdown of Smc3 results in reduced regenerate length, segment length and cell proliferation

In my first publication I have reported that Esco2 is essential for regenerate length, segment length and cell proliferation in the regenerating fins (Banerji et al., 2016). To provide evidence that cohesins may mediate these Esco2-dependent effects, I designed two independent non-overlapping MOs that target Smc3: one targeting *smc3* ATG (MO1) and the second targeting the first splice site junction (exon1-intron1; e1i1) of *smc3* gene (MO2) (Figure 3.2A). Thus, MO1 blocks translation of Smc3 whereas MO2 alters the *smc3* pre-mRNA proper splicing. All results were compared to a standard negative control MO (Std-MO) as previously described (Banerji et al., 2016; Bhadra et al., 2015).

I first validated the efficiency of the two *smc3* MOs. MO1 efficiency was tested by monitoring Smc3 protein levels in AB9 cells transfected with either MO1or Std-MO (Bhadra et al., 2015). AB9 cells are primary fibroblasts derived from regenerating caudal fins of the adult zebrafish (Bhadra et al., 2015). The results reveal that the Smc3 protein levels were significantly reduced (60%) in the Smc3 knockdown lysates compared to the control lysates (Figure 3.2B). To confirm the effectiveness of splice blocking MO2, I performed RT-PCR in 4 dpa regenerating fins. RT-PCR results reveal that intron1 was

retrieved only when fins were injected with MO2 and not when injected with Std-MO (Figure 3.2C).

Using both MOs I carried out microinjection and electroporation as previously described (Govindan et al., 2016; Banerji et al., 2016) (Figure 3.2D). All MOs are tagged with fluorescein, allowing us to validate cellular uptake microscopically 1 day post electroporation (dpe) or 4 dpa. Only MO-positive fins were selected for further experiments. For measurement of regenerate length and segment length, Smc3 knockdown/Std-MO fins were calcein stained at 4 dpe/7 dpa and measured. To reduce the effect of fin-to-fin variation, I utilized the percent similarity method in which 100% indicates no difference between injected and non-injected sides of the same fin, whereas a value less than 100% indicates differences between the injected and non-injected sides of the same fin (Govindan et al., 2016; Bhadra and Iovine, 2015; Banerji et al., 2016). Quantification of regenerate length was based on the distance from the plane of amputation to the distal end of the 3rd fin ray. Quantification of bone segment length was based on measurements obtained from the first segment distal to the amputation plane of the 3rd fin ray. The Std-MO injected fins showed a high percent similarity to the uninjected side, indicating that the control MO had no effect on regenerate and bone segment length as expected. In contrast, both MO1 and MO2 showed low percentage of similarities, indicating significant differences between the injected and non-injected sides. Thus Smc3 is critical for both regenerate length and segment length similar to Esco2 (Figure 3.3A-D).

Esco2 knockdown also results in reduced cell proliferation (Banerji et al., 2016). Thus, I next addressed whether the effect of Smc3 knockdown on both regenerate length

and segment length was based on altered cell proliferation rates. To test this, I quantified the number of mitotic cells by staining for Histone-3 phosphate (H3P) on 1 dpe Smc3 knockdown (MO1 and MO2) and Std-MO injected fins. The results reveal significant reduction in H3P-positive cells in Smc3 knockdown fins compared to the control fins (Figure 3.3E, F). Thus, Smc3-dependent phenotypes are similar to both Esco2 and Cx43-dependent phenotypes previously reported (i.e. reduced regenerate length, segment length and cell proliferation) (Banerji et al., 2016; Iovine et al., 2005). Having validated Smc3 knockdown phenotypes using two non-overlapping MOs, all subsequent experiments were performed using a single targeting MO (MO1).

***smc3* and *esco2* function together during skeletal regeneration**

esco2 is critical for *cx43* expression, although the basis for this regulation remains unknown (Banerji et al., 2016). Thus, it became important to determine if Smc3 knockdown also influences *cx43* expression. I performed whole mount in situ hybridization with *cx43* probe on Smc3 knockdown fins. Half of the fin was injected with MO1 or Std-MO and the other half was kept uninjected as an internal control. Remarkably, the Smc3 knockdown side exhibited significantly reduced expression of *cx43* compared to the uninjected side (Figure 3.4A). In contrast, the Std-MO injected side showed no difference in *cx43* expression compared to the uninjected side (Figure 3.4B).

To determine the genetic relationship between *smc3* and*,* I tested for rescue of *smc3*-MO phenotypes by over expressing *cx43* (Banerji et al., 2016). For this purpose, I used the transgenic line, *Tg(hsp70:miR-133sp^pd48)* that indirectly over express *cx43* in both regenerating heart and fins (Yin et al., 2012; Banerji et al., 2016). The three groups

of fish for this experiment were as follows: (1) transgene positive and heat shocked (Tg+HS+), (2) transgene negative and heat shocked (Tg-HS+) and (3) transgene positive but not heat shocked (Tg+HS-) (Figure 3.5A). Importantly, three independent heat shock trials revealed that both regenerate length and bone segment length defects otherwise exhibited in Smc3 knockdown were significantly rescued in the Tg+HS+ group (Figure 3.5B). This rescue was specific to transgene activation and was not induced by heat shock alone or in combination with any other group. These findings support an exciting model that Smc3 functions upstream to regulate *cx43* gene expression, similar to Esco2.

AB9 cells are suitable for testing the *smc3/esco2-cx43* skeletal pathway

What is the basis through which both Esco2 and Smc3 regulate *cx43* expression? To address this issue, I switched to AB9 fibroblast cell line, that are less complex than regenerating fish fin tissue and previously reported to express Cx43 (Bhadra et al., 2015). I first tested whether AB9 cells also express Esco2 and Smc3. AB9 cells grown on a coverslip were fixed and processed for immunofluorescence. The results show that anti-Esco2 antibody and anti-Smc3 antibody co-localize and overlap with the DAPI-stained nuclei (Figure 3.6A). I next tested whether either *esco2-* or *smc3-* similarly regulate Cx43 protein levels as occurs in regenerating fins. Cx43 protein levels were monitored by Western blot in AB9 cells knocked down for either *esco2* MO or *smc3* MO. The results show that Esco2 or Smc3 proteins were each reduced using their respective knockdown morpholinos (Figure 3.6B). Critically, Cx43 protein levels also were reduced following either knockdown (Figure 6B). Therefore thes AB9 system recapitulates the effect of

Esco2 and Smc3 knockdown in reducing Cx43 expression levels, similar to results

obtained in regenerating fins (Banerji et al., 2016).

Smc3 directly binds to a specific region of the *cx43* promoter

It is well established that cohesins bind directly and stabilize DNA-tethering

structures required for efficient gene expression (Dorsett, 2016; Merkenschlager and

Nora, 2016; Jeppsson et al., 2014). Thus, I hypothesized that Smc3, as a part of the

cohesin complex, directly binds to a segment of the *cx43* promoter. The *cx43* promoter is

approximately 6.7 kb in length, adjacent to an additional connexin gene (*cx32.2*) that

resides upstream of the *cx43* coding sequence (Chatterjee et al., 2005; Figure 3.7A). I

assayed Smc3 binding to the *cx43* promoter by performing Chromatin

Immunoprecipitation (ChIP) on AB9 cells. I first optimized the ChIP procedure using

Smc3 as the target antibody and IgG as the negative control. Since this is the first time

that protein binding to the putative *cx43* promoter is investigated, I performed qualitative

PCR analysis. I designed 31 primers pairs that, in overlapping fashion, span the entire 6.7

kb promoter (Table 3.1). Positive binding was observed for primers 2-6 (800bp), primer

11 (250bp) and primers 18-28 (1.5kb). In contrast, the negative control (IgG) exhibited

little to no binding throughout the promoter length (Figure 3.7A).

To investigate in detail the specific regions of the *cx43* promoter to which Smc3

binds, I next performed qRT-PCR. I designed 5 primer pairs that spanned the Smc3

positive binding regions obtained from the qualitative PCR analysis (p2- p6) and 2 primer

pairs as negative controls that fall within zones devoid of Smc3 binding (p1 and p7). The

results reveal significant binding of Smc3 specifically within one region (p2) of the *cx43*

109

promoter (Figure 3.7B). Binding was also observed at p3-p6, but at levels that did not rise

to statistically significant levels. The negative controls (p1 and p7) showed negligible

binding. These ChIP results provide strong evidence that Smc3 binds directly to the *cx43*

promoter.

3.5 Discussion

Esco2 mutations are the only known etiologic agent for RBS. Previously, I established Esco2 knockdown in regenerating fin as a powerful system from which to elucidate the molecular basis of RBS. One major revelation is that Smc3 functions in a similar manner as Esco2 during fin regeneration. First, *smc3* mRNA expression coincides with *esco2* expression, specifically in the proliferative blastemal compartment of the regenerating fin. Second, morpholino-mediated Smc3 knockdown revealed that Smc3-dependent phenotypes i.e. reduced regenerate length and segment length and decreased cell proliferation, recapitulate the *esco2*/*cx43*-dependent phenotypes. Third, I see a reduction in the *cx43* expression levels in Smc3 knockdown fins. Finally, *cx43* overexpression rescues Smc3-dependent phenotypes to a similar degree as Esco2-dependent phenotypes. In combination with my previous findings (Banerji et al., 2016), these results provide strong evidence that Esco2, Smc3, and Cx43 function in a common pathway and that RBS is a transcriptional malady similar to CdLS.

A popular model is that Esco2 deficiency results in mitotic failure and progenitor cell death through apoptosis. A second revelation is that, a subset of RBS-type phenotypes may instead arise directly from defects in cohesin (Smc3) binding to the promoter of clinically relevant development genes. As proof of concept, the ChIP experiments demonstrate that Smc3 physically binds to the *cx43* promoter and is required, along with Esco2, for efficient *cx43* expression. Cx43 represents a valuable and informative target given that mutation in human *CX43* results in ODDD, and that CdLS models similarly report aberrant expression of *CX43* (Monnich et al., 2011; Kawauchi et al., 2009). These results, combined with the established role for Esco2 in Smc3-

acetylation, provide compelling support for a model in which Esco2 and Smc3 act on the promoters of skeletal genes (i.e. *cx43*) to regulate transcription and thereby mediate proper skeletal development and morphogenesis (Figure 3.8).

Extensive research has been carried out to understand the structure of the cohesin complex and auxiliary factors, and their role(s) in mediating various DNA tethering events, with the intention of elucidating molecular mechanisms underlying cohesinopathies. Surprisingly, while both CdLS and RBS are grouped under a similar disease category, the etiologies of these sister maladies are considered different. Transcriptional deregulation is considered to be the primary mechanism underlying CdLS (Krantz et al., 2004; Tonkin et al., 2004; Gillis et al., 2004; Musio et al., 2006; Deardorff et al., 2007;Deardorff et al., 2012a, Deardorff et al., 2012b; Zhang et al., 2009). For example, defects in *cis*-DNA tethering events result in severe to mild phenotypes observed in CdLS. Cohesin subunits (SMC1A and SMC3) and NIPBL interact with Mediator complexes along with RNA polymerase II that bring long-distance enhancers to close proximity of the promoter of transcriptionally active genes via a *cis*-mediated DNA looping event (Kagey et al., 2010). The molecular mechanism underlying RBS is thought to occur through *trans*-tethering mitotic defects. It is true that mitotic failure and modest levels of apoptotic cells are often accompanied in mouse and zebrafish embryo studies of RBS. The current findings do not rule out the possibility that these can promote developmental defects (Monnich et al., 2011; Horsfield et al., 2012; Mehta et al., 2013; Whelan et al., 2012). However, the findings that RBS-type phenotypes can occur in the absence of apoptosis greatly diminishes these models. Instead, the data suggests a unified mechanism for both RBS and CdLS through transcriptional deregulation.

Why do RBS cells often exhibit cohesion defects (Vega et al., 2005; Schule et al., 2005)? Why do CdLS cells appear devoid of elevated levels of mitotic failure and apoptosis? I suggest contributions of gene dosage. For instance, an elegant study performed in yeast revealed differential dosage effects on a subset of cohesin related functions (Heidinger-Pauli et al., 2010). In humans, CdLS arises due to heterozygous dominant mutations in cohesion pathway genes. Thus, one functional copy of the gene may be sufficient to support cohesion but may not be sufficient to prevent changes in gene transcription. In contrast, RBS arises due to homozygous recessive mutations. Therefore, both copies of the *ESCO2* gene are defective, which blocks all cohesion pathway function such that mitotic defects appear more prevalent. My studies demonstrating that Esco2 and Smc3 function together to regulate *cx43* expression provide compelling evidence for a more unified model linking the underlying mechanisms of CdLS and RBS cohesinopathies.

3.6 Figures
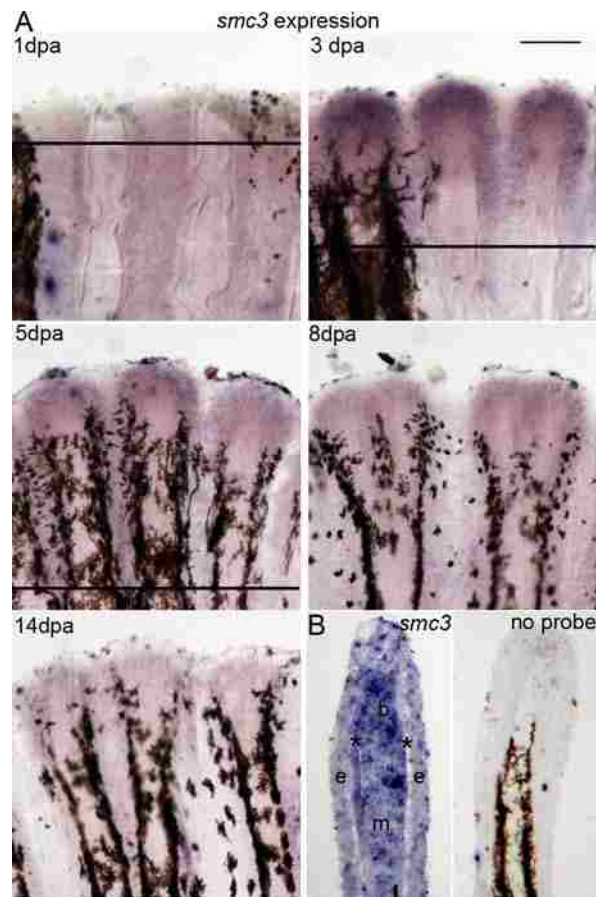
Figure 3.1: Expression of *smc3* in whole mount and cryosectioned regenerating fins. (A) Expression of *smc3* by whole mount in situ hybridization at various time points (1, 3, 5, 8 and 14 days post amputation; dpa) (n=6 per timepoint). A solid line except in 8 dpa and 14 dpa regenerating fin indicates the amputation plane, unless it is out of the field of view. (B) In situ hybridization on 3 dpa longitudinal cryosectioned fin showing the tissue-specific localization of *smc3* mRNA. The expression is observed in most compartments of the regenerating fin, being localized strongly at the blastemal compartment (b) with moderate expression in epidermis (e), mesenchyme (m) and skeletal precursor cells (*). The no probe control (3 dpa cryosectioned fin, right panel) shows no expression of *smc3*. Three independent trials were performed with different fin sections from 3 different fins. Scale bar is 50 μm (shown in 3 dpa panel) for all panels.
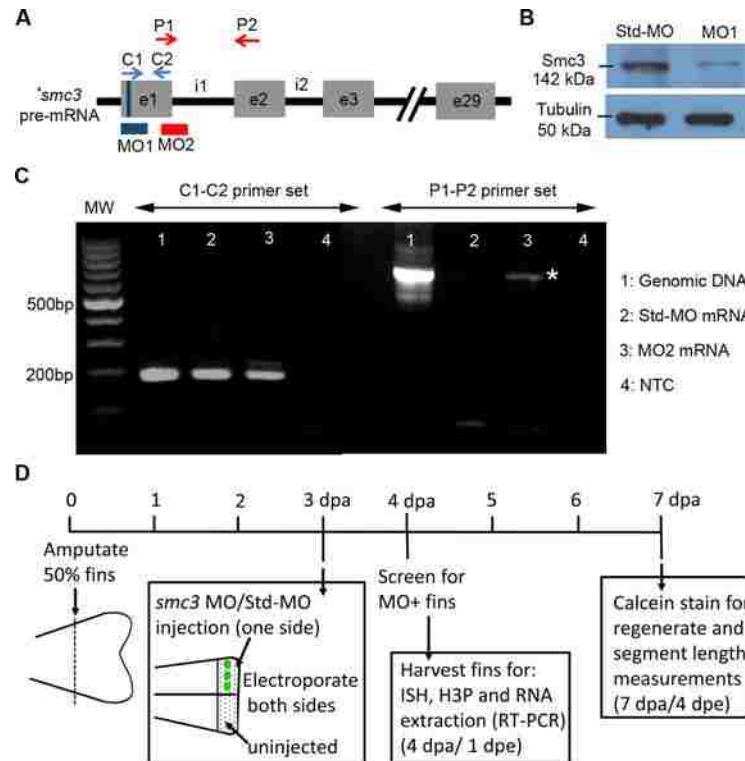
Figure 3.2:Validating the efficiency of *smc3* **morpholinos.** (A) Schematic representation of the zebrafish *smc3* pre-mRNA with exons (e) represented with grey boxes and the regions between the exons are the introns (i). The position of MO1 (ATG blocker) at the start codon of the *smc3* gene is indicated by a blue bar (indicated on e1 with a vertical line). MO2 is positioned at the first exon and intron junction of the splice donor site (e1i1). The positions of the control primer pairs (C1-C2) are indicated with blue arrows whereas the position of the target primer pairs (P1-P2) is indicated with red arrows. (B) Western blots confirming Smc3 protein reduction (60%) in MO1 injected AB9 cell lysate (lane 2) compared to the Std-MO injected lysate (lane 1). Tubulin was used as a loading control. Similar findings were observed in each of three trials (n=10 fins per trial). (C) Results of RT-PCR analysis using CI-C2 and P1-P2 primer pairs for verifying the efficiency of MO2. The templates for both these primer pairs are numbered from 1 to 4 as follows: (1) genomic DNA extracted from regenerating fins, (2) cDNA from fins injected with Std-MO, (3) cDNA from fins injected with MO2 and (4) no template control (NTC). I used 3 fins to generate genomic DNA and 10 fins to generate cDNA. The C1-C2 primer pair amplified an expected 210 bp product. In contrast, the P1-P2 pair amplified a 729 bp product in lane 3 (marked with *) due to the inclusion of intron1 (as predicted for MO2 injected sample) compared to lane 2 which did not amplify any product (as expected for Std-MO injected sample). (D) Schematic outline of knockdown experiments. Fins are amputated (50% level) and permitted to regenerate for 3 days. At 3 dpa, either *smc3* MOs (MO1 and MO2) or Std-MO (Standard control morpholino) was microinjected to one half of the regenerating fin keeping other half uninjected. This was immediately followed by electroporation on both injected and uninjected sides of the fin. The next day i.e.1 day post electroporation (dpe) or 4 dpa, the injected part of the fins were evaluated for MO uptake using a fluorescence microscope.

115

Only those fish that showed a strong signal of the fluorescein –tagged MO were used for further experiments. For experiments such as in situ hybridization (ISH), histone-3-phosphate (H3P) and RNA extraction for RT-PCR, the fins were harvested at 1 dpe or 4 dpa. Note that for RNA extraction, all fin rays across the fin were injected with MO and electroporated before harvesting. For regenerate length and segment length measurement and analysis, fins were allowed to regenerate for longer period and were calcein stained at 4 dpe or 7 dpa. For each experiment n=8 per trial and at least 3 independent trials were performed.
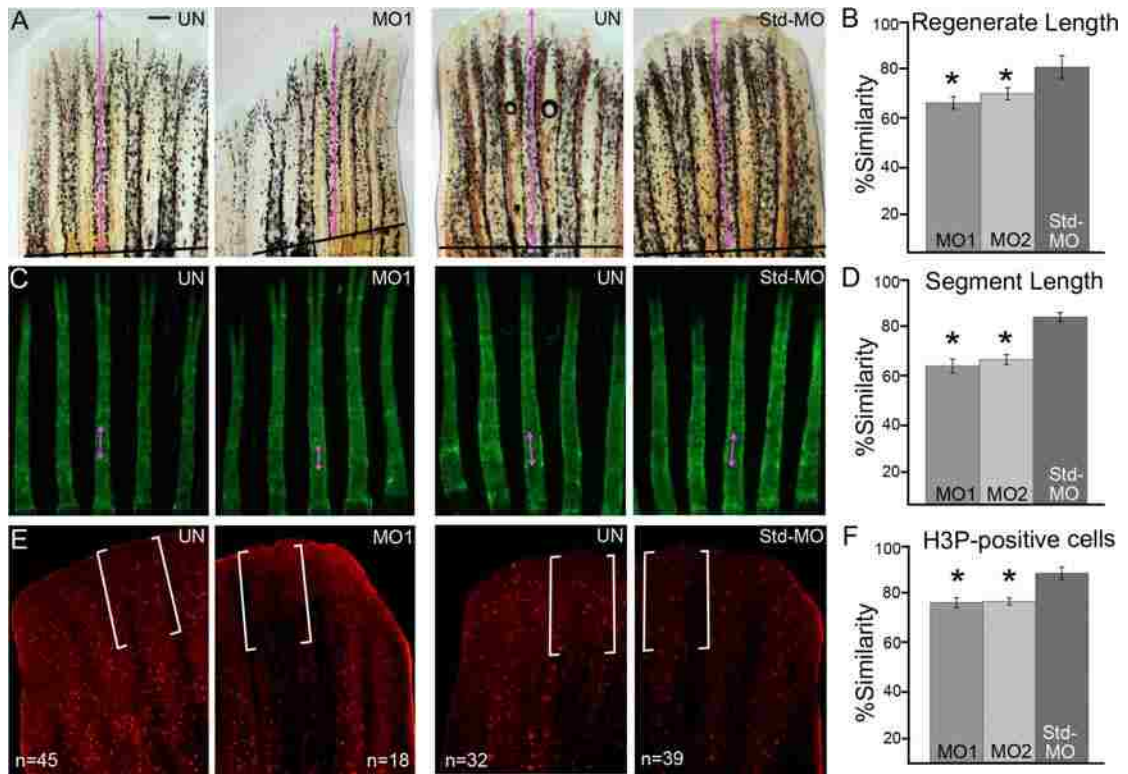
Figure 3.3: Morpholino mediated Smc3 knockdown results in regenerate length, segment length and cell proliferation reduction. (A) Representative images of uninjected (UN), *smc3* MO injected (MO1) and Std-MO injected fins. Total regenerate length was calculated by measuring the distance between the amputation plane (indicated by a solid black line) to the distal end of the 3rd fin ray (purple arrows indicates the length measured). (B) Graph shows the significant reduction (indicated by *) of regenerate length in Smc3 knockdown fins (for both MO1 and MO2) compared to the Std-MO injected fins using the percent similarity method. (C) Representative images of calcein stained fins of uninjected (UN), *smc3* MO injected (MO1) and Std-MO injected fins. Segment length was calculated by measuring the distance between first two joints in the 3rd fin ray (purple arrows indicates the length measured). (D) Graph shows that significant reduction (indicated by *) of segment length in Smc3 knockdown (for both MO1 and MO2) compared to Std-MO injected fins using the percent similarity method. (E) Representative images of H3P-positive cells in uninjected (UN), *smc3* MO injected (MO1) and Std-MO injected fins. Measurements were taken from the distal most 250μm of the 3rd ray. White bracket marks the defined area and n represents the number of H3P-positive cells in that area. (F) Graph shows the significant reduction (indicated by *) in the number of H3P-positive cells in Smc3 knockdown (for both MO1 and MO2) compared to Std-MO injected fins using the percent similarity method. For each experiment n=8 fins per trial and 3 independent trials were performed. For statistical significance, two tailed unpaired student's *t*-test was used where $P<0.05$. Mean± s.e.m. is represented by error bars. Scale bar is 50 μm for all panels.
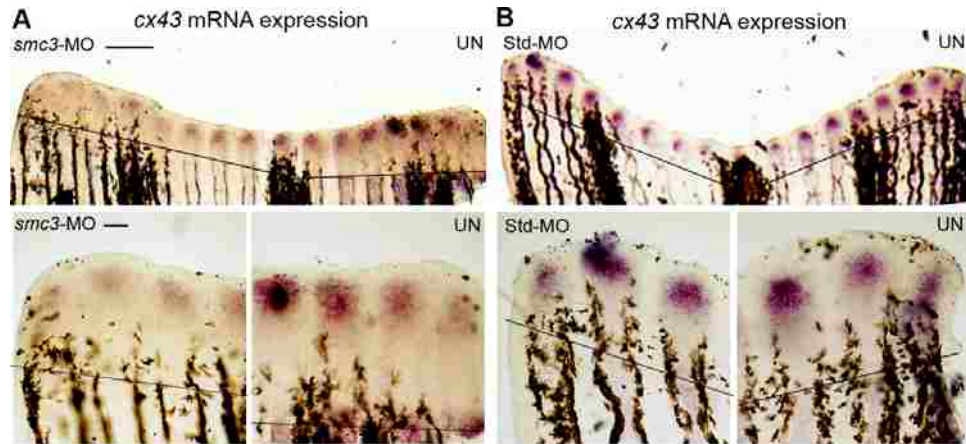
Figure 3.4: *smc3* **regulates the expression of** *cx43* **in regenerating fins.** (A) Representative image of a fin with Smc3 knockdown side (*smc3*-MO) showing decreased *cx43* staining compared to the uninjected side (UN). Higher magnification of the Smc3 knockdown side of the same fin shows reduced levels of *cx43* expression compared to the uninjected side (UN), which shows normal *cx43* levels. (B) Representative image of Std-MO injected fin revealing similar *cx43* levels in both injected and uninjected side (UN). Higher magnification of the same fin shows normal and similar levels of *cx43* expression in both injected and uninjected sides (UN). For this experiment n=6 fins per trial and 3 independent trials were performed. A solid line indicates the amputation plane and scale bar is 100 μm and 50 μm.
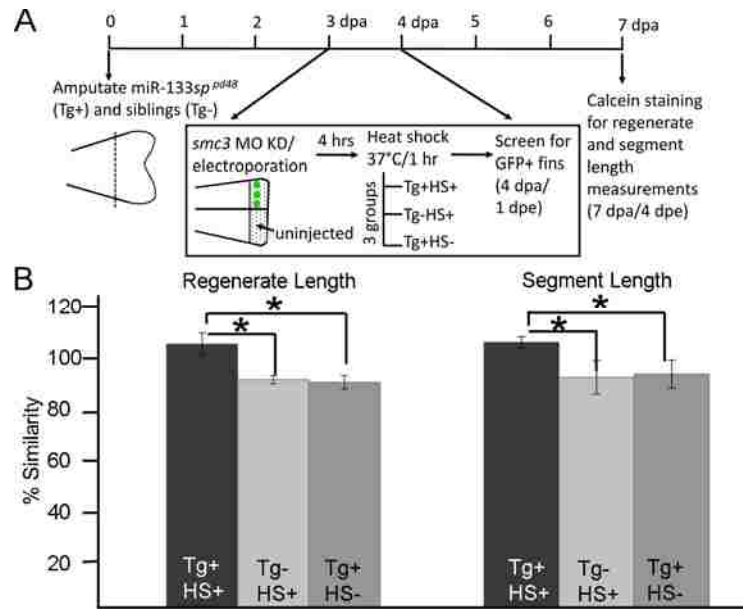
Figure 3.5: Over expression of *cx43* rescues *smc3-dependent skeletal* phenotypes.
(A) Experimental timeline providing details of the fin amputation, MO
injection/electroporation, heat shock and data analysis process. Fin amputation (50%
level) was performed on transgenic *hsp70:miR-133sp^{pd48}* fish (Tg+) and their siblings
(Tg-). At 3 dpa, *smc3* MO was injected in one half of the fin keeping the other half
uninjected. This step was immediately followed by electroporating both sides of the fin.
After a period of 4 hours, the heat shock process began. At this point there were total 3
groups of fish: (1) Tg+HS+ is the transgenic-positive fish that were heat shocked at 37°C
for 1 hour, (2) Tg+HS- is the transgenic-positive fish but were not heat shocked and (3)
Tg-HS+ were the siblings (transgenic-negative) that were similarly heat shocked as
Tg+HS+. At 4 dpa or 1 dpe the Tg+HS+ fins were screened for positive GFP expression,
which indicated transgene induction. The control groups (Tg+HS- and Tg-HS+) were
GFP-negative indicating absence of transgene induction. For regenerate length and
segment length measurement and data analysis, fins were calcein stained at 7 dpa or 4
dpe. (B) The graph reveals significant (indicated by *) rescue of *smc3*-dependent
regenerate and segment length defects in Tg+HS- Smc3 knockdown fins compared to the
control groups (Tg-HS+ and Tg+HS-). For each experiment n=8 fins per trial and 3
independent trials were performed. For statistical significance, two tailed unpaired
student's *t*-test was used where $P<0.05$. Mean$\pm$ s.e.m. is represented by error bars. Scale
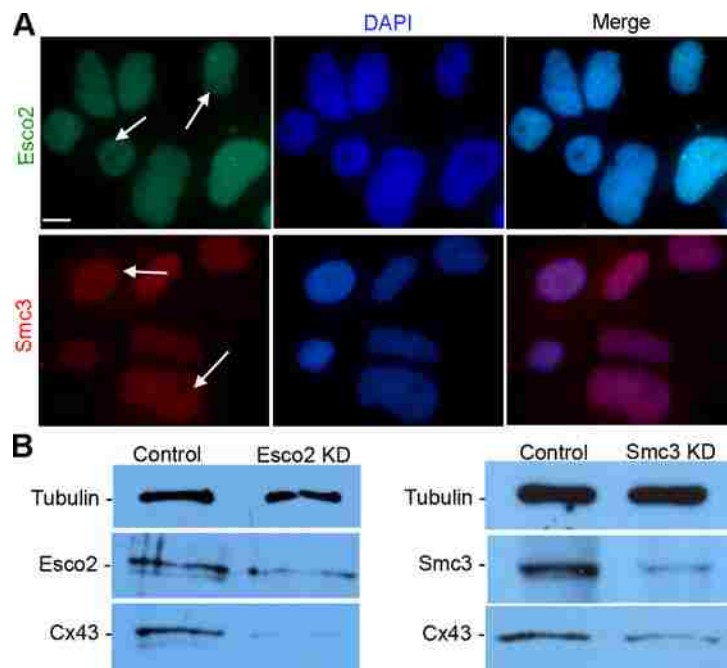bar is 50 µm for all panels.

Figure 3.6: AB9 cells as a system to evaluate cohesin-binding at the *cx43* promoter.
(A) Expression of Esco2 and Smc3 are detected in AB9 cells by immunofluorescence.
The anti-Esco2 antibody and anti-Smc3 antibody stains the nuclei of the cells (DAPI,
blue), indicated with arrows. For each protein, 3 independent trials were performed. Scale
bar is 10 μm (B) Western blot analysis detects the Esco2 in Std-MO electroporated
control cell lysates (Lane1: Control) at a predicted size of 68 kDa. A reduction in Esco2
protein levels in MO1-electroporated Esco2 knockdown cell lysate (lane 2: Esco2 KD)
was observed when compared to the control sample (lane 1: Control). The results with
anti-Cx43 antibody reveals reduced Cx43 protein levels (detected at 43 kDa as predicted)
in Esco2 KD compared to control. Western blot analysis detects Smc3 in Std-MO
electroporated control cell lysates (lane1: Control) at a predicted size of 142 kDa. A
reduction in Smc3 protein levels in MO1-electroporated Smc3 knockdown cell lysate
(lane 2: Smc3 KD) was observed when compared to the control sample (lane 1: Control).
The results with anti-Cx43 antibody reveals reduced Cx43 protein levels (detected at 43
kDa as predicted) in Smc3 KD compared to control. Tubulin detected at 50 kDa was used
as the loading control for both blots. Image J software was used for analysis of relative
band intensity from data of 3 independent trials.
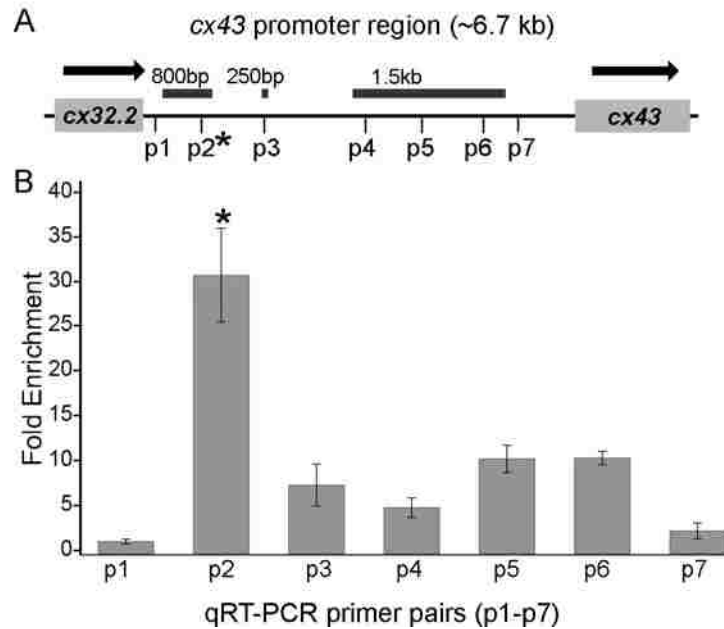
Figure 3.7: Smc3 binds at a specific location of the *cx43* promoter (A) Schematic representation of the zebrafish *cx43* promoter. It is approximately 6.7 kb in length, adjacent to an additional connexin gene (*cx32.2*). The horizontal bars indicate the binding regions of Smc3 inferred from qualitative PCR results. The positions of the seven qRT-PCR primer pairs (p1-p6) are indicated on the promoter region. The two primer pairs (p1 and p7) are the negative controls, since they lie at a region not predicted from previous PCR results. (B) The graph represents the fold enrichment of Smc3 binding (normalized to IgG) at different regions of the *cx43* promoter. Significant enrichment was observed at p2 location of the promoter suggesting positive binding of Smc3 at the p2 region. Statistical significance was determined by one-way ANOVA test (P<0.001) and indicated with *. The mean$\pm$ s.e.m. is represented by error bars for 3 independent trials.
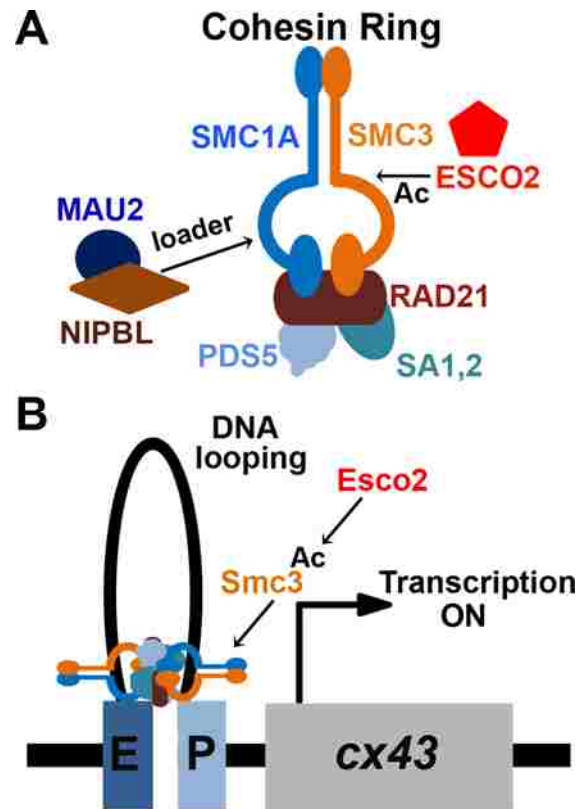
Figure 3.8: Esco2-dependent *cis*-DNA looping model underlying the etiology of RBS.
(A) Schematic representation of the cohesin ring complex. It is composed of two
structural maintenance of chromosome (SMC) subunits (SMC1A and SMC3) and three
non-SMC subunits (RAD21, SA1, 2 and PDS5). The cohesin auxiliary factor, NIPBL-
MAU2 heterodimer complex helps in cohesin ring opening/closing reactions that loads
cohesins onto DNA. Another auxiliary factor, *ESCO2* is a member of the *ESCO* family of
N-acetyltransferases that acetylates the SMC3 cohesin subunit. (B) A model depicting the
Esco2-dependent *cis*-DNA tethering mechanism underlying RBS in which the
acetyltransferace Esco2 activates its target, Smc3 (denoted by Ac) that binds the *cx43*
promoter, thus activating *cx43* transcription. This process is believed to occur through a
cis-DNA looping mechanism that connects the enhancer (E) and promoter (P) of the *cx43*
gene.

3.5 Tables

Table 3.1: PCR Primer sequences

Name	Primer sequence (5'-->3")	PCR product
Fp1	5'- AAA GGG TCA CGA AAC ACC -3'	Negative
Rp1	5'- TCA AAG ATG TCA CAT TTT ACC G -3'	
Fp2	5'- GGG TTG AGA CTA GAT GTC TGT -3'	Positive
Rp2	5'- GTT AAA TGT CTG TTG AAG GAG C -3'	
Fp3	5'- CCA CTT GAG TAT TAG ACT GTT TG -3'	Positive
Rp3	5'- TGT CAC TTT ATT TTG ATG GTC GG -3'	
Fp4	5'- GGC ATG TAG ATG CAA TGT AAC T -3'	Positive
Rp4	5'- GGA ACT AGA GGA GTA GTC TTG G -3'	
Fp5	5'- GCT TAT TCA ATC CAA GAC TAC TC -3'	Positive
Rp5	5'- ATG AAT GAG ATC AAA AAA GTA TGC -3	
Fp6	5'- GCA CGT AAA CTG TAA ACT TGC A -3'	Positive
Rp6	5'- GTC GAC AAG TTA AAA CCA GCC -3'	
Fp7	5'- GCT GAA ATC AGC CTA GGC -3'	Negative
Rp7	5'- GTT GGC TGC TTT TAG TTG G -3'	
Fp8	5'- GGC TGG TCA ACC AAC TAA A -3'	Negative
Rp8	5'- CCA ATG AAA AGG TGT GAA GC -3'	
Fp9	5'- GGT TGC TTT TTG TGC TTC ACA C -3'	Negative
Rp9	5'- ACA GCA CTA CCT ACT GCG -3'	
Fp10	5'- GCT AAA GTC ACA CTA GGG G -3'	Negative
Rp10	5'- CCA TCT CTG GGA AAC ATC C -3'	
Fp11	5'- CGT AGT GTA TGA GTG TGT GT -3'	Positive
Rp11	5'- ATG CAT ATG ACT GCT ATG GC -3'	
Fp12	5'- CCT TTT TCG ATG GGT TAT TTT CAC -3'	Negative
Rp12	5'- AAT ATT TTG CAA AAC AAC GAA CC -3'	
Fp13	5'- CCC ATA ACT CTG TGG TTC GTT -3'	Negative
Rp13	5'- CTT GTA GAG ACA GGA GTT CGG -3'	
Fp14	5'- GCA CTC GCT AAA CCG AA -3'	Negative
Rp14	5'- CGC AGG TAT TAT TTG AGT AGG C -3'	
Fp15	5'- CCG ACA GAA AGA AAC ACA CA -3'	Negative
Rp15	5'- CTT TCA TAA AAG GGG TTG ATC C -3'	
Fp16	5'- GGC TAG TAA TTG ACT TTT CAA GT -3'	Negative
Rp16	5'- AAA ACA AGT TGT AAC CTA TAG GC -3'	
Fp17	5'- CCA TTG TAG CCT ATA GGT TAC AA -3'	Negative
Rp17	5'- GGG TTT CCT CCA CAA TCC -3'	

Fp18	5'- CCG AAT GTC TTT GGA TTG TG -3'	Positive
Rp18	5'- CCT TGT AGC CTA AAC TCG C -3'	
Fp19	5'- GGA TCA AGT GAG CGA GTT TA -3'	Positive
Rp19	5'- CTG GAA AGA AGT AAA GAG TGG -3'	
Fp20	5'- GGC TCT CCA CTC TTT ACT TC -3'	Positive
Rp20	5'- CAA ATA TGA ATC ATA TCA TGG CG -3'	
Fp21	5'- CGC CAT GAT ATG ATT CAT ATT TG -3'	Positive
Rp21	5'- AAT TTG TGA CTT CTA TTG AGG C -3'	
Fp22	5'- GGA ATA ACT TTT TGT TTT TGG GAG -3'	Positive
Rp22	5'- AGA ATT GCA GGT TAA AGT TTG C -3'	
Fp23	5'- CCT TCA TTT CAT GTA ACT CTG C -3'	Positive
Rp23	5'- ATA ATT GGA CAT GTT TGT GTC C -3'	
Fp24	5'- GGC AAT ATT AAA ATT CCA TCA CTT -3'	Positive
Rp24	5'- GGA ACC TAG CAT GAC ATA TAC G -3'	
Fp25	5'- CCA CGC AAG ACA AAG AAA TTA A -3'	Positive
Rp25	5'- GCA TAA CAC TAT TGA GGT GG -3'	
Fp26	5'- CCC TAA CCT TAC CCG TAT TC -3'	Positive
Rp26	5'- AGA AAA CAA GCA CAA TGC G -3'	
Fp27	5'- CCC ACT TAT TGT CTA AAC AAG AAT -3'	Positive
Rp27	5'- GCA TGG AAA GTC AAA TAT CAT AAG G -3'	
Fp28	5'- GGC AGT TCT TTA GAA CTT CTT AAA -3'	Positive
Rp28	5'- CAG CAA GTG AGT CAT CAT CC -3'	
Fp29	5'- GCT TGG CAA TGT TTT TTA ATG GT -3'	Negative
Rp29	5'- TGA AAA TAA TCA TGA AAG CTG ACC -3'	
Fp30	5'- CCT GAG GTC AGC TTT CAT GAT -3'	Negative
Rp30	5'- AAC AGT CCA TCA CTT TTA CTG C -3'	
Fp31	5'- GCA TGA ACT TGA AGG GGA A -3'	Negative
Rp31	5'- GAG TTC TAG CTG AAA ATA GAA AGC -3'	
Forward primer-fp and reverse primer-rp. Positive indicates the presence of a amplified PCR product for that primer pair and negative indicates no PCR product for that primer pair.		

Table 3.2: PCR Primer sequences for ChIP- qRT PCR

Name	Primer sequence (5'-->3")
p1	fp- 5'-TGTGTCCCACATTGCCAAA-3'
	rp- 5'-GATCTCATGGCTGTGACGTAG-3'
p2	fp- 5'-GGTGTGAAGATTTATGGTTGCC-3'
	rp- 5'-AGGTGTGGAACTAGAGGAGTAG-3'
p3	fp- 5'-GCATGTTCTCCTTGCGTTTG-3'
	rp- 5'-CATCCACACACACTCATACA-3'
p4	fp- 5'-CAGACTTGCCATTGTAGCCTAT-3'
	rp- 5'-GGCGAGCCCTGATGAATAAA-3'
p5	fp- 5'-AGGATCAAGTGAGCGAGTTTAG-3'
	rp- 5'-TCAGAGGGAAGAAAGTGGAAAG-3'
p6	fp- 5'-GATGGCTTTCTCCCGCTTAT-3'
	rp- 5'-CTATCTGTGGAACCTAGCATGAC-3'
p7	fp- 5'-TATCCGAGACCAGGTGTAGTT-3'
	rp- 5'-GCACCTGCTGAGGATGTTAT-3'

3.7 References

Banerji, R., Eble, D. M., Iovine, M. K. & Skibbens, R. V. 2016. Esco2 regulates cx43 expression during skeletal regeneration in the zebrafish fin. *Dev Dyn,* 245, 7-21.

Bellows, A. M., Kenna, M. A., Cassimeris, L. & Skibbens, R. V. 2003. Human EFO1p exhibits acetyltransferase activity and is a unique combination of linker histone and Ctf7p/Eco1p chromatid cohesion establishment domains. *Nucleic Acids Res,* 31, 6334-43.

Bhadra, J., Banerji, R., Singh, J., Sallada, N., Eble, D.M & Iovine, M.K. 2015. The zebrafish fibroblast cell line AB9 as a tool to complement gene regulation studies. *Musculoskeletal Regeneration,* 1, 2:e992.

Bhadra, J. & Iovine, M. K. 2015. Hsp47 mediates Cx43-dependent skeletal growth and patterning in the regenerating fin. *Mech Dev,* 138 Pt 3, 364-74.

Chatterjee, B., Chin, A. J., Valdimarsson, G., Finis, C., Sonntag, J. M., Choi, B. Y., Tao, L., Balasubramanian, K., Bell, C., Krufka, A., et al. 2005. Developmental regulation and expression of the zebrafish connexin43 gene. *Dev Dyn,* 233, 890-906.

Deardorff, M. A., Kaur, M., Yaeger, D., Rampuria, A., Korolev, S., Pie, J., Gil-Rodriguez, C., Arnedo, M., Loeys, B., Kline, A. D., et al. 2007. Mutations in cohesin complex members SMC3 and SMC1A cause a mild variant of cornelia de Lange syndrome with predominant mental retardation. *Am J Hum Genet,* 80, 485-94.

Deardorff, M. A., Bando, M., Nakato, R., Watrin, E., Itoh, T., Minamino, M., Saitoh, K., Komata, M., Katou, Y., Clark, D., et al. 2012a. HDAC8 mutations in Cornelia de Lange syndrome affect the cohesin acetylation cycle. *Nature,* 489, 313-7.

Deardorff, M. A., Wilde, J. J., Albrecht, M., Dickinson, E., Tennstedt, S., Braunholz, D., Monnich, M., Yan, Y., Xu, W., Gil-Rodriguez, M. C., et al. 2012b. RAD21 mutations cause a human cohesinopathy. *Am J Hum Genet,* 90, 1014-27.

Dorsett, D. 2016. The Drosophila melanogaster model for Cornelia de Lange syndrome: Implications for etiology and therapeutics. *Am J Med Genet C Semin Med Genet,* 172, 129-37.

Dorsett, D. & Merkenschlager, M. 2013. Cohesin at active genes: a unifying theme for cohesin and gene expression from model organisms to humans. *Curr Opin Cell Biol,* 25, 327-33.

Du, S. J., Frenkel, V., Kindschi, G. & Zohar, Y. 2001. Visualizing normal and defective bone development in zebrafish embryos using the fluorescent chromophore calcein. *Dev Biol,* 238, 239-46.

Flenniken, A. M., Osborne, L. R., Anderson, N., Ciliberti, N., Fleming, C., Gittens, J. E., Gong, X. Q., Kelsey, L. B., Lounsbury, C., Moreno, L., et al. 2005. A Gja1 missense mutation in a mouse model of oculodentodigital dysplasia. *Development,* 132, 4375-86.

Gillis, L. A., McCallum, J., Kaur, M., DeScipio, C., Yaeger, D., Mariani, A., Kline, A. D., Li, H. H., Devoto, M., Jackson, L. G., et al. 2004. NIPBL mutational analysis in 120 individuals with Cornelia de Lange syndrome and evaluation of genotype-phenotype correlations. *Am J Hum Genet,* 75, 610-23.

Goodenough, D. A., Goliger, J. A. & Paul, D. L. 1996. Connexins, connexons, and intercellular communication. *Annu Rev Biochem,* 65, 475-502.

Gordillo, M., Vega, H., Trainer, A. H., Hou, F., Sakai, N., Luque, R., Kayserili, H., Basaran, S., Skovby, F., Hennekam, R. C., et al. 2008. The molecular mechanism underlying Roberts syndrome involves loss of ESCO2 acetyltransferase activity. *Hum Mol Genet,* 17, 2172-80.

Govindan, J., Tun, K. M. & Iovine, M. K. 2016. Cx43-Dependent Skeletal Phenotypes Are Mediated by Interactions between the Hapln1a-ECM and Sema3d during Fin Regeneration. *PLoS One,* 11, e0148202.

Heidinger-Pauli, J. M., Mert, O., Davenport, C., Guacci, V. & Koshland, D. 2010. Systematic reduction of cohesin differentially affects chromosome segregation, condensation, and DNA repair. *Curr Biol,* 20, 957-63.

Hoptak-Solga, A. D., Nielsen, S., Jain, I., Thummel, R., Hyde, D. R. & Iovine, M. K. 2008. Connexin43 (GJA1) is required in the population of dividing cells during fin regeneration. *Dev Biol,* 317, 541-8.

Horsfield, J. A., Print, C. G. & Monnich, M. 2012. Diverse developmental disorders from the one ring: distinct molecular pathways underlie the cohesinopathies. *Front Genet,* 3, 171.

Hou, F. & Zou, H. 2005. Two human orthologues of Eco1/Ctf7 acetyltransferases are both required for proper sister-chromatid cohesion. *Mol Biol Cell,* 16, 3908-18.

Iovine, M. K. 2007. Conserved mechanisms regulate outgrowth in zebrafish fins. *Nat Chem Biol,* 3, 613-8.

Iovine, M. K., Higgins, E. P., Hindes, A., Coblitz, B. & Johnson, S. L. 2005. Mutations in connexin43 (GJA1) perturb bone growth in zebrafish fins. *Dev Biol,* 278, 208-19.

Ivanova, A. V. & Ivanov, S. V. 2002. Differential display analysis of gene expression in yeast. *Cell Mol Life Sci,* 59, 1241-5.

Jeppsson, K., Kanno, T., Shirahige, K. & Sjogren, C. 2014. The maintenance of chromosome structure: positioning and functioning of SMC complexes. *Nat Rev Mol Cell Biol,* 15, 601-14.

Jones, S. J., Gray, C., Sakamaki, H., Arora, M., Boyde, A., Gourdie, R. & Green, C. 1993. The incidence and size of gap junctions between the bone cells in rat calvaria. *Anat Embryol (Berl),* 187, 343-52.

Kagey, M. H., Newman, J. J., Bilodeau, S., Zhan, Y., Orlando, D. A., van Berkum, N. L., Ebmeier, C. C., Goossens, J., Rahl, P. B., Levine, S. S., et al. 2010. Mediator and cohesin connect gene expression and chromatin architecture. *Nature,* 467, 430-5.

Kawauchi, S., Calof, A. L., Santos, R., Lopez-Burks, M. E., Young, C. M., Hoang, M. P., Chua, A., Lao, T., Lechner, M. S., Daniel, J. A., et al. 2009. Multiple organ system defects and transcriptional dysregulation in the Nipbl(+/-) mouse, a model of Cornelia de Lange Syndrome. *PLoS Genet,* 5, e1000650.

Krantz, I. D., McCallum, J., DeScipio, C., Kaur, M., Gillis, L. A., Yaeger, D., Jukofsky, L., Wasserman, N., Bottani, A., Morris, C. A., et al. 2004. Cornelia de Lange syndrome is caused by mutations in NIPBL, the human homolog of Drosophila melanogaster Nipped-B. *Nat Genet,* 36, 631-5.

Lee, Y., Grill, S., Sanchez, A., Murphy-Ryan, M. & Poss, K. D. 2005. Fgf signaling instructs position-dependent growth rate during zebrafish fin regeneration. *Development,* 132, 5173-83.

Liu, J. & Krantz, I. D. 2009. Cornelia de Lange syndrome, cohesin, and beyond. *Clin Genet,* 76, 303-14.

Mannini, L., Liu, J., Krantz, I. D. & Musio, A. 2010. Spectrum and consequences of SMC1A mutations: the unexpected involvement of a core component of cohesin in human disease. *Hum Mutat,* 31, 5-10.

Marston, A. L. 2014. Chromosome segregation in budding yeast: sister chromatid cohesion and related mechanisms. *Genetics,* 196, 31-63.

Mehta, G. D., Kumar, R., Srivastava, S. & Ghosh, S. K. 2013. Cohesin: functions beyond sister chromatid cohesion. *FEBS Lett,* 587, 2299-312.

Merkenschlager, M. & Nora, E. P. 2016. CTCF and Cohesin in Genome Folding and Transcriptional Gene Regulation. *Annu Rev Genomics Hum Genet,* 17, 17-43.

Monnich, M., Kuriger, Z., Print, C. G. & Horsfield, J. A. 2011. A zebrafish model of Roberts syndrome reveals that Esco2 depletion interferes with development by disrupting the cell cycle. *PLoS One,* 6, e20051.

Morita, A., Nakahira, K., Hasegawa, T., Uchida, K., Taniguchi, Y., Takeda, S., Toyoda, A., Sakaki, Y., Shimada, A., Takeda, H., et al. 2012. Establishment and characterization of Roberts syndrome and SC phocomelia model medaka (Oryzias latipes). *Dev Growth Differ,* 54, 588-604.

Musio, A., Selicorni, A., Focarelli, M. L., Gervasini, C., Milani, D., Russo, S., Vezzoni, P. & Larizza, L. 2006. X-linked Cornelia de Lange syndrome owing to SMC1L1 mutations. *Nat Genet,* 38, 528-30.

Paznekas, W. A., Boyadjiev, S. A., Shapiro, R. E., Daniels, O., Wollnik, B., Keegan, C. E., Innis, J. W., Dinulos, M. B., Christian, C., Hannibal, M. C., et al. 2003. Connexin 43 (GJA1) mutations cause the pleiotropic phenotype of oculodentodigital dysplasia. *Am J Hum Genet,* 72, 408-18.

Percival, S. M., Thomas, H. R., Amsterdam, A., Carroll, A. J., Lees, J. A., Yost, H. J. & Parant, J. M. 2015. Variations in dysfunction of sister chromatid cohesion in esco2 mutant zebrafish reflect the phenotypic diversity of Roberts syndrome. *Dis Model Mech,* 8, 941-55.

Rolef Ben-Shahar, T., Heeger, S., Lehane, C., East, P., Flynn, H., Skehel, M. & Uhlmann, F. 2008. Eco1-dependent cohesin acetylation during establishment of sister chromatid cohesion. *Science,* 321, 563-6.

Schule, B., Oviedo, A., Johnston, K., Pai, S. & Francke, U. 2005. Inactivating mutations in ESCO2 cause SC phocomelia and Roberts syndrome: no phenotype-genotype correlation. *Am J Hum Genet,* 77, 1117-28.

Skibbens, R. V. 2016. Of Rings and Rods: Regulating Cohesin Entrapment of DNA to Generate Intra- and Intermolecular Tethers. *PLoS Genet,* 12, e1006337.

Skibbens, R. V., Corson, L. B., Koshland, D. & Hieter, P. 1999. Ctf7p is essential for sister chromatid cohesion and links mitotic chromosome structure to the DNA replication machinery. *Genes Dev,* 13, 307-19.

Ton, Q. V. & Iovine, M. K. 2013. Determining how defects in connexin43 cause skeletal disease. *Genesis,* 51, 75-82.

Tonkin, E. T., Wang, T. J., Lisgo, S., Bamshad, M. J. & Strachan, T. 2004. NIPBL, encoding a homolog of fungal Scc2-type sister chromatid cohesion proteins and fly Nipped-B, is mutated in Cornelia de Lange syndrome. *Nat Genet,* 36, 636-41.

Toth, A., Ciosk, R., Uhlmann, F., Galova, M., Schleiffer, A. & Nasmyth, K. 1999. Yeast cohesin complex requires a conserved protein, Eco1p(Ctf7), to establish cohesion between sister chromatids during DNA replication. *Genes Dev,* 13, 320-33.

Unal, E., Heidinger-Pauli, J. M., Kim, W., Guacci, V., Onn, I., Gygi, S. P. & Koshland, D. E. 2008. A molecular determinant for the establishment of sister chromatid cohesion. *Science,* 321, 566-9.

Van den Berg, D. J. & Francke, U. 1993. Sensitivity of Roberts syndrome cells to gamma radiation, mitomycin C, and protein synthesis inhibitors. *Somat Cell Mol Genet,* 19, 377-92.

Vega, H., Waisfisz, Q., Gordillo, M., Sakai, N., Yanagihara, I., Yamada, M., van Gosliga, D., Kayserili, H., Xu, C., Ozono, K., et al. 2005. Roberts syndrome is caused by mutations in ESCO2, a human homolog of yeast ECO1 that is essential for the establishment of sister chromatid cohesion. *Nat Genet,* 37, 468-70.

Westerfield, M. 1993. The zebrafish: a guide for the laboratory use of zebrafish (*Brachydanio reriro*). Inst. of Neuroscience, University of Oregon.

Whelan, G., Kreidl, E., Wutz, G., Egner, A., Peters, J. M. & Eichele, G. 2012. Cohesin acetyltransferase Esco2 is a cell viability factor and is required for cohesion in pericentric heterochromatin. *EMBO J,* 31, 71-82.

Xu, B., Lee, K. K., Zhang, L. & Gerton, J. L. 2013. Stimulation of mTORC1 with L-leucine rescues defects associated with Roberts syndrome. *PLoS Genet,* 9, e1003857.

Xu, B., Lu, S. & Gerton, J. L. 2014. Roberts syndrome: A deficit in acetylated cohesin leads to nucleolar dysfunction. *Rare Dis,* 2, e27743.

Yin, V. P., Lepilina, A., Smith, A. & Poss, K. D. 2012. Regulation of zebrafish heart regeneration by miR-133. *Dev Biol,* 365, 319-27.

Yuan, B., Pehlivan, D., Karaca, E., Patel, N., Charng, W. L., Gambin, T., Gonzaga-Jauregui, C., Sutton, V. R., Yesil, G., Bozdogan, S. T., et al. 2015. Global transcriptional disturbances underlie Cornelia de Lange syndrome and related phenotypes. *J Clin Invest,* 125, 636-51.

Zhang, B., Chang, J., Fu, M., Huang, J., Kashyap, R., Salavaggione, E., Jain, S., Kulkarni, S., Deardorff, M. A., Uzielli, M. L., et al. 2009. Dosage effects of cohesin regulatory factor PDS5 on mammalian development: implications for cohesinopathies. *PLoS One,* 4, e5232.

Zhang, J., Shi, X., Li, Y., Kim, B. J., Jia, J., Huang, Z., Yang, T., Fu, X., Jung, S. Y., Wang, Y., et al. 2008. Acetylation of Smc3 by Eco1 is required for S phase sister chromatid cohesion in both human and yeast. *Mol Cell,* 31, 143-51.

CHAPTER 4

Conclusions and Future Directions

4.1 Conclusions

It has been a long-standing question in the cohesinopathy field as to what is the underlying molecular mechanism of RBS/CdLS phenotypes, in part due to the diverse roles of cohesin and its auxiliary factors in various *cis* and *trans*-DNA tethering events such as cell division, chromatin organization and transcriptional processes (Ball et al., 2014; Barbero, 2014; Gerton, 2012; Horsfield et al., 2012; Mehta et al., 2013; Skibbens., 2013; Dorsett, 2016; Cucco and Musio, 2015; Zakari et al., 2015; Bose et al., 2012; Liu and Krantz, 2008; Rudra and Skibbens, 2013; Kawauch et al., 2016; Dorsett D, Merkenschlager et al., 2013; Dorsett and Krantz et al., 2009; Banerji et al, 2016; Banerji et al., 2017). The past few years have witnessed important advances made in this field, however, crucial questions regarding the etiology of RBS in particular still remained unanswered. My research exploits the zebrafish regenerating caudal fin to uncover a transcriptional basis for RBS. My findings provide strong evidence that ESCO2 plays a transcriptional role and suggests that the skeletal phenotypes of RBS arise through *cis*-DNA tethering defects resulting in transcriptional deregulation of developmental programs (Banerji et al., 2016; Banerji et al, 2017 submitted).

In Chapter 2, I provide details of my findings that suggest that Esco2 knockdown results in transcriptional deregulation, independent of apoptosis, thus challenging the popular mitotic model of RBS. Using ISH and qRT-PCR techniques I show that Esco2 regulates the expression of clinically relevant *cx43* gene, linked to a similar skeletal disorder, ODDD. By using a transgenic Cx43 overexpression line, I demonstrate rescue of Esco2-dependent skeletal phenotypes. These results provide strong evidence that link Esco2 with Cx43 during bone growth and skeletal patterning (Banerji et al., 2016). These

findings open up crucial questions regarding the mechanism underlying the Esco2-Cx43 skeletal pathway. One such question I became interested in was if Esco2 functions in a cohesin-dependent manner in regulating *cx43* expression? In Chapter 3, I extend my previous findings by testing the role of the cohesin subunit, Smc3 (a known target of Esco2) in regulating the expression of *cx43*. I show that MO-mediated knockdown of Smc3 perturbs bone and tissue regeneration. The results are similar to those previously reported for Esco2 knockdown that includes defects in bone segment growth, tissue regeneration and *cx43* expression (discussed in Chapter 2). Additionally, I provide evidence of rescue of Smc3-dependent bone and tissue regeneration defects using the transgenic *cx43* overexpression line. These findings provide evidence that Smc3 directly contributes to RBS-type phenotypes in the regenerating fin model. Moreover, ChIP assays using zebrafish AB9 cells revealed that Smc3 binds to a discrete region of the *cx43* promoter, suggesting that Esco2 exerts transcriptional regulation of *cx43* through modification of Smc3 bound to the *cx43* promoter (Banerji et al., 2017, in revision, *Biology Open*). Combined findings from Chapter 2 and 3, combined with the established role for Esco2 in Smc3-acetylation, I provide compelling support for a model where Esco2 and Smc3 act on the promoters of skeletal genes (i.e. *cx43*) to regulate transcription and thereby mediate phenotypes of RBS (Figure 3.8).

Overall, the work compiled in this dissertation highlights the following important revelations regarding the etiology of RBS. First, Esco2 knockdown in regenerating fin is established as a powerful system for elucidating the molecular basis of RBS. Second, a novel role of *esco2* in regulating the transcription of a clinically important gene, *cx43* is uncovered. Third, I show that cohesin subunit, Smc3 functions in a similar manner as

Esco2 in regulating the expression of *cx43* gene. Fourth, I provide mechanistic insights into how Esco2 regulates *cx43* expression i.e. Smc3 binds to a discrete region of the *cx43* promoter. These findings suggest a unified transcriptional mechanism that underlies both RBS and CdLS.

Proposed unified model of Cohesinopathy diseases

Considering the findings from my research work, along with evidence from other groups, I challenge the notion that CdLS and RBS represent separate syndromes (Banerji et al., 2016; Choi et al., 2010; Kim et al., 2008; Morita et al., 2012; Kaur et al., 2005; Ghiselli et al., 2006; Fazio et al., 2016; Pistochhi et al., 2013; Schuster et al., 2015; Leem et al., 2011; Xu et al., 2016). My work provides tangible evidence for a unified mechanism underlying RBS and CdLS (discussed in the review article, Banerji et al., 2017, in revision). It is important to take into consideration findings from various groups and reinterpret the underlying mechanisms of RBS/CdLS. Currently, there is enough evidence that mutations in *esco2* not only impact apoptosis but also transcriptional regulation. Furthermore, along with transcriptional deregulation there is evidence that mutations in genes associated with CdLS also cause apoptosis through mitotic failure (Kaur et al., 2005; Ghiselli, 2006; Fazio et al., 2016; 306 Schuster et al., 2015; Pistocchi et al., 2013; Leem et al., 2011, Choi et al., 2010, Banerji et al., 2016, Xu et al., 2016; Cucco and Musio, 2016). But why do cells from RBS and CdLS exhibit distinct morphology? Why are cohesion defects a prominent feature of RBS and not apparent in CdLS?

I speculate that the lack of cohesion defects in CdLS is due to the heterozygosity involved in the disease. CdLS arise due to dominant mutations in genes coding for structural components of the cohesion ring (Krantz et al., 2004; Tonkin et al., 2004; Musio et al., 2006; Deardorff et al., 2007; Deardorff et al., 2012a; Deardorff et al., 2012b; Yuan et al., 2015; Liu and Krantz, 2009). In contrast, RBS is caused by recessive mutations in the gene coding for an enzymatic activity that regulates ring closure (Vega et al., 2005; Schule et al., 2005; Gordillo et al., 2008). Thus dosage of the cohesion pathway genes may play a vital role in this purpose. For instance, RBS cells and model systems exhibit significant loss of cohesion function resulting from *trans*-DNA tethering defects (Monnich et al., 2011; Morita et al., 2012; Percival et al., 2015; Whelan et al., 2012; Van der Lejij et al., 2009). These mitotic failures, and the subsequent induction of apoptosis, potentially disguise underlying *cis*-DNA tethering defects. My PhD. thesis work suggests that a moderate loss of Esco2 function results primarily in *cis*-DNA tethering defects. Autosomal recessive transmission for RBS is consistent with requiring a greater decrease in ESCO2 to achieve transcriptional defects. At this reduced level of ESCO2 function, chromosome segregation defects also are prominent. On the other hand, autosomal dominant transmission requires only a modest loss of cohesion pathway activity, leading to defects in transcription. At this level of function, mitotic defects are not prominent. Therefore, I can propose that transcriptional deregulation is the predominant mechanism through which both RBS and CdLS arise, although the contributing role for mitotic failure and apoptosis cannot be ruled out (Figure 4.1). Further studies are required for support for the unified model of cohesinopathies. Below,

I summarize some of the future directions that would provide additional evidence for the transcriptional model of RBS.

4.2 Future Direction

(1) To determine if the Smc3 association with the *cx43* promoter is dependent on Esco2 acetylation

In Chapter 3, I provide evidence of Smc3 binding to the *cx43* promoter region and provide support of a cohesin-mediated Esco2-dependent model of RBS (Figure 3.8). In this model, it is proposed that acetyltransferace activity of Esco2 is required for the activation its target, Smc3 that binds the *cx43* promoter, thus regulating *cx43* transcription. This model is based on the consideration that Esco2 functions as its established role of an acetlytransferase (Bellows et al., 2003; Skibbens et al., 1999; Toth et al., 1999; Ivanov et al., 2002; Zhang et al., 2008; Unal et al., 2008; Ben-Shahar et al., 2008; Hou and Zou, 2005). Thus it will be interesting to test the established role of Esco2 in regulating *cx43* expression. To functionally link Smc3 binding and gene regulation with Esco2 activity, it is important to test if Smc3 binds to the *cx43* promoter in a Esco2-dependent fashion. This could be achieved by performing Smc3-ChIP at the *cx43* promoter on Esco2 knockdown AB9 cells. If significant Smc3 binding is not observed at the p2 region of the *cx43* promoter in Esco2 knockdown cell lysates, then that infers the Esco2 dependency in the proposed cohesin-mediated transcriptional model of RBS, supporting the hypothesis. The results for this experiment are extremely important to further strengthen the proposed model and provide evidence that Esco2 functions as an acetyltransferase and thus activating cohesins.

(2) Promoter analysis of *cx43* to determine the functional sequence required for Smc3 binding for regulating *cx43* expression

Future studies should be aimed to quantify and detect measurable changes in transcription from the putative *cx43* promoter. For achieving this goal reporter constructs for *cx43* can be generated. The zebrafish *cx43* promoter is approximately 6.7 kb in length, adjacent to an additional connexin gene (*cx32.2*) that resides upstream of the *cx43* coding sequence (Chatterjee et al., 2005). AB9 cells can be transfected with *cx43*-luciferase reporters followed by detection of transcription. This experiment is important to answer two important questions. First, with this set up the functional impact of Esco2 dependency can be tested. For example, the luciferase assay (Solberg and Krauss, 2013) can be performed on Esco2 knockdown AB9 cells followed by luciferase quantification that will determine the functional requirement of Esco2 on *cx43* transcription. Second, in order to determine the functional promoter sequence requirement, *cx43* reporter constructs with point mutations and deletions in the *cx43* promoter can be generated followed by measurement of transcription. These experiments would provide additional evidence in support of the RBS transcriptional model (Figure 3.8).

(3) To demonstrate chromosome looping as a mechanism of transcriptional regulation in RBS

Genome-wide studies show strong evidence of direct association of cohesin subunits and its auxiliary factors with developmental genes. One of the possible mechanisms underlying the transcriptional regulation of cohesin is via long distance DNA loops. The DNA loop formation during transcription is not new concept, as there are historical

evidence of such phenomenon in bacteria and bacteriophage systems (Ptashne, 1986; Hoover et al., 1990; Luijsterburg et al., 2008; Saiz and Vilar, 2006; Kagey et al., 2010). There are several evidences from various groups that show cohesin facilitates such looping mechanism (Hadjur et al., 2009, Mishiro et al., 2009; Nativio et al., 2009; Hou et al., 2010). Interestingly, in mouse embryonic stem cells cohesin binding initiates enhancer-promoter interaction via DNA loops in transcriptionally active genes (Kagey et al., 2010). This study provides *in vivo* evidence of physical interaction and co-occupancy of the cohesin, mediator and NIBPL at the enhancer and core promoter regions of particularly active genes (Figure 1.2). Keeping this mechanism as a common notion during transcriptional regulation, I propose a cohesion-mediated Esco2 dependent model of RBS (Figure 3.8), where activated Smc3 binds to the *cx43* promoter region that facilitates conformational changes bringing the enhancer- *cx43* promoter in close proximity. In Chapter 3, I provide evidence of Smc3 association with the *cx43* promoter region, but it is important to test if the mechanism is via chromatin looping and also the involvement of enhancers in *cx43* regulation. The spatial organization of chromatin can be tested by performing Chromosome conformation capture (3C) technique (Kagey et al., 2010).

(4) To determine if Esco2 regulates *cx43* transcription via association of transcription factors

I provide support of a cohesin-dependent mechanism of *cx43* regulation, which is one of the many ways that *cx43* could be regulated by Esco2 (Chapter 3). There lies a possibility that the link between Esco2 and Cx43 is cohesin-independent (Figure 4.2).

Transcription factors can bind to Esco2 in regulating *cx43* expression. One potential candidate is *notch*, since a similar role of Esco2 in regulating *notch* transcription has been previously reported (Leem et al., 2011). Notch signaling is evolutionary conserved in all vertebrates and is crucial for regulating various developmental programs. The transcription factor *notch* associates with Esco2 and is sequestered away from the promoter binding sites during the differentiation of neuronal cells. Another study reported reduction in *notch1a* expression in Esco2 depleted medaka mutants (*esco2^{R80S}*) providing additional evidence of Esco2 and Notch association (Morita et al., 2012).

Another potential transcription factor that may also play an important role is CTCF. There are many evidence that link cohesin and CTCF and suggest their role in gene expression (Wendt and Peters, 2009; Wendt et al., 2008; Hadjur et al., 2009; Hou et al., 2010; Kagey et al., 2010; Ball et al., 2014; Parelho et al., 2008; Rubio et al., 2008; Degner et al., 2011; Nativio et al., 2011; Majumder and Boss, 2011; Guo et al., 2012). In a 2008 study, 9000 cohesin sites were mapped in the entire non-repetitive part of the human genome, which showed 89% of these sites identical with CTCF sites (Wendt et al. 2008). It will be interesting to see if these factors are dependent on Esco2 and if yes, then how is *cx43* expression affected. This is important to understand the alternative mechanisms that may link Esco2 and Cx43 during skeletal growth and patterning. If this model is true, it will provide evidence that Esco2-binding factors may regulate *cx43* expression, which is separate from its well-established acetyltransferase role. The schematic of the proposed model is depicted in Figure 4.2.

Additionally there are few transcription factors that are reported to associate with *cx43* but their dependency on Esco2 is yet to be tested. The list of genes that can be

included to test the model (Figure 4.2) are *Nkx2.5*, *Runx2*, *Tbx2* and *Tbx3*, *SOX4*, and

SOX2, *β-catenin*, and *Msx1* (Chatterjee et al., 2005; Boogerd et al., 2011; Xia et al., 2010;

Boogerd et al., 2008; Chen et al., 1995; Chatterjee et al., 2001). These factors could either

induce or repress *cx43* expression but their link with Esco2 needs to be tested.

(5) To determine if Esco2 regulate *cx43* transcription by the association of

chromatin-remodeling complexes

It is now widely accepted that eukaryotic gene expression is regulated not only by

basal transcriptional machinery but also by chromatin structural changes. Thus it is

possible that Esco2 recruits chromatin-remodeling complexes to *cx43* promoter for

regulating its transcription. There are evidence that suggest association of Esco2 with the

CoREST complex and also with other chromatin modifying enzymes (Kim et al., 2008).

Other evidence show chromatin- remodeling complexes such as methyltransferases

(SETDB1, G9a and suv39h1) and demethylases (LSD1) bind to Esco2 independent of

acetyltransferase activity (Choi et al., 2010; Skibbens et al., 2013). Involvement of such

factors will provide additional mechanisms through which Esco2-binding factors may

regulate *cx43* expression which is separate from it's well established acetyltransferase

role. The schematic of the proposed model is depicted in Figure 4.2. Similarly, it will be

interesting to test the Esco2 dependency on this model and to determine how *cx43*

expression is affected.

(6) To determine novel binding partners of Esco2 in regulating *cx43* expression

Currently, very few known partners of Esco2 have been identified. In order to understand the alternative mechanisms underlying Esco2-Cx43 regulation it will be valuable to adapt *a priori* approach for identifying novel binding partners of Esco2. Since my findings show that Esco2 knockdown results in reduction of *cx43* expression, it is possible that there are novel partners that participate in direct binding of repressors away from the *cx43* promoter. To address this strategy, mass spectrometric analysis can be performed to identify Esco2 associated factors. This should be followed by testing for candidate factor binding to *cx43* promoter in the presence and absence of Esco2. Generation of a candidate list will be extremely helpful for testing the physical link between the candidates and Esco2. This strategy of producing a candidate list of Esco2-dependent binding factors will open up new ways to identify possible mechanisms underlying Roberts Syndrome.

4.3 Figures
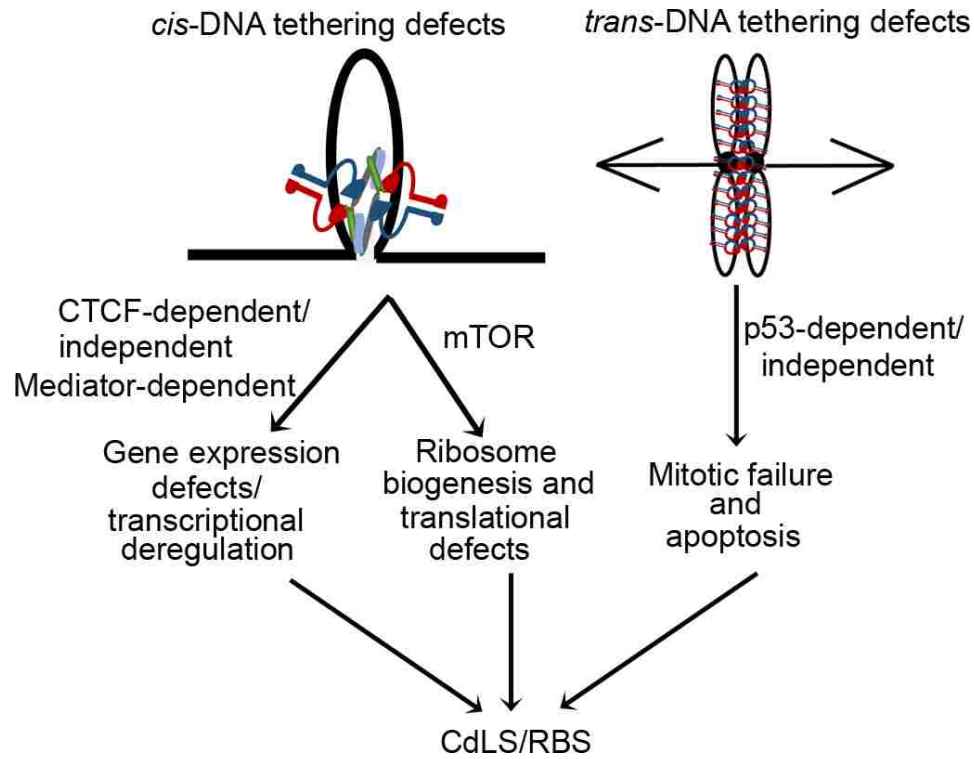
Figure 4.1: Mechanisms of cohesinopathies. Transcriptional deregulation caused by defects in *cis*-DNA tethering events is the predominant mechanism through which both RBS and CdLS arise. The extent to which mitotic failure and apoptosis caused by defects in *trans*-DNA tethering events contribute to cohesinopathies requires further inquiry.

Source: Review article, Banerji et al., 2017, (In press, Developmental Dynamics)
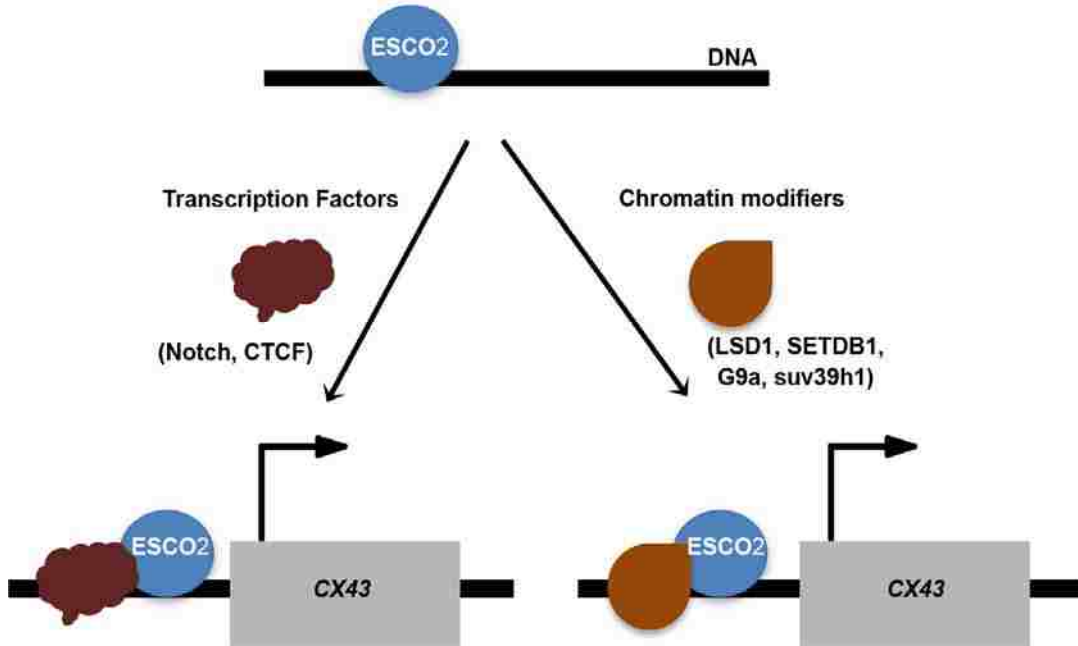
Figure 4.2: Cohesin-independent model of Esco2-Cx43 regulation. Proposed model of Esco2 regulating *cx43* transcription via transcription factors or chromatin remodeling complexes. Chromatin modifiers or transcription factors bind Esco2 may be recruited to the *cx43* promoter for transcriptional regulation.

4.4 References

Ball, A. R., Jr., Chen, Y. Y. & Yokomori, K. 2014. Mechanisms of cohesin-mediated gene regulation and lessons learned from cohesinopathies. *Biochim Biophys Acta,* 1839, 191-202.

Banerji, R., Eble, D.M., Iovine, M.K. and Skibbens, R.V., 2016. Esco2 regulates cx43 expression during skeletal regeneration in the zebrafish fin. *Developmental Dynamics*, 245(1), pp.7-21.

Banerji, R., Iovine, M.K. and Skibbens, R.V., 2017. Cohesin mediates Esco2-dependent transcriptional regulation in zebrafish regenerating fin model of Roberts syndrome *Biology Open*, (submitted).

Banerji, R., Iovine, M.K. and Skibbens, R.V., 2017. How many roads lead to cohesinopathies? *Developmental Dynamics*, (In revision).

Barbero, J.L., 2013. Genetic basis of cohesinopathies. *Appl Clin Genet*, *6*, pp.15-23.

Bellows, A. M., Kenna, M. A., Cassimeris, L. & Skibbens, R. V. 2003. Human EFO1p exhibits acetyltransferase activity and is a unique combination of linker histone and Ctf7p/Eco1p chromatid cohesion establishment domains. *Nucleic Acids Res,* 31, 6334-43.

Ben-Shahar, T.R., Heeger, S., Lehane, C., East, P., Flynn, H., Skehel, M. and Uhlmann, F., 2008. Eco1-dependent cohesin acetylation during establishment of sister chromatid cohesion. *Science*, 32*1*(5888), pp.563-566.

Boogerd, C.J.J., Wong, L.Y.E., van den Boogaard, M., Bakker, M.L., Tessadori, F., Bakkers, J., Moorman, A.F., Christoffels, V.M. and Barnett, P., 2011. Sox4 mediates Tbx3 transcriptional regulation of the gap junction protein Cx43. *Cellular and molecular life sciences*, 68(23), pp.3949-3961.

Boogerd, K.J., Wong, L.E., Christoffels, V.M., Klarenbeek, M., Ruijter, J.M., Moorman, A.F. and Barnett, P., 2008. Msx1 and Msx2 are functional interacting partners of T-box factors in the regulation of Connexin43. *Cardiovascular research*, 78(3), pp.485-493.

Bose T, Lee KK, Lu S, Xu B, Harris B, et al. 2012. Cohesin proteins promote ribosomal RNA production and protein translation in yeast and human cells. *PLoS Genet* 8(6): e1002749.

Chatterjee, B., Chin, A.J., Valdimarsson, G., Finis, C., Sonntag, J.M., Choi, B.Y., Tao, L., Balasubramanian, K., Bell, C., Krufka, A. and Kozlowski, D.J., 2005. Developmental regulation and expression of the zebrafish connexin43 gene. *Developmental dynamics*, 233(3), pp.890-906.

Chatterjee, B., Li, Y.X., Zdanowicz, M., Sonntag, J.M., Chin, A.J., Kozlowski, D.J., Valdimarsson, G., Kirby, M.L. and Lo, C.W., 2001. Analysis of Cx43α1 promoter function in the developing zebrafish embryo. *Cell communication & adhesion*, *8*(4-6), pp.289-292.

Chen, S.C., Pelletier, D.B., Ao, P. and Boynton, A.L., 1995. Connexin43 reverses the phenotype of transformed cells and alters their expression of cyclin/cyclin-dependent kinases. *Cell growth & differentiation: the molecular biology journal of the American Association for Cancer Research*, *6*(6), pp.681-690.

Choi, H. K., Kim, B. J., Seo, J. H., Kang, J. S., Cho, H. & Kim, S. T. 2010. Cohesion establishment factor, Eco1 represses transcription via association with histone demethylase, LSD1. *Biochem Biophys Res Commun,* 394, 1063-8.

Cucco, F. and Musio, A., 2016, June. Genome stability: What we have learned from cohesinopathies. *American Journal of Medical Genetics Part C: Seminars in Medical Genetics* Vol. 172, No. 2, pp. 171-178.

Deardorff, M. A., Bando, M., Nakato, R., Watrin, E., Itoh, T., Minamino, M., Saitoh, K., Komata, M., Katou, Y., Clark, D., et al. 2012a. HDAC8 mutations in Cornelia de Lange syndrome affect the cohesin acetylation cycle. *Nature,* 489, 313-7.

Deardorff, M. A., Kaur, M., Yaeger, D., Rampuria, A., Korolev, S., Pie, J., Gil-Rodriguez, C., Arnedo, M., Loeys, B., Kline, A. D., et al. 2007. Mutations in cohesin complex members SMC3 and SMC1A cause a mild variant of cornelia de Lange syndrome with predominant mental retardation. *Am J Hum Genet,* 80, 485-94.

Deardorff, M. A., Wilde, J. J., Albrecht, M., Dickinson, E., Tennstedt, S., Braunholz, D., Monnich, M., Yan, Y., Xu, W., Gil-Rodriguez, M. C., et al. 2012b. RAD21 mutations cause a human cohesinopathy. *Am J Hum Genet,* 90, 1014-27.

Degner, S. C., Verma-Gaur, J., Wong, T. P., Bossen, C., Iverson, G. M., Torkamani, A., Vettermann, C., Lin, Y. C., Ju, Z., Schulz, D., et al. 2011. CCCTC-binding factor (CTCF) and cohesin influence the genomic architecture of the Igh locus and antisense transcription in pro-B cells. *Proc Natl Acad Sci U S A,* 108, 9566-71.

Dorsett, D. 2016. The Drosophila melanogaster model for Cornelia de Lange syndrome: Implications for etiology and therapeutics. *Am J Med Genet C Semin Med Genet,* 172, 129-37.

Dorsett D, Merkenschlager M. (2013) Cohesin at active genes: A unifying theme for cohesin and gene expression from model organisms to humans. *Curr Opin Cell Biol* 25(3): 327-333.

Dorsett, D. and Krantz, I.D., 2009. On the molecular etiology of Cornelia de Lange syndrome. *Annals of the New York Academy of Sciences*, 1151(1), pp.22-37.

Fazio, G., Gaston-Massuet, C., Bettini, L. R., Graziola, F., Scagliotti, V., Cereda, A., Ferrari, L., Mazzola, M., Cazzaniga, G., Giordano, A., et al. 2016. CyclinD1 Down-Regulation and Increased Apoptosis Are Common Features of Cohesinopathies. *J Cell Physiol,* 231, 613-22.

Gerton JL. 2012. Translational mechanisms at work in the cohesinopathies. Nucleus 3(6): 520-525.

Ghiselli, G. 2006. SMC3 knockdown triggers genomic instability and p53-dependent apoptosis in human and zebrafish cells. *Mol Cancer,* 5, 52.

Gordillo, M., Vega, H., Trainer, A. H., Hou, F., Sakai, N., Luque, R., Kayserili, H., Basaran, S., Skovby, F., Hennekam, R. C., et al. 2008. The molecular mechanism underlying Roberts syndrome involves loss of ESCO2 acetyltransferase activity. *Hum Mol Genet,* 17, 2172-80.

Guo, Y., Monahan, K., Wu, H., Gertz, J., Varley, K.E., Li, W., Myers, R.M., Maniatis, T. and Wu, Q., 2012. CTCF/cohesin-mediated DNA looping is required for protocadherin α promoter choice. *Proceedings of the National Academy of Sciences*, 109(51), pp.21081-21086.

Hadjur, S., Williams, L. M., Ryan, N. K., Cobb, B. S., Sexton, T., Fraser, P., Fisher, A. G. & Merkenschlager, M. 2009. Cohesins form chromosomal cis-interactions at the developmentally regulated IFNG locus. *Nature,* 460, 410-3.

Horsfield, J. A., Print, C. G. & Monnich, M. 2012. Diverse developmental disorders from the one ring: distinct molecular pathways underlie the cohesinopathies. *Front Genet,* 3, 171.

Hoover, T.R., Santero, E., Porter, S. and Kustu, S., 1990. The integration host factor stimulates interaction of RNA polymerase with NIFA, the transcriptional activator for nitrogen fixation operons. *Cell*, 63(1), pp.11-22.

Hou, C., Dale, R. & Dean, A. 2010. Cell type specificity of chromatin organization mediated by CTCF and cohesin. *Proc Natl Acad Sci U S A,* 107, 3651-6.

Hou, F. & Zou, H. 2005. Two human orthologues of Eco1/Ctf7 acetyltransferases are both required for proper sister-chromatid cohesion. *Mol Biol Cell,* 16, 3908-18.

Ivanov, D., Schleiffer, A., Eisenhaber, F., Mechtler, K., Haering, C.H. and Nasmyth, K., 2002. Eco1 is a novel acetyltransferase that can acetylate proteins involved in cohesion. *Current biology*, 12(4), pp.323-328.

Kagey, M. H., Newman, J. J., Bilodeau, S., Zhan, Y., Orlando, D. A., van Berkum, N. L., Ebmeier, C. C., Goossens, J., Rahl, P. B., Levine, S. S., et al. 2010. Mediator and cohesin connect gene expression and chromatin architecture. *Nature,* 467, 430-5.

Kaur, M., DeScipio, C., McCallum, J., Yaeger, D., Devoto, M., Jackson, L. G., Spinner, N. B. & Krantz, I. D. 2005. Precocious sister chromatid separation (PSCS) in Cornelia de Lange syndrome. *Am J Med Genet A,* 138, 27-31.

Kawauchi, S., Santos, R., Muto, A., Lopez-Burks, M.E., Schilling, T.F., Lander, A.D. and Calof, A.L., 2016, June. Using mouse and zebrafish models to understand the etiology of developmental defects in Cornelia de Lange Syndrome. In *American Journal of Medical Genetics Part C: Seminars in Medical Genetics* (Vol. 172, No. 2, pp. 138-145).

Kim, B. J., Kang, K. M., Jung, S. Y., Choi, H. K., Seo, J. H., Chae, J. H., Cho, E. J., Youn, H. D., Qin, J. & Kim, S. T. 2008. Esco2 is a novel corepressor that associates with various chromatin modifying enzymes. *Biochem Biophys Res Commun,* 372, 298-304.

Krantz, I. D., McCallum, J., DeScipio, C., Kaur, M., Gillis, L. A., Yaeger, D., Jukofsky, L., Wasserman, N., Bottani, A., Morris, C. A., et al. 2004. Cornelia de Lange syndrome is caused by mutations in NIPBL, the human homolog of Drosophila melanogaster Nipped-B. *Nat Genet,* 36, 631-5.

Leem, Y. E., Choi, H. K., Jung, S. Y., Kim, B. J., Lee, K. Y., Yoon, K., Qin, J., Kang, J. S. & Kim, S. T. 2011. Esco2 promotes neuronal differentiation by repressing Notch signaling. *Cell Signal,* 23, 1876-84.

Liu, J. & Krantz, I. D. 2009. Cornelia de Lange syndrome, cohesin, and beyond. *Clin Genet,* 76, 303-14.

Luijsterburg, M.S., White, M.F., van Driel, R. and Dame, R.T., 2008. The major architects of chromatin: architectural proteins in bacteria, archaea and eukaryotes. *Critical reviews in biochemistry and molecular biology*, 43(6), pp.393-418.

Majumder, P. & Boss, J. M. 2011. Cohesin regulates MHC class II genes through interactions with MHC class II insulators. *J Immunol,* 187, 4236-44.

Mehta GD, Kumar R, Srivastava S, Ghosh SK. 2013. Cohesin: Functions beyond sister chromatid cohesion. *FEBS Lett* 587(15): 2299-2312.

Mishiro, T., Ishihara, K., Hino, S., Tsutsumi, S., Aburatani, H., Shirahige, K., & Nakao, M. 2009. Architectural roles of multiple chromatin insulators at the human apolipoprotein gene cluster. *The EMBO journal*, 28(9), 1234-1245.

Misulovin, Z., Schwartz, Y. B., Li, X. Y., Kahn, T. G., Gause, M., MacArthur, S., Fay, J. C., Eisen, M. B., Pirrotta, V., Biggin, M. D., et al. 2008. Association of cohesin and Nipped-B with transcriptionally active regions of the Drosophila melanogaster genome. *Chromosoma,* 117, 89-102.

Monnich, M., Kuriger, Z., Print, C. G. & Horsfield, J. A. 2011. A zebrafish model of Roberts syndrome reveals that Esco2 depletion interferes with development by disrupting the cell cycle. *PLoS One,* 6, e20051.

Morita, A., Nakahira, K., Hasegawa, T., Uchida, K., Taniguchi, Y., Takeda, S., Toyoda, A., Sakaki, Y., Shimada, A., Takeda, H., et al. 2012. Establishment and characterization of Roberts syndrome and SC phocomelia model medaka (Oryzias latipes). *Dev Growth Differ,* 54, 588-604.

Musio, A., Selicorni, A., Focarelli, M. L., Gervasini, C., Milani, D., Russo, S., Vezzoni, P. & Larizza, L. 2006. X-linked Cornelia de Lange syndrome owing to SMC1L1 mutations. *Nat Genet,* 38, 528-30.

Nativio, R., Sparago, A., Ito, Y., Weksberg, R., Riccio, A. & Murrell, A. 2011. Disruption of genomic neighbourhood at the imprinted IGF2-H19 locus in Beckwith-Wiedemann syndrome and Silver-Russell syndrome. *Hum Mol Genet,* 20, 1363-74.

Percival, S. M., Thomas, H. R., Amsterdam, A., Carroll, A. J., Lees, J. A., Yost, H. J. & Parant, J. M. 2015. Variations in dysfunction of sister chromatid cohesion in esco2 mutant zebrafish reflect the phenotypic diversity of Roberts syndrome. *Dis Model Mech,* 8, 941-55.

Pistocchi, A., Fazio, G., Cereda, A., Ferrari, L., Bettini, L. R., Messina, G., Cotelli, F., Biondi, A., Selicorni, A. & Massa, V. 2013. Cornelia de Lange Syndrome: NIPBL haploinsufficiency downregulates canonical Wnt pathway in zebrafish embryos and patients fibroblasts. *Cell Death Dis,* 4, e866.

Ptashne, M., 1986. Gene regulation by proteins acting nearby and at a distance. *Nature, 322*, pp.697-701.

Rolef Ben-Shahar, T., Heeger, S., Lehane, C., East, P., Flynn, H., Skehel, M. & Uhlmann, F. 2008. Eco1-dependent cohesin acetylation during establishment of sister chromatid cohesion. *Science,* 321, 563-6.

Rudra, S. and Skibbens, R.V., 2013. Cohesin codes–interpreting chromatin architecture and the many facets of cohesin function. *J Cell Sci*, *126*(1), pp.31-41.

Saiz, L. and Vilar, J.M., 2006. DNA looping: the consequences and its control. *Current opinion in structural biology*, 16(3), pp.344-350.

Schule, B., Oviedo, A., Johnston, K., Pai, S. & Francke, U. 2005. Inactivating mutations in ESCO2 cause SC phocomelia and Roberts syndrome: no phenotype-genotype correlation. *Am J Hum Genet,* 77, 1117-28.

Schuster, K., Leeke, B., Meier, M., Wang, Y., Newman, T., Burgess, S. & Horsfield, J. A. 2015. A neural crest origin for cohesinopathy heart defects. *Hum Mol Genet,* 24, 7005-16.

Skibbens, R. V. 2016. Of Rings and Rods: Regulating Cohesin Entrapment of DNA to Generate Intra- and Intermolecular Tethers. *PLoS Genet,* 12, e1006337.

Skibbens, R. V., Corson, L. B., Koshland, D. & Hieter, P. 1999. Ctf7p is essential for sister chromatid cohesion and links mitotic chromosome structure to the DNA replication machinery. *Genes Dev,* 13, 307-19.

Skibbens RV, Colquhoun JM, Green MJ, Molnar CA, Sin DN, Sullivan BJ, Tanzosh EE. 2013. Cohesinopathies of a feather flock together. *PLoS Genet* 9(12): e1004036.

Solberg, N. and Krauss, S., 2013. Luciferase assay to study the activity of a cloned promoter DNA fragment. *Gene Regulation: Methods and Protocols*, pp.65-78.

Tonkin, E. T., Wang, T. J., Lisgo, S., Bamshad, M. J. & Strachan, T. 2004. NIPBL, encoding a homolog of fungal Scc2-type sister chromatid cohesion proteins and fly Nipped-B, is mutated in Cornelia de Lange syndrome. *Nat Genet,* 36, 636-41.

Toth, A., Ciosk, R., Uhlmann, F., Galova, M., Schleiffer, A. & Nasmyth, K. 1999. Yeast cohesin complex requires a conserved protein, Eco1p(Ctf7), to establish cohesion between sister chromatids during DNA replication. *Genes Dev,* 13, 320-33.

Unal E, Arbel-Eden A, Sattler U, Shroff R, Lichten M, et al. 2004. DNA damage response pathway uses histone modification to assemble a double-strand break-specific cohesin domain. *Mol Cell* 16(6): 991-1002.

van der Lelij, P., Godthelp, B. C., van Zon, W., van Gosliga, D., Oostra, A. B., Steltenpool, J., de Groot, J., Scheper, R. J., Wolthuis, R. M., Waisfisz, Q., et al. 2009. The cellular phenotype of Roberts syndrome fibroblasts as revealed by ectopic expression of ESCO2. *PLoS One,* 4, e6936.

Vega, H., Waisfisz, Q., Gordillo, M., Sakai, N., Yanagihara, I., Yamada, M., van Gosliga, D., Kayserili, H., Xu, C., Ozono, K., et al. 2005. Roberts syndrome is caused by mutations in ESCO2, a human homolog of yeast ECO1 that is essential for the establishment of sister chromatid cohesion. *Nat Genet,* 37, 468-70.

Wendt, K. S. & Peters, J. M. 2009. How cohesin and CTCF cooperate in regulating gene expression. *Chromosome Res,* 17, 201-14.

Wendt, K. S., Yoshida, K., Itoh, T., Bando, M., Koch, B., Schirghuber, E., Tsutsumi, S., Nagae, G., Ishihara, K., Mishiro, T., et al. 2008. Cohesin mediates transcriptional insulation by CCCTC-binding factor. *Nature,* 451, 796-801.

Whelan, G., Kreidl, E., Wutz, G., Egner, A., Peters, J. M. & Eichele, G. 2012. Cohesin acetyltransferase Esco2 is a cell viability factor and is required for cohesion in pericentric heterochromatin. *EMBO J,* 31, 71-82.

Xia, X., Batra, N., Shi, Q., Bonewald, L.F., Sprague, E. and Jiang, J.X., 2010. Prostaglandin promotion of osteocyte gap junction function through transcriptional regulation of connexin 43 by glycogen synthase kinase 3/β-catenin signaling. *Molecular and cellular biology*, *30*(1), pp.206-219.

Xu, B., Gogol, M., Gaudenz, K. & Gerton, J. L. 2016. Improved transcription and translation with L-leucine stimulation of mTORC1 in Roberts syndrome. *BMC Genomics,* 17, 25.

Yuan, B., Pehlivan, D., Karaca, E., Patel, N., Charng, W.L., Gambin, T., Gonzaga-Jauregui, C., Sutton, V.R., Yesil, G., Bozdogan, S.T. and Tos, T., 2015. Global transcriptional disturbances underlie Cornelia de Lange syndrome and related phenotypes. *The Journal of clinical investigation*, 125(2), pp.636-651.

Zakari, M., Yuen, K. & Gerton, J. L. 2015. Etiology and pathogenesis of the cohesinopathies. *Wiley Interdiscip Rev Dev Biol,* 4, 489-504.

Zhang, J., Shi, X., Li, Y., Kim, B. J., Jia, J., Huang, Z., Yang, T., Fu, X., Jung, S. Y., Wang, Y., et al. 2008. Acetylation of Smc3 by Eco1 is required for S phase sister chromatid cohesion in both human and yeast. *Mol Cell,* 31, 143-51.

<div align="center">

Rajeswari Banerji
Curriculum Vitae

Lehigh University
Department of Biological Sciences
111 Research Drive, B-217
Bethlehem, PA 18015

</div>

Education:

2011 – May, 2017	**Ph.D. Candidate, Cell and Molecular Biology** Lehigh University, Bethlehem, PA Advisor: Mary Kathryn Iovine, Ph.D. Co-Advisor: Robert V. Skibbens Title: The regenerating fin as a model to examine the skeletal defects of Roberts Syndrome **Current GPA: 4.0**
2005- 2007	**M.Sc., Biotechnology, Amity Institute of Biotechnology.** Amity University, Noida, India, CGPA – 8.27
2002- 2005	**B.Sc. (Hons.), Biotechnology, Amity Institute of Biotechnology.** CCS University, Meerut, India First division, 72%

Experience:

Lehigh University, Bethlehem, PA Department of Biological Sciences Graduate Research/Teaching Assistant	August 2011 – Present
The Centre for Genomic Application, New Delhi Research Biologist, Microarray Department	February 2008 – September 2009
International Medical Research Organization, Kolkata Clinical Research Associate	May 2005- June 2005

Training:

Master's degree:

1. Undertook a 2 months training during M.Sc. (Sem-II) at Department of Biological Chemistry, Indian Association for Cultivation of Science, Kolkata, under a project

<div align="center">

149

</div>

entitled '*Isolation of Fungi having Chitosanase Activity followed by Partial Purification of Chitosanase*'.

2. All India Institute of Medicinal Sciences (AIIMS), Ocular Biochemistry, Project title: '*Study of Various Biochemical Parameters in Uveitis*'.

3. The Centre for Genomic Applications (TCGA), Delhi. Project title: '*Analysis of loci 5, 6, 10 and 15 of IS900 element in the Indian 'Bison type' MAP isolate 'S5''*'. Techniques applied in the project were Polymerase Chain Reaction, DNA sequencing and Multiple Alignment by Clustal W.

Undergraduate degree:

4. Amity Institute of Biotechnology. Project title: *'Isolation and Assessment of Bacterial Activity in Yamuna Water'*. The aim was to show the water balance in New Delhi and the harmful effects it could cause.

5. Training during M.Sc. (Semester-II) at Department of Biological Chemistry, Indian Association for Cultivation of Science, Kolkata.

Fellowships:

1. Lehigh University, College of Arts & Sciences Summer Research Fellowship, 2013

2. Lehigh University, Nemes Fellowship, Fall 2015

Manuscripts:

1. **Banerji R**, Eble D. M., Iovine M. K. and Skibbens R. V. (2016). Esco2 regulates *cx43* expression during skeletal regeneration in the zebrafish fin. *Developmental Dynamics*, 245(1), 7-21. doi: 10.1002/dvdy.24354

2. Bhadra J, **Banerji R**, Singh J, Sallada N, Eble D. M. and Iovine M. K. (2015). The Zebrafish fibroblast cell line AB9 as a tool to complement gene regulation studies. *Musculoskeletal Regeneration*, 1. ***doi***: 10.14800/mr.992

3. **Banerji R**, Skibbens R. V. and Iovine M. K. How many roads lead to cohesinopathies? Invited review*, Developmental Dynamics Special Issue* (In press)

4. **Banerji R**, Skibbens R. V.and Iovine M. K. Cohesin mediates Esco2-dependent transcriptional regulation in zebrafish regenerating fin model of Roberts Syndrome (in revision, *Biology Open*)

Conferences:

1. **R. Banerji**, D. M. Eble, R. V. Skibbens and M. K. Iovine. *Development of a Model for Roberts Syndrome in Zebrafish regenerating fins.* **(Invited talk)** 2013 Mid-Atlantic SDB Meeting, April 19 -21. College of William & Mary, Williamsburg, VA.
2. **R. Banerji**, D. M. Eble, R. V. Skibbens and M. K. Iovine. *Esco2 regulates cx43 expression during skeletal regeneration in the zebrafish fin.* 2014 International Zebrafish Meeting, Wisconsin, Madison.
3. **R. Banerji**, R. V. Skibbens and M. K. Iovine. *Esco2 regulates cx43 expression during skeletal regeneration in the zebrafish fin.* 2015 Mid-Atlantic SDB Meeting, Princeton University, NJ.
4. **R. Banerji**, R. V. Skibbens and M. K. Iovine. *The regenerating fin as a model to examine the skeletal defects of Roberts Syndrome.* 2016 The Allied Genetics Conference, Orlando, FL.
5. **Banerji R**, Skibbens R. V. and Iovine M. K. *The regenerating fin as a model to examine the skeletal defects of Roberts Syndrome.* **(Invited talk)** 2017 MARZ Meeting, Baltimore.